AFRL-VA-WP-TR-2001-3008

SMALL CRACK GROWTH AT PIN LOADED HOLES

Arvind Nagar

Analytical Structural Mechanics Branch (AFRL/VASM)
Structures Division
Air Force Research Laboratory, Air Force Materiel Command
Wright-Patterson Air Force Base, OH 45433-7542

JUNE 2003

Final Report for 20 January 2000 – 30 June 2003

AIR VEHICLES DIRECTORATE
AIR FORCE RESEARCH LABORATORY
AIR FORCE MATERIEL COMMAND
WRIGHT-PATTERSON AIR FORCE BASE, OH 45433-7542

NOTICE

USING GOVERNMENT DRAWINGS, SPECIFICATIONS, OR OTHER DATA INCLUDED IN THIS DOCUMENT FOR ANY PURPOSE OTHER THAN GOVERNMENT PROCUREMENT DOES NOT IN ANY WAY OBLIGATE THE U.S. GOVERNMENT. THE FACT THAT THE GOVERNMENT FORMULATED OR SUPPLIED THE DRAWINGS, SPECIFICATIONS, OR OTHER DATA DOES NOT LICENSE THE HOLDER OR ANY OTHER PERSON OR CORPORATION; OR CONVEY AND RIGHTS OR PERMISSION TO MANUFACTURE, USE, OR SELL ANY PATENTED INVENTION THAT MAY RELATE TO THEM.

THIS REPORT HAS BEEN REVIEWED BY THE OFFICE OF PUBLIC AFFAIRS (ASC/PA) AND IS RELEASABLE TO THE NATIONAL TECHNICAL INFORMATION SERVICE (NTIS). AT NTIS, IT WILL BE AVAILABLE TO THE GENERAL PUBLIC, INCLUDING FOREIGN NATIONS.

THIS TECHNICAL REPORT HAS BEEN REVIEWED AND IS APPROVED FOR PUBLICATION.

/s/
ARVIND NAGAR
Aerospace Engineer
Structural Mechanics Branch
Structures Division

/s/
JAMES W. ROGERS JR., MAJ, USAF
Chief, Structural Mechanics Branch
Structures Division

/s/
JOHN A. BOWLUS
Chief
Structures Division

Do not return copies of this report unless contractual obligations or notice on a specific document require its return.

REPORT DOCUMENTATION PAGE

Form Approved
OMB No. 0704-0188

1. REPORT DATE *(DD-MM-YY)*	2. REPORT TYPE	3. DATES COVERED *(From - To)*
June 2003	Final	01/20/2000 – 06/30/2003

4. TITLE AND SUBTITLE
SMALL CRACK GROWTH AT PIN LOADED HOLES

5a. CONTRACT NUMBER
IN-HOUSE

5b. GRANT NUMBER

5c. PROGRAM ELEMENT NUMBER
N/A

6. AUTHOR(S)
Arvind Nagar

5d. PROJECT NUMBER
N/A

5e. TASK NUMBER
N/A

5f. WORK UNIT NUMBER
N/A

7. PERFORMING ORGANIZATION NAME(S) AND ADDRESS(ES)
Analytical Structural Mechanics Branch (AFRL/VASM)
Structures Division
Air Force Research Laboratory, Air Force Materiel Command
Wright-Patterson Air Force Base, OH 45433-7542

8. PERFORMING ORGANIZATION REPORT NUMBER
AFRL-VA-WP-TR-2001-3008

9. SPONSORING/MONITORING AGENCY NAME(S) AND ADDRESS(ES)
Air Vehicles Directorate
Air Force Research Laboratory
Air Force Materiel Command
Wright-Patterson Air Force Base, OH 45433-7542

10. SPONSORING/MONITORING AGENCY ACRONYM(S)
AFRL/VASM

11. SPONSORING/MONITORING AGENCY REPORT NUMBER(S)
AFRL-VA-WP-TR-2001-3008

12. DISTRIBUTION/AVAILABILITY STATEMENT
Approved for public release; distribution is unlimited.

13. SUPPLEMENTARY NOTES
This technical report was prepared in cooperation with Federal Aviation Administration (FAA/AAR), Hughes Technical Center and Boeing West, Long Beach. The testing was sponsored by FAA/AAR. Report contains color.

14. ABSTRACT *(Maximum 200 Words)*
This report describes the results of an experimental study conducted to verify analytical methods for small crack growth prediction at pin-loaded holes under varying load transfer rates. The study was conducted on 2024-T3 joint specimens with an initial 0.003-inch radial thru crack under constant amplitude cyclic and spectrum loads. The test specimens were joined using three different types of doublers. Crack growth data in the small crack regime and the long crack regime was developed. Strain data on doubler plates during testing was obtained.

15. SUBJECT TERMS
Crack Growth, Small Cracks, Load Transfer, Pin Loaded, Strain Surveys

16. SECURITY CLASSIFICATION OF:			17. LIMITATION OF ABSTRACT:	18. NUMBER OF PAGES	19a. NAME OF RESPONSIBLE PERSON (Monitor)
a. REPORT	b. ABSTRACT	c. THIS PAGE			Arvind Nagar
Unclassified	Unclassified	Unclassified	SAR	144	19b. TELEPHONE NUMBER *(Include Area Code)* (937) 904-6777

Table of Contents

List of Figures

List of Tables

Foreword

A widespread fatigue damage evaluation program was initiated jointly by FAA, AFRL and Boeing to develop a procedure for predicting the residual strength of an aircraft structure and to better understand the multiple site damage initiation and small crack behavior. The small crack growth experimental study was one of the many tasks in the WFD program.

Federal Aviation Administration (FAA/AAR) sponsored the small cracks experimental program. Boeing-Long Beach developed the initial experimental plans and supplied the test specimens. Air Force Research Laboratory (AFRL/VASM) fabricated the test specimen assemblies; cold worked the required holes, developed the experimental strains and small fatigue crack growth data and conducted failure analysis of failed specimens. SelecTech and AdTech provided support for this AFRL in-house effort.

The small crack effects on crack growth predictions based on established practices have been known for a long time. With the advancements in crack measurement technologies, it is now possible to determine smaller crack lengths. The small crack behavior of cracks at loaded holes under loads with variable amplitudes was the objective of this work. This report documents the findings of this study.

Acknowledgements

The testing task of this work was sponsored by the Federal Aviation Administration (FAA-TC) under a wide spread fatigue damage program. Boeing West (J. Lo) provided the specimens and preliminary experimental plans. Tests were conducted by SelecTech Services (S. Coghlan). The SEM analysis was performed by AFRL/VASM (B. Smyers) and AdTech Systems (S. Soni) provided computer support and documentation of results.

1. Introduction

This report describes the results of an experimental study to verify analytical methods for small fatigue crack growth prediction in pin-loaded holes under varying load transfer. The study was conducted under a joint Federal Aviation Administration, Air Force Research Laboratory and Boeing cooperative program. The experiments were conducted in house using AFRL/VASM Fatigue and Fracture Laboratory test facilities. FAA sponsored the study under a MIPR DTFA03-96-C-0027 WFD Evaluation Program.

The primary objective was to study small fatigue crack growth behavior at pin-loaded holes in structural joints where small cracks are often observed. Experiments were conducted on 2024-T3 joint specimens with an initial .003 inch radial thru crack. The cracks were grown from a notch at the smaller hole. The hole was enlarged to machine out the notch and leaving a small crack at the hole. The test specimens with three different types of doublers of varying stiffness were joined by pins through two holes to provide a variation in the magnitude of load transfer rates at the cracked hole. The other hole without a crack was cold worked to prevent any crack initiation or crack growth. Static loads were applied for strain surveys and three types of cyclic loads to develop crack growth data. The cyclic loads with constant amplitude, cyclic load with variation in maximum stress and EIFS spectrum loads of variable maximum stresses and variable load amplitudes.

A comparison of structural joint small crack growth data with FASTRAN predictions shows that FASTRAN predicts small crack behavior under constant amplitude loading reasonably well. However, the plasticity induced closure based predictions by FASTRAN do not correlate with the small crack growth data under periodic over loads (marker bands) as good. The predictions of small crack life under spectrum loads (EIFS) were even farther off. In general, the crack growth rates are lower than predicted. Thus there is a question whether FASTRAN can be employed reliably to predict small crack growth in joints with loading histories.

The experimental strain data developed during this program also indicated that the load transfer rates for steel doublers can not be predicted using the same technique as used in NASTRAN which have been used for calculations of fastener load transfer with aluminum doublers. Due to the large amount of test data developed during this program, the raw strain measurements and raw crack growth data is presented in the Appendices.

Overall, this experimental program provided major challenges in the areas of precise small crack measurements at machined holes, precise machining of parts and holes for pinhole interference fit. The test results were further affected as the tests progressed and damage and wear of mating surfaces occurred during cycling and disassembly of components.

2. Background

Damage tolerant structural design requires that a pre-existing, initial crack at a critical location in a structural detail must not reach the critical size required to maintain the minimum load bearing capability during its design life. The design life of a damage tolerant structure i.e. the number of flights required to grow an initial crack to a critical size, is calculated from the crack growth relations. For safety of flight, it is assumed that cracks initially exist at fatigue critical locations in primary structures. For structures with close tolerance fasteners, the initial primary damage size is .05 inch. A crack size of .005 inch for continuing damage at the holes is recommended. These assumptions for initial crack lengths are based on NDI capability of the designer. With improved NDI techniques, cracks smaller than .05 can be detected. The small crack growth behavior discussed here provides guidelines for crack growth analysis if an initial crack smaller than .05 is assumed in the damage tolerant design of structural members [1,5].

The design guidelines and linear elastic fracture mechanics based life prediction methods are applicable to long crack only. From mechanics considerations, the development of crack occurs in three distinct stages: crack initiation, small crack development and long crack progression. The subject of crack initiation and nucleation is outside the scope of this study. A long crack has a dominant singularity in the continuum domain. A crack is considered small when it is smaller than the long crack for a small crack, the similitude rules break down. The crack size is comparable to one or few grains, the plastic zone size is not small compared to the size of the crack and the assumption of a linearly elastic material at the crack tip region is not realistic. A discussion of similitude rules is presented by Leis et.al [2].

It has been experimentally observed that small crack growth behavior is different from the behavior of long cracks. The small crack effects have been observed in both notched and un-notched specimens. The un-notched small crack growth behavior has been attributed to crack grain boundary interaction effects not accounted for in the fracture mechanics based predictions of small crack growth. In the case of long cracks, the crack growth in the plastic wake is averaged over many grains. It has been argued by Leis et. al. [2] and Blom et al. [3] that the difference in crack growth at notches is not due to the breakdown of similitude rules but inaccurate calculations of the stress intensity factors .

Based on observations of small crack growth in 2024-T3, Blom reported that the short crack effects are due to plasticity induced crack closure and roughness induced closure effects. He also concluded that in this material a crack should be al least four grains in length before qualifying as a long crack. In Newman's study of small cracks in 2024-T3 and 7075-T6 specimens, the crack closure transients have been found to be the cause of crack growth effects [4]. There is transient behavior of crack opening stress as the crack progresses from small crack size to long crack. At higher stress ratios (stress ratios over .5), the crack may be assumed to be open and thus has no significant effect on crack opening stress. At higher negative stress ratios (i.e. at R=-2), the effects have been found to be more significant. A fatigue crack growth analysis computer code "FASTRAN"

based on plasticity-induced closure has been developed and currently available at NASA Computer Management and Software Information Center.

The upper limit of the crack size below which the small crack effects start and the conventional long crack growth behavior resumes is not well established. The crack lengths from .040 in. to .070 in. have been proposed. The following observations of small crack behavior from experimental data have been reported in the literature. It has been demonstrated from the crack growth data under both the constant amplitude loads and the spectrum loads that the small crack growth rates are higher than those for long cracks. Higher crack growth rates result in non-conservative predictions of fatigue life. A small crack can grow even when the applied stress intensity factor is well below the threshold limit. The threshold stress intensity factor range is dependent on the stress ratio. The experimental results show that the small crack effects are more pronounced at extreme values of stress ratios. The behavior of small cracks initiated at holes is different from the behavior of small cracks in un-notched materials.

Because of these differences, an understanding of the mechanics of small crack growth and mechanisms of cracking in the small crack regime is necessary. The structural designer should have the appropriate design tools to incorporate the effects a small crack may have on crack growth rate and resulting life prediction. The small crack effects are present either because the similitude rule for LEFM application to crack growth breaks down or inappropriate evaluation of the damage parameters such as the stress intensity factor "K" or the "J" integral used for steady state crack growth rate prediction. The similitude rules are a set of requirements on structural crack geometry and the mode and extent of crack-tip deformation of a material under loading.

The results presented in this report extend the understanding and behavior of small cracks in conventional material specimens to cracks emanating from holes in structural joints. The small fatigue crack at the central hole in rectangular panel is developed under cyclic loads. The rectangular panel is then joined with doublers to form a pin fastened structural joint. The crack propagation behavior of the fatigue crack at the pin-loaded hole is studied under variable load transfer rates. The results have been previously summarized [1 and 5] by the author. The experimental results in detail are presented in this report.

3. Experimental Procedure

3.1. Test Specimen Description

The nominal dimensions of the test specimens were 18 x 3 x .063 machined from 2024-T3 aluminum bare sheet (QQ-A-250/4 Temp T3). Each specimen had a .063 diameter hole and a .010 long saw cut notch normal to the longitudinal direction of the specimen and along the width of the specimen.

The test specimens were pre-cracked until the total length of the notch and the crack reached .065 in. The hole was then enlarged to a size (nominal .187 in.) so that a .003 inch long crack remains at the enlarged hole. The preliminary test plan for pre-cracking was revised due to the load interaction effects on crack growth. Another load stage was added to avoid crack growth retardation effects. The stress ratio was also changed to 0.1 so that the specimen is not subjected to near zero loads during unloading. The pre-cracking was performed in three stages to grow the .01-inch notch to approximately .096 inch from the center of the hole as shown in Table 1. Once the desired length was reached at approximately 100, 000 cycle, the specimens were finish machined to the test specimen configuration. This included enlargement of the cracked hole and final reaming to leave a .003-inch sharp crack.

Table 3.1.1 Pre-cracking Loads (Frequency 10 Hertz)

Stage	Max. Stress (Ksi)	Stress ratio	Initial size	Final size (in.)
I. Crack information	24.6	.1	.010	.025
II. Crack Sharpening	19.0	.1	.025	.035
III. Crack Finishing	14.3	.1	.035	.065

The diameters of 30 titanium pins were measured with in .0001 inch and based on the size of the pin; the hole size was selected for a pin/hole tolerance of plus .0000 and minus .0005 inch. The hole size was also to be selected from the measured crack size at the end of pre-cracking so that the drilled hole leaves a .003-inch crack at the hole. It was decided that hole-pin fit was more important than the variation in the initial size of the crack. The initial crack size was therefore measured after the drilling and cold working. The pre-cracked specimens, calibration base plates and doublers were then stack drilled with two holes of sizes as determined above 2.56 inches from the centerline of the specimen. The hole, which did not have the crack, was cold worked with the FTI tool number 6-0-N and the procedure established in coordination with FTI.

Starting Hole Diameter	.180 max/. 177 min
Mandrel Minor Diameter	.1610
Mandrel Major Diameter	.1740 nom. / .1734 min
Sleeve thickness	.0060

Max allowable finished hole diameter with this procedure is .2130

The test specimen assembly consisted of a pair of doublers, 6 in. by 2 in. of different materials and thickness. There were three groups of doublers. Group I was .063 thick al, group II had .125 thick al and group III was -.063-inch thick steel. The test specimens and doublers were assembled for zero clearance using assorted aluminum shims. Each specimen-doubler assembly was joined by two pre-designated Ti 6-4 pins passing through the holes in the doublers and the specimen as shown in Figure 1. The pins were locked in place by means of cotter pins on the side of the shims. A strain gage was installed at the center of each doubler as shown in Figure 2. Thus the strains were measured at the center of the doublers as shown in the side view of Figure 1 of test specimen assembly.

In addition to test specimen assemblies, strain calibration assemblies were fabricated for each doubler group. The calibration assembly used the same joining components as the test specimen assembly except that its two halves, each 9 inches long and 3 inches wide replaced the 18 in. by 3 in. test specimen. The calibration assemblies were used to measure strains under hundred percent load transfer.

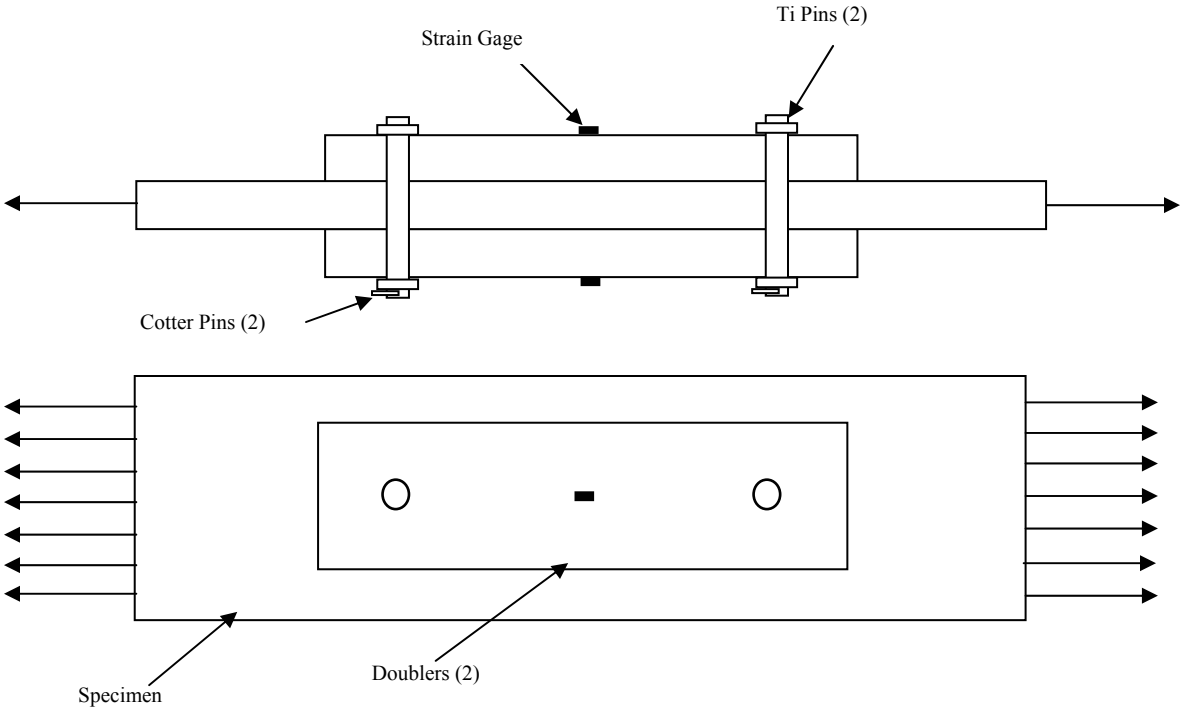

Figure 3.1.1: Test Specimen Assembly – Small Crack Growth Test

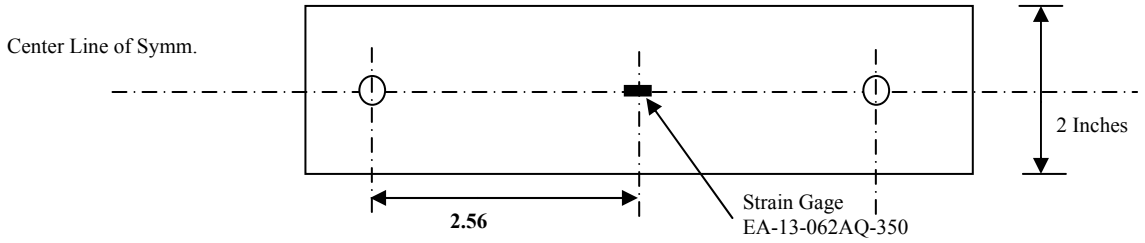

Figure 3.1.2: Doublers Used in Small Crack Growth Test (Thicknesses. 0.0625 Al, 0.125 Al and 0.0625 Steel)

3.2. Test loads

Four types of loads were applied in the small crack growth study:

1. Static loads for strain surveys
2. Constant amplitude loads
3. Constant amplitude loads with variable maximum stress (marker bands)
4. EIFS spectrum loads

The following tables show the applied loads as revised.

3.2.1. Static Loads – Strain Surveys

The specimens with matching doublers, holes and pins were assembled as marked. Assorted shims and washers were used for zero clearance. The strain readings were zeroed in only before the calibration surveys for each specimen. After that just the readings are taken for each specimen. MATE computer program was used for the strain measurements. The crack growth was measured first and then the strain reading at each inspection. The strain survey load (Ksi) for different specimen assemblies are listed in Table 3.2.1.

Table 3.2.1 Static Loads for Strain Surveys

	Specimen	Min. Load	Max. Load
Calibration Assy.	SCG 1-15	0	3.3
		0	4.5
Test Specimen Assy.	SCG 1-5	0	6
		0	12
	SCG 6-10	0	6
		0	10
	SCG 10-15	0	6
		0	8

3.2.2. Constant Amplitude Cyclic Loads:

All cyclic loads were applied at a frequency of 10 hz and a stress ratio of 0.1. The max. loads for open hole specimens were 15.8 ksi unless indicated other wise.

3.2.3 Marker Band load Tests

A typical marker band cyclic test loads sequence is shown in Table 3.2.3 for15 ksi peak stress. For other peak stresses, the maximum and min. load values were scaled down or up by the same factor. The stress ratio of .10 was maintained.

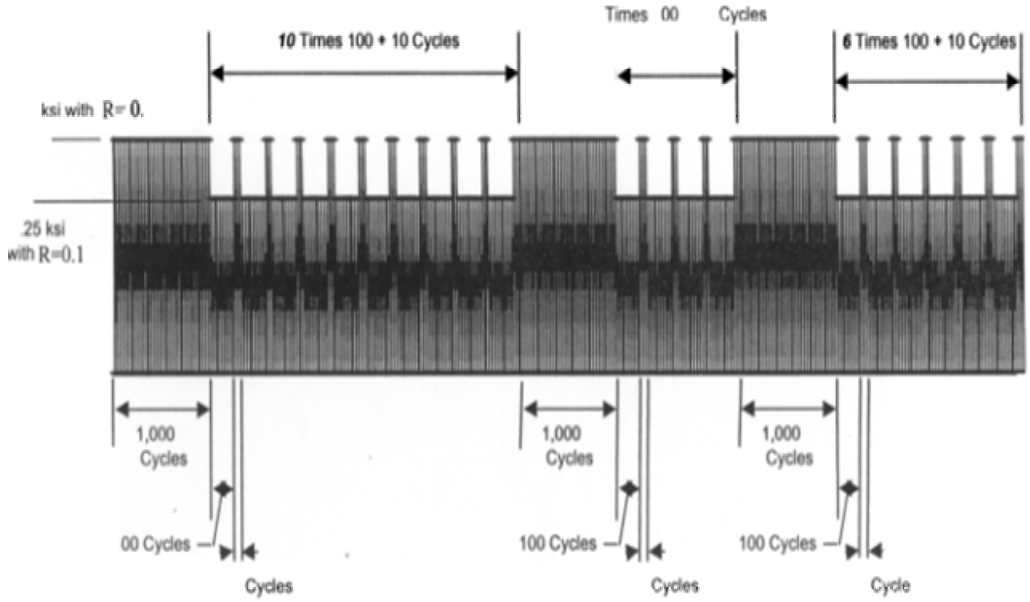

Figure 3.2.3: Marker Cyclic load for an average flight

Table 3.2.3 Marker Band Cyclic Test Loads

Load (Ksi)			Cycles	Remarks
Minimum	Maximum	Frequency		
1.5	15	10	1000	(a),(b)
1.125	11.25	10	100	
1.5	15	10	10	
1.125	11.25	10	100	
1.5	15	10	10	
1.125	11.25	10	100	
1.5	15	10	10	
1.125	11.25	10	100	
1.5	15	10	10	
1.125	11.25	10	100	
1.5	15	10	10	
1.125	11.25	10	100	
1.5	15	10	10	
1.125	11.25	10	100	
1.5	15	10	10	
1.125	11.25	10	100	
1.5	15	10	10	
1.125	11.25	10	100	
1.5	15	10	10	
1.125	11.25	10	100	
1.5	15	10	1010	
1.125	11.25	10	100	
1.5	15	10	10	
1.125	11.25	10	100	
1.5	15	10	10	
1.125	11.25	10	100	
1.5	15	10	10	
1.125	11.25	10	100	
1.5	15	10	1010	
1.125	11.25	10	100	
1.5	15	10	10	
1.125	11.25	10	100	
1.5	15	10	10	
1.125	11.25	10	100	
1.5	15	10	10	
1.125	11.25	10	100	
1.5	15	10	10	
1.125	11.25	10	100	
1.5	15	10	10	
1.125	11.25	10	100	
1.5	15	10	10	

(a) R = 0.1, (b) a Vs N Data

3.2.4. EIFS Spectrum Loads

EIFS spectrum loads for a 24.34-ksi-peak stress value are summarized below:

Total Cycles	8566
Average Cycles (Per Flight)	8566
Highest Peak	24.337 Ksi
Lowest Valley	0.0
Largest Range	24.337 Ksi

Table 3.2.4 lists the peak stress, valley/peak ratio and stress range distributions in more detail. The spectrum for a different peak stresses was scaled down. The number of cycles in an average flight was 8566.

3.3. Test Procedure

All the small crack growth specimens were tested on a 10 kip MTS axial servo-hydraulic load frame. The control software was called Lab MATE written by University of Dayton Research Institute for the Air Force Research Laboratory. This software provides for application of spectrum based loads such as the marker bands and random EIFS loads used for this study. The loads were applied under load control. The EIFS spectrum load rate was 20 kips per second.

3.3.1. Test Plan Revisions

The original test plan was revised due to bearing failure of first specimen during strain surveys. This was caused by a very high bearing stress developed at the holes due to pin loading. To prevent further bearing failures, the strain survey loads and the crack growth test loads were revised as given in the following Table 3.3.1.

Table 3.2.4 EIFS Spectrum Loads table

Peak Distribution Ratio			Range Distribution			Valley/Peak (V/P)		
Peak Stress Cycles		Cycles	Stress Range		Cycles	Distribution		Cycles
Below	-5	0	Below	0	0	Below	-2.0	0
-5	-4	0	0	1	0	-2.00	-1.90	0
-4	-3	0	1	2	0	-1.90	-1.80	0
-3	-2	0	2	3	0	-1.80	-1.70	0
-2	-1	0	3	4	0	-1.70	-1.60	0
-1	0	0	4	5	0	-1.60	-1.50	0
0	1	0	5	6	0	-1.50	-1.40	0
1	2	0	6	7	1736	-1.40	-1.30	0
2	3	0	7	8	172	-1.30	-1.20	0
3	4	0	8	9	414	-1.20	-1.10	0
4	5	0	9	10	31	-1.10	-1.00	0
5	6	0	10	11	127	-1.00	-0.90	0
6	7	0	11	12	9	-0.90	-0.80	0
7	8	0	12	13	41	-0.80	-0.70	0
8	9	0	13	14	5	-0.70	-0.60	0
9	10	0	14	15	18	-0.60	-0.50	0
10	11	0	15	16	2539	-0.50	-0.40	0
11	12	0	16	17	2382	-0.40	-0.30	0
12	13	0	17	18	784	-0.30	-0.20	0
13	14	1	18	19	218	-0.20	-0.10	0
14	15	355	19	20	69	-0.10	0.00	6000
15	16	2669	20	21	9	0.00	0.10	0
16	17	2882	21	22	9	0.10	0.20	4
17	18	1825	22	23	0	0.20	0.30	26
18	19	569	23	24	1	0.30	0.40	84
19	20	177	24	25	2	0.40	0.50	322
20	21	53	25	26	0	0.50	0.60	1167
21	22	24	26	27	0	0.60	0.70	963
22	23	6	27	28	0	0.70	0.80	0
23	24	4	28	29	0	0.80	0.90	0
24	25	1	29	30	0	0.90	1.00	0
25	26	0	30	31	0	1.00	1.10	0
26	27	0	31	32	0	1.10	1.20	0
27	28	0	32	33	0	1.20	1.30	0
28	29	0	33	34	0	1.30	1.40	0
29	30	0	34	35	0	1.40	1.50	0
30	31	0	35	36	0	1.50	1.60	0
31	32	0	36	37	0	1.60	1.70	0
32	33	0	37	38	0	1.70	1.80	0
33	34	0	38	39	0	1.80	1.90	0
34	35	0	39	40	0	1.90	2.00	0
Above	35	0	Above	40	0	Above	2.0	0

Table 3.3.1 Test Load Revisions

Group	Spec. No.	Load Type	Original Load Stress (Ksi)	Revised Load	
				Stress Ratio	Stress (Ksi)
I	1,2	Static	12 Max		4.5 Max
	3,4	Static	19.4 Max		4.5 Max
	3,4	EIFS	24.3 Peak		15.8 Peak (65%)
	5 Spare				
II	6,7	Static	12 Max		4.5 Max
	6,7	Marker Band	15 Peak	0.1	12.5 Peak
	8,9	Static	19.4 Max		4.5
	8,9	EIFS	24.3		13.4 Peak (55%)
	10 Spare				
III	11,12	Static	12 Max		4.5 Max
	11,12	Marker Band	15	0.1	10
	13,14	Static	19.4		4.5
	13,14	EIFS	24.3 Peak		11.0 Peak (45%)
	15 Spare				

Each group had a different type of doubler as described earlier. An application of original test loads caused excessive plastic deformation at the notch due to overloads during pre-cracking of first specimen (specimen number 1). The specimen number 3 was lost due to bearing failure. The strain measurements on specimen number 4 gave erroneous results due to switch in doublers caused by the test engineer. As tests were conducted on available specimens, it was noticed that the specimen numbering lost their original numbering sequence. To keep the intent of the original test plan and to maintain continuity of specimen numbering for each load and joint type category, the original specimen numbers were revised as shown in Table 3.3.2. The specimen numbers were changed from 1S to 4S, 4S to 1S, 14 to 11, 13 to 12, 11S to 13S, 15 to 14, 12 to 16 and from 12S to 17S.

Table 3.3.2 Specimen Number Revisions

Group	Load Type	Current Number	Previous Number
I	EIFS	4S	(1S)
I	Marker Band	1S	(4S)
II	-	No Changes	
III	Marker Band	11	(14)
III	Marker Band	12	(13)
III	EIFS	13S	(11S)
III	EIFS	14	(15)
IV	Marker Band	16	(12)
IV	Marker Band	17S	(12S)

3.3.2. Test Matrix

With the revised specimen numbers, the doubler configurations and revised test loads, the small crack growth test matrix is shown in Table 3.3.3. This includes tests on open hole specimens and additional specimens, AFRL tested to develop a crack growth rate baseline.

A total of 21 specimens were tested. Boeing West, Lon Beach, provided first 15 specimens with .063 in. diameter holes and-.010-inch notch, calibration plates, doublers and fasteners. The Air Force Research Laboratory provided other specimens including the replacements for damaged specimens. The letter "S" following the specimen numbers is used to identify the specimens, which did not belong to the original batch of material from which Boeing fabricated the 15 specimens.

Table 3.3.3 WFD Small Crack Growth Revised Test Matrix

Spec. No.	Doubler	Load Type	Stress Ratio	Peak Stress (Ksi.)	Remarks
1S	.063 Al	Marker Band	0.1	15	
2					
5					
3S	.063 Al	EIFS Spectrum	N/A	15.8	
4S					
6	.125 Al	Marker Band	0.1	12.5	
7					
8	.125 Al	EIFS Spectrum	N/A	13.4	
9					
11	.063 Steel	Marker Band	0.1	10.0	
12					
13S	.063 Steel	EIFS Spectrum	N/A	11.0	
14					
16	W/O doublers	Marker Band	0.1	15.0	(a)
17S					
18S	-	EIFS Spectrum	N/A	15.8	(a)
19S					
20S	-	Const. Amplitude	0.1	15.8	(a)
21					

(a) No load transfer in open hole specimens

3.3.3. Strain Surveys and Crack Growth:

The first test activity was the strain calibrations. The experimental strains as a function of applied load for each calibration specimen assembly was recorded during the test. The loads were applied monotonically to about 2/3rd of the maximum strain load, unloaded and then reloaded to the maximum load. The measured strains versus applied

loads were recorded during both loadings and unloading. The doublers and fasteners used in the calibration assembly were also used for the test specimen assemblies. All specimens, doublers, holes, titanium pins and cotter pins were marked for orientation, front/back and top/bottom prior to assembling the test specimens so that all parts are in their original place and orientation every time they are re-assembled at inspection intervals.

The crack growth testing and strain surveys during tests were the primary objective of this program. However, it was discovered that the existing test system lacked the capability to record the strains simultaneously with the application of cyclic loads to the specimen assembly. Test loads were applied to grow the crack from its initial small length (approx. .003 in.) to a final length of approximately 0.25 in. Minimums of 8 inspections were planned during crack growth testing of each specimen. At each inspection, the following tasks were performed:

1. Crack measurement
2. Disassemble
3. Crack measurement
4. Assemble
5. Strain Assembly

The crack length was measured with an optical microscope while the specimen is still in the grips and partially loaded. The specimen was then disassembled and placed under a Nicon microscope. The crack is observed under 1000X. The observed crack length was read up to 4 decimal places. The specimen is assembled again and placed back in test frame. The strain surveys were then conducted. The specimen was loaded and unloaded in accordance with the test plan for strain survey loads. The load versus strain data for all specimens was recorded.

After measurement of initial crack, the crack growth testing started. If crack is not visible at the start of the test, a static load of 8-ksi max was applied and while holding the load, the crack was observed again. If the crack is still not detected under load, apply constant amplitude cyclic loads, 14.3-ksi max/ 1.43-ksi min. and check the crack length after 100 cycle intervals until the initial crack is detected. The initial crack size was then recorded. Apply marker band or EIFS spectrum loads for the maximum or peak stress and record the crack size and number of cycles. Take 8 to 10 crack length readings and corresponding number of cycles. At least 4 readings to be before the crack length reaches .070 inch. When the crack became .250 inch long, the final number of cycles were recorded. At the conclusion of the test, all specimens were loaded under static load until failure of the specimen. The failure load representing the residual strength of the specimen was recorded. The final failure loads varied slightly from the average load of about 8.5 Kips.

3.3.4. SEM Analysis:

The SEM analysis of failed specimens was conducted. The objective of this task was to correlate and verify small crack growth test data with SEM observations and to develop crack shapes during propagation. The fractographic features at various locations on fracture surfaces were examined. The following SEM procedure was followed:

a. Machine failed specimens to size suitable for SEM observations. Mark specimen with assigned numbers and store in environmental chamber.

b. Protect fracture surfaces from degradation due to environment, handling and other effects during SEM examinations.

c. Get an overview photograph of fracture surface of each specimen.

d. Photomicrographs of fracture surfaces of selected specimens with visible features, marker band load marks (approx. 10) at various locations on the surface.

   Total: approx. 100

e. Determine initial crack size for each specimen. Measure marker band lengths.

f. Establish reference point for both the data crack and the SEM crack and correlate and compare the crack growth for each specimen versus the number of applied load cycles.

g. Record crack growth vs. load cycles data for each specimen.

h. Pictorially document crack shapes.

4. Results

4.1. Strain Surveys

The strain survey data on calibration assemblies, and initial strains (zero cycles), strains measured near 50, 000 cycles on test specimens are presented in the following figures. A list of specimen numbers and the associated strain plots discussed here is presented in table 4.1. For specimens SCG-8 and 9 the cracks grew very slowly and the strain readings were taken after a large number of cycles (well above 50K). The strains data on the doublers for calibration sheets (full load transfer) was available only up to 4.5 ksi of applied load due to the high bearing stresses developed at the hole in the calibration specimens at increasing stresses. For other test specimen assemblies, the strains were measured for higher applied stresses up to 12.64 ksi anticipating reduced load transfer rates. At these stress levels (well below the yield strength), the deviation from linearity of load versus strain relations as shown in the plots for specimens (1,6,9,11) was not expected. The strain data also indicate that as the number of cycles increased, the strains tend to decrease slightly indicating a reduction in the load transfer rates. This may be due to the fastener and hole gap variations in the joint as higher number of fatigue cycles.

The strain data on calibration assemblies is very good The measured strain data for calibration specimens show a near 100 percent agreement with analytic calculations for all three types of doubler joints i.e.

$$S= P/2AE \quad (1)$$

Where S is the measured strain, P is the applied load, A is the cross section of the doubler and E is the elastic modulus of the doubler material. The agreement in analytic/measured strains show that the strain gage was placed far enough from the pin load concentrated at the doubler hole.

However when the test specimen is assembled with the doublers, the strain data is good only for the aluminum doublers specifically the thin .063 in. doublers which have the same thickness as the thickness of the specimens. The data obtained for the steel doublers show marked variations in strains measured at the front and back of the specimens (11,12). For some specimens, the strains were even compressive as the load was applied and gradually increased becoming positive strains as the load increased. The complete data on strains for all the specimens during each inspection and at various test cycles is presented in Appendix –A. The front to back strain variations is due to misalignment of holes, increase in pinhole clearance with load cycling and wearing of hole and pin surfaces. Also, the cyclic life of a strain gage is about 1 million tensile-tensile cycles so any data taken above these cycles may not be reliable.

Table 4.1: Strain Data Summary

Spec. No.	Calibration	Test Load Cycles
1S	1	2 (0,51.8K)
2	1	2 (0,38K)
5	1	2 (0,52.5K)
6	1	2 (0,52.2K)
7	1	2 (0,45.3K)
8	1	2 (0,325K)
9	1	2 (0,1.1K)
11	1	2 (0,50K)
12	1	1 (0)

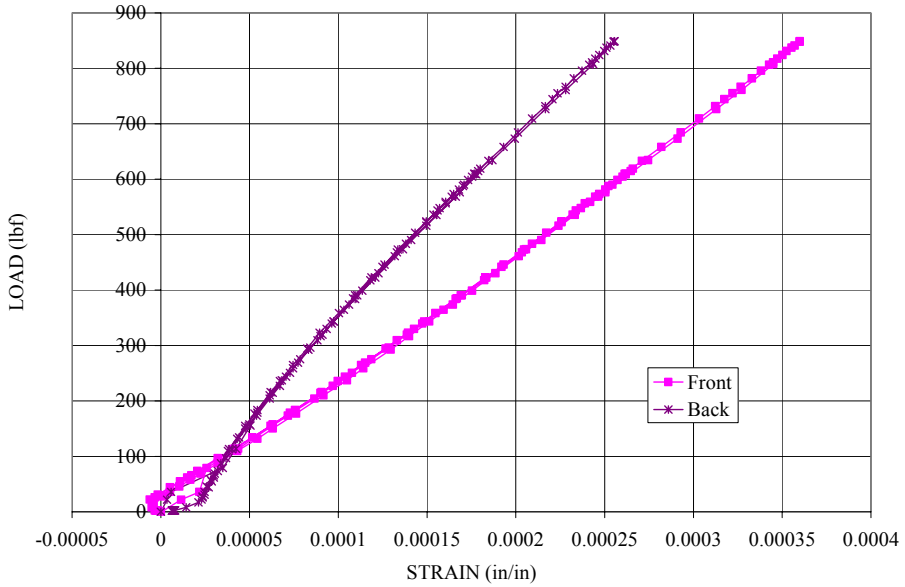

Figure 4.1.1:Load vs. Strain Data for SCG-1S; Calibration

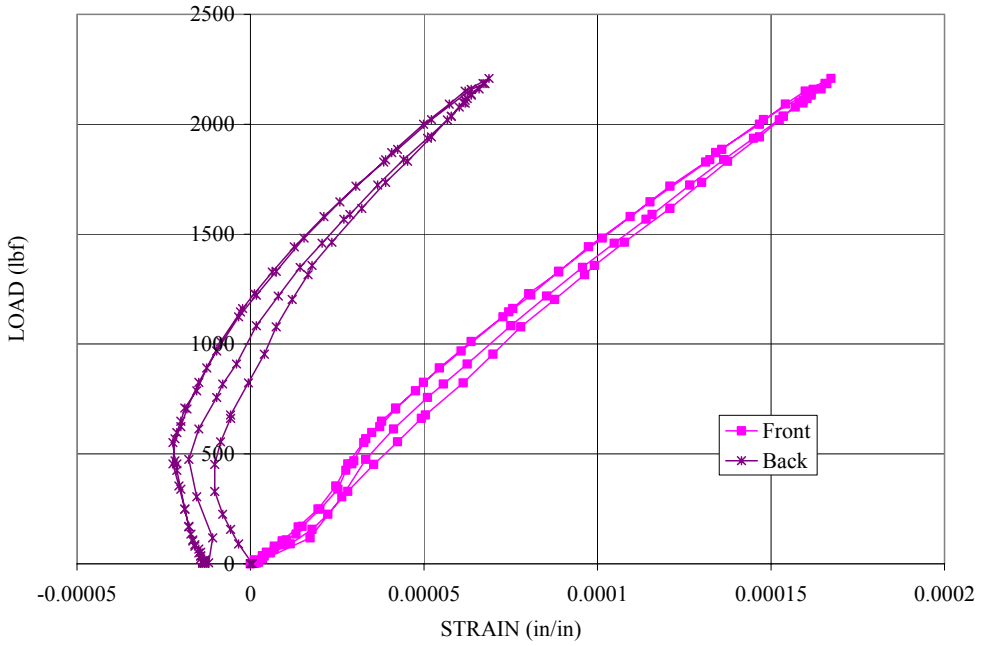

Figure 4.1.2: Load vs. Strain Data for SCG-1S; 0 cycles

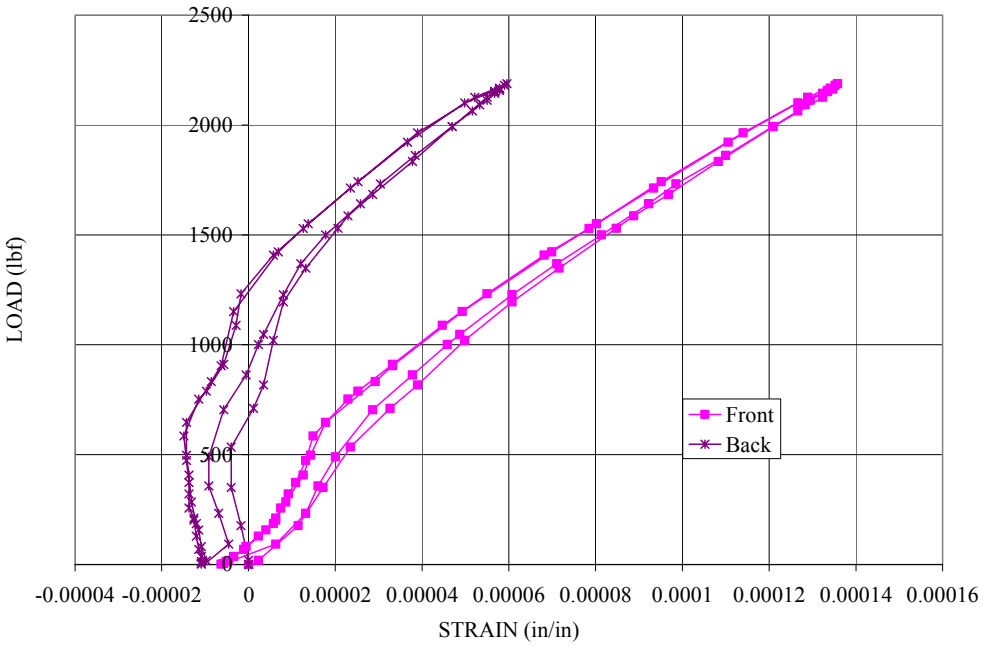

Figure 4.1.3: Load vs. Strain Data for SCG-1S; 51.8k cycles

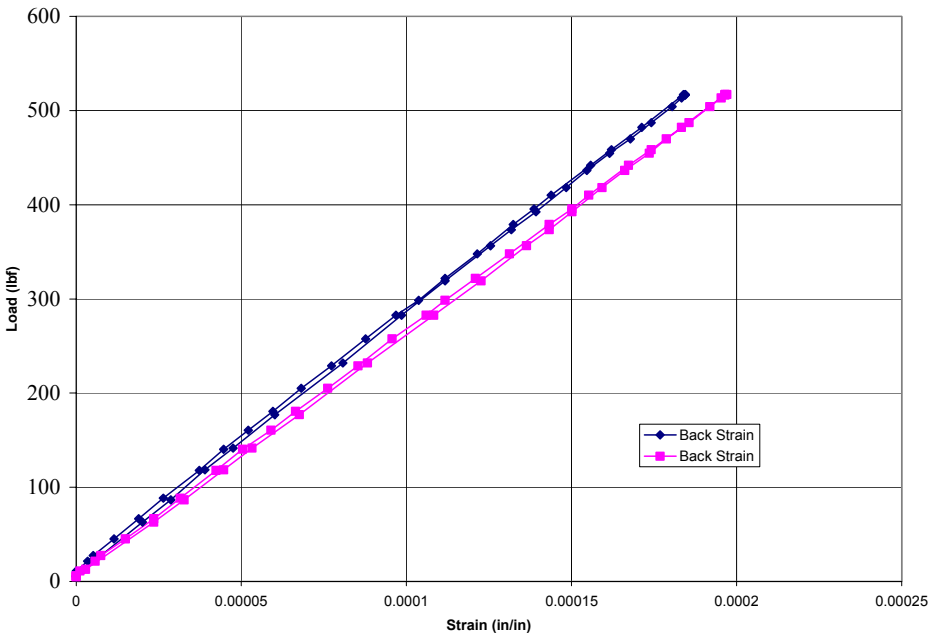

Figure 4.1.4: Load vs. Strain Data for SCG-2; Calibration

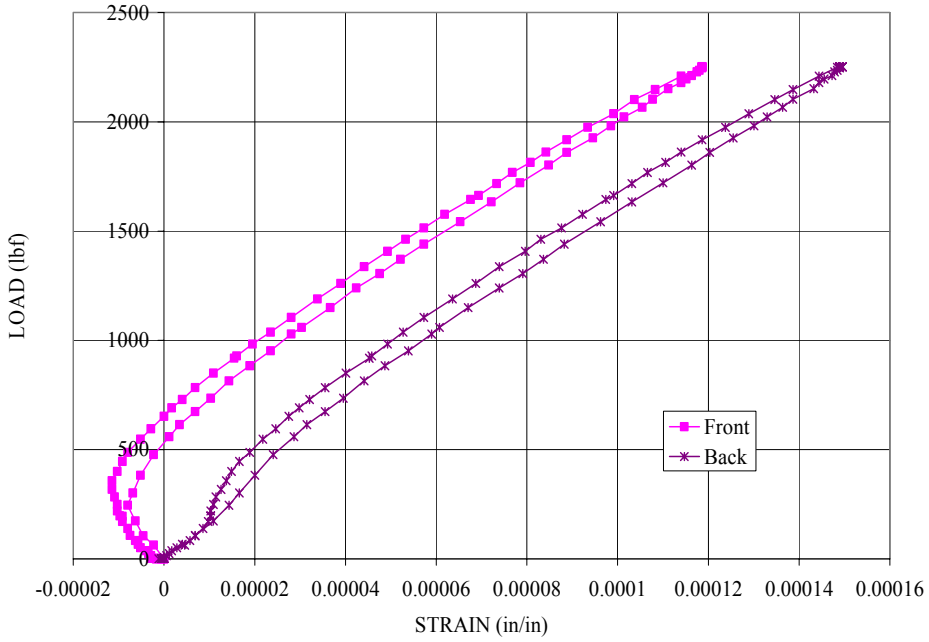

Figure 4.1.5: Load vs. Strain Data for SCG-2; 0 cycles

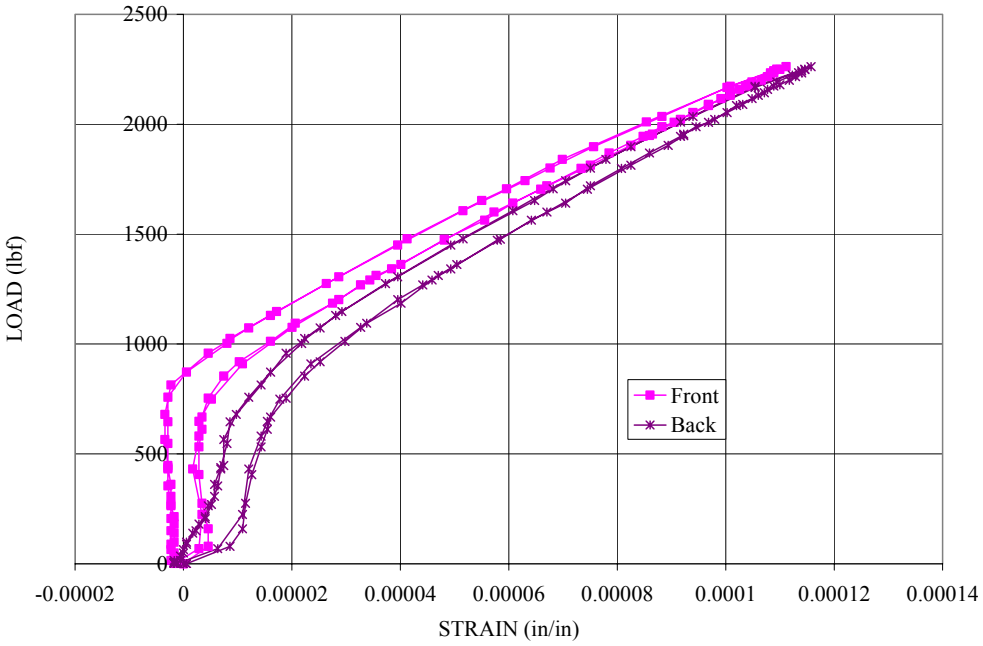

Figure 4.1.6: Load vs. Strain Data for SCG-2; 38K cycles

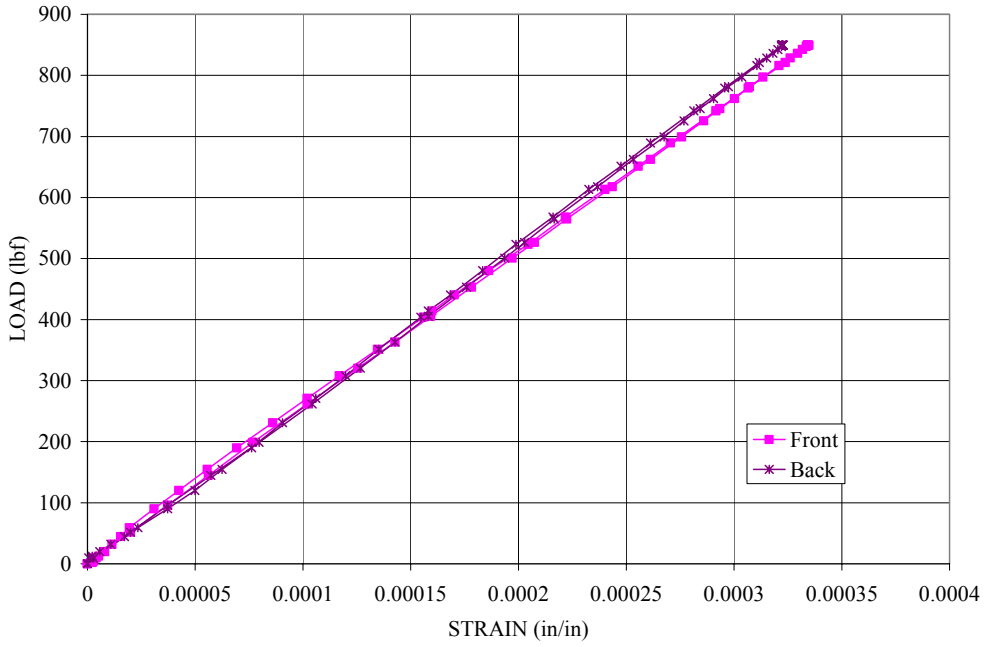

Figure 4.1.7: Load vs. Strain Data for SCG-5; Calibration

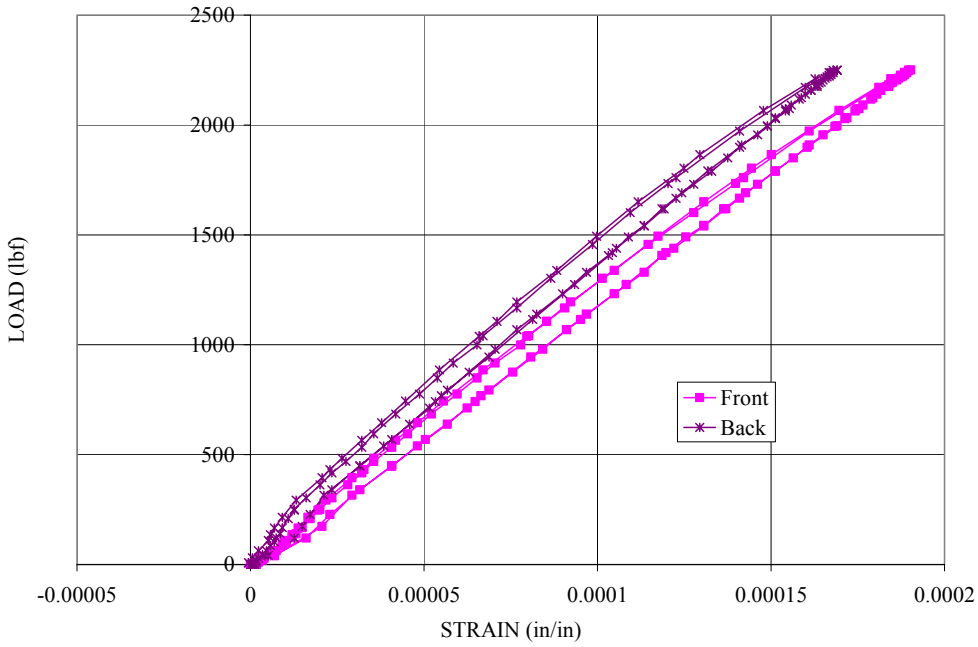

Figure 4.1.8: Load vs. Strain Data for SCG-5; 0 Cycles

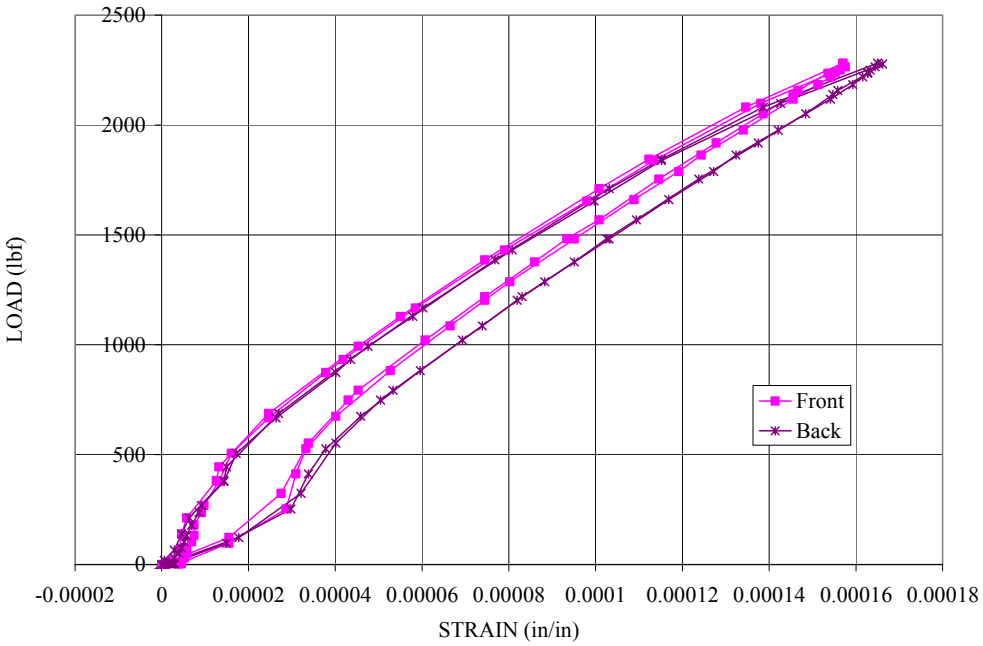

Figure 4.1.9: Load vs. Strain Data for SCG-5; 52.5K Cycles

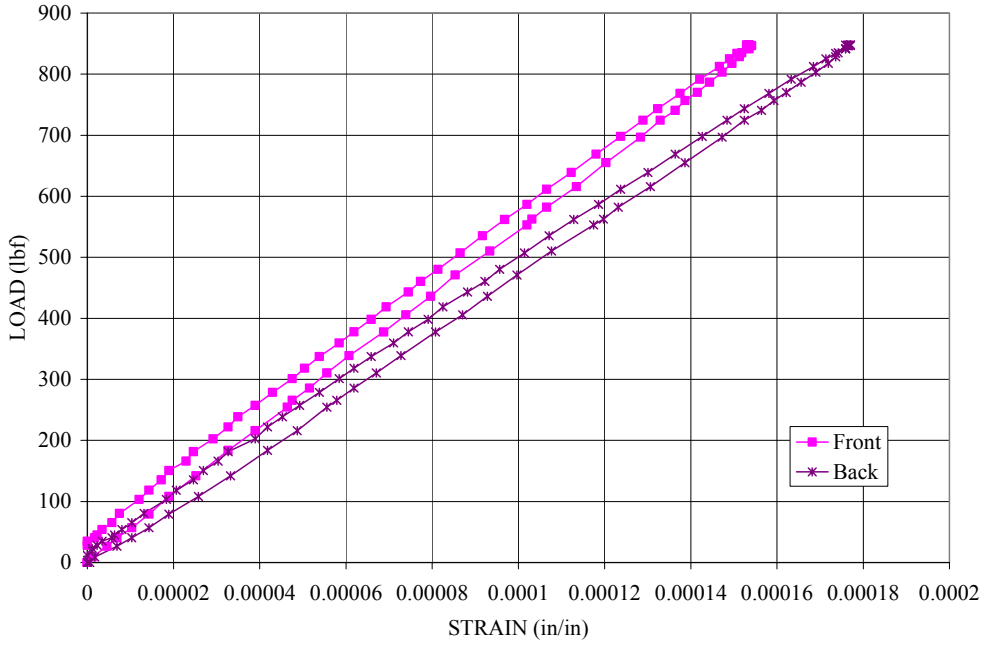

Figure 4.1.10: Load vs. Strain Data for SCG-6; Calibration

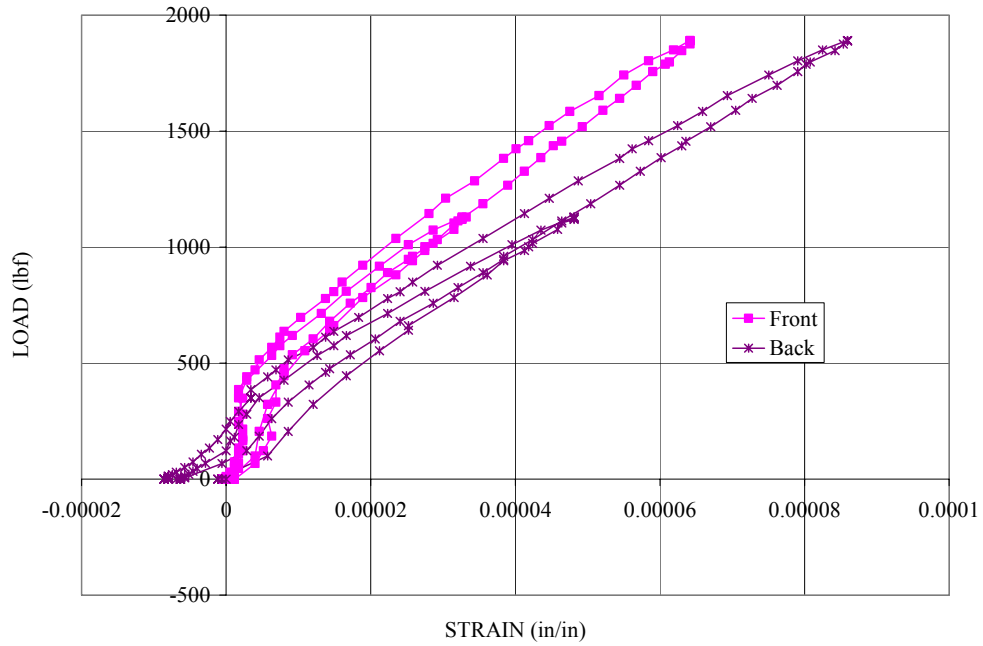

Figure 4.1.11: Load vs. Strain Data for SCG-6; 0 cycles

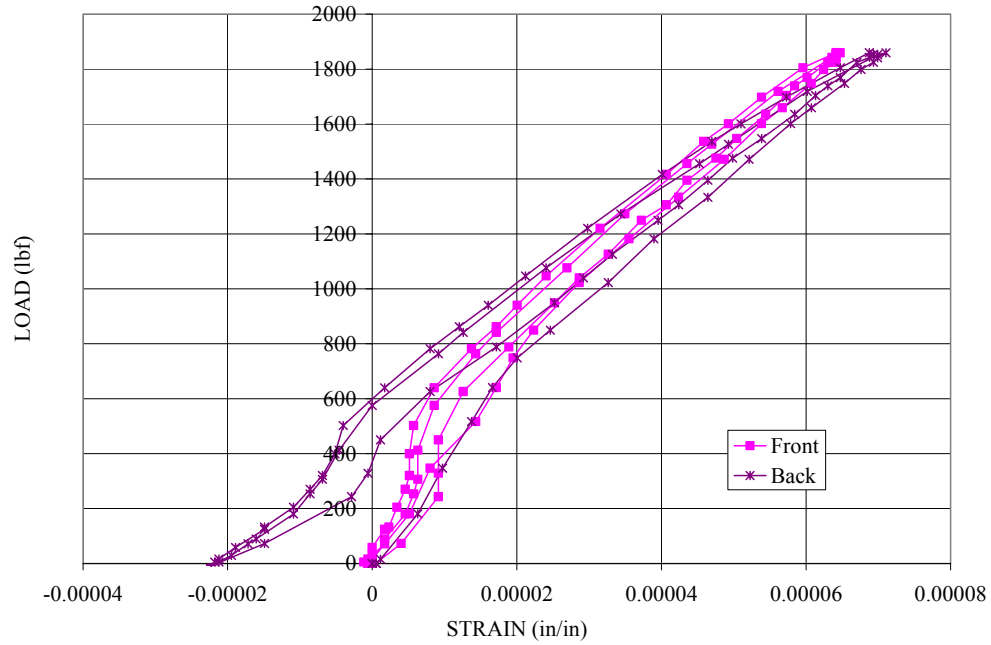

Figure 4.1.12: Load vs. Strain Data for SCG-6; 52.2K Cycles

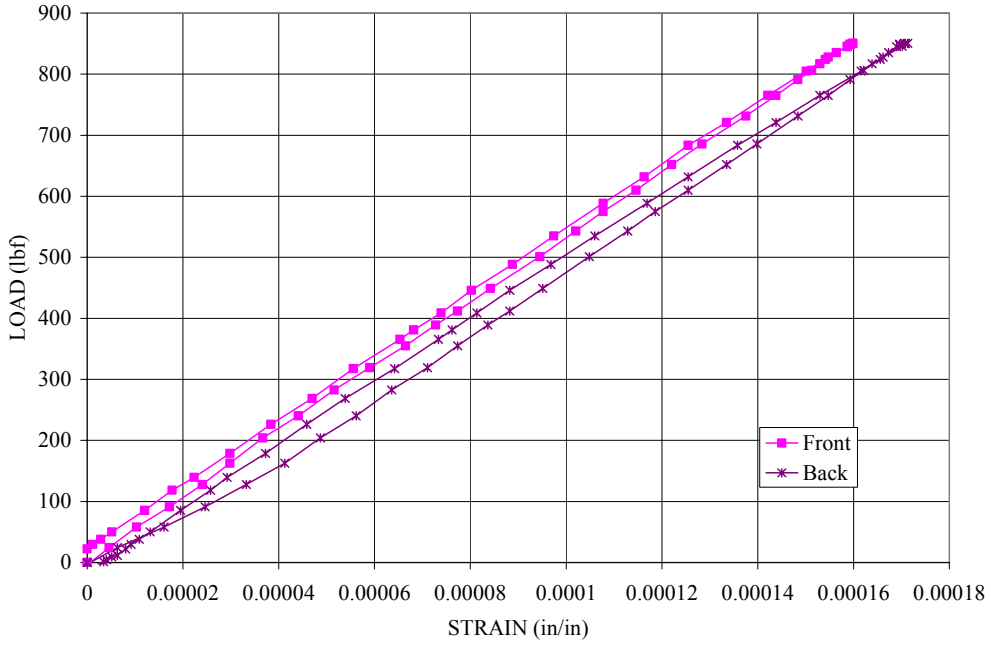

Figure 4.1.13: Load vs. Strain Data for SCG-7; Calibration

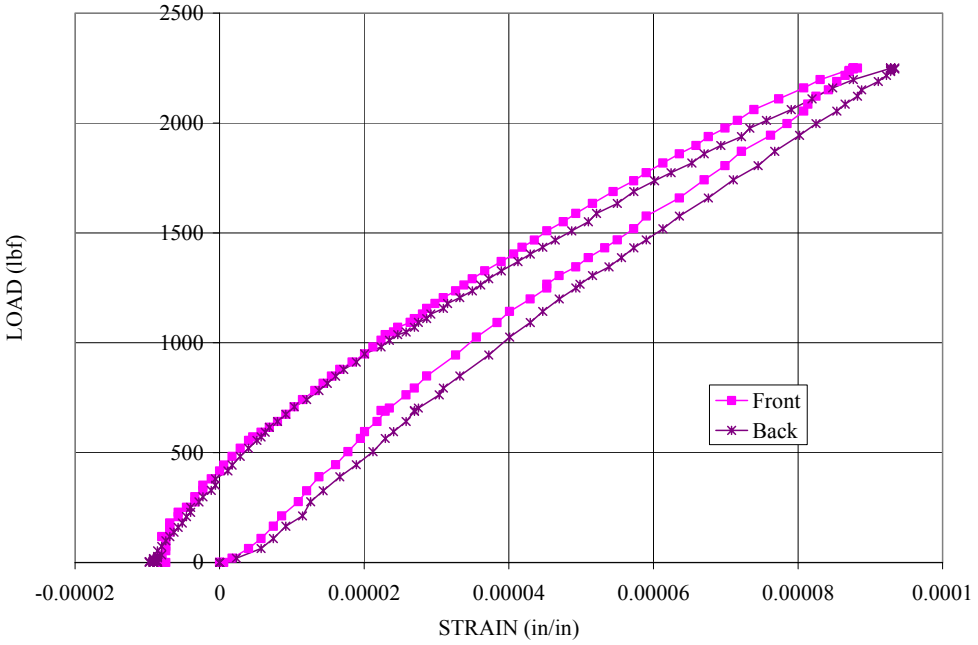

Figure 4.1.14: Load vs. Strain Data for SCG-7; 0 Cycles

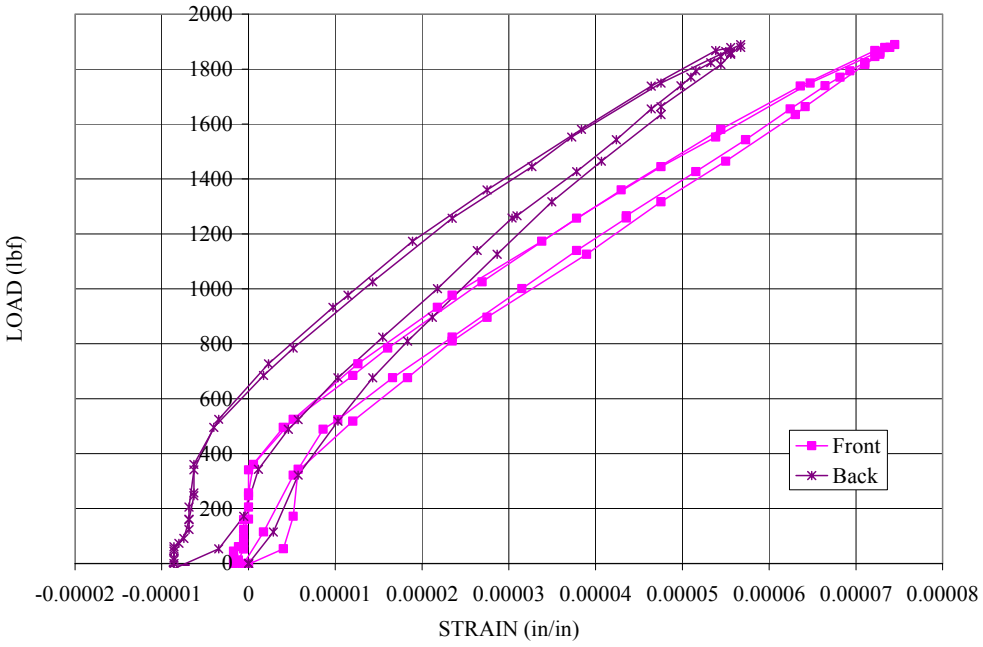

Figure 4.1.15: Load vs. Strain Data for SCG-7; 45.3K Cycles

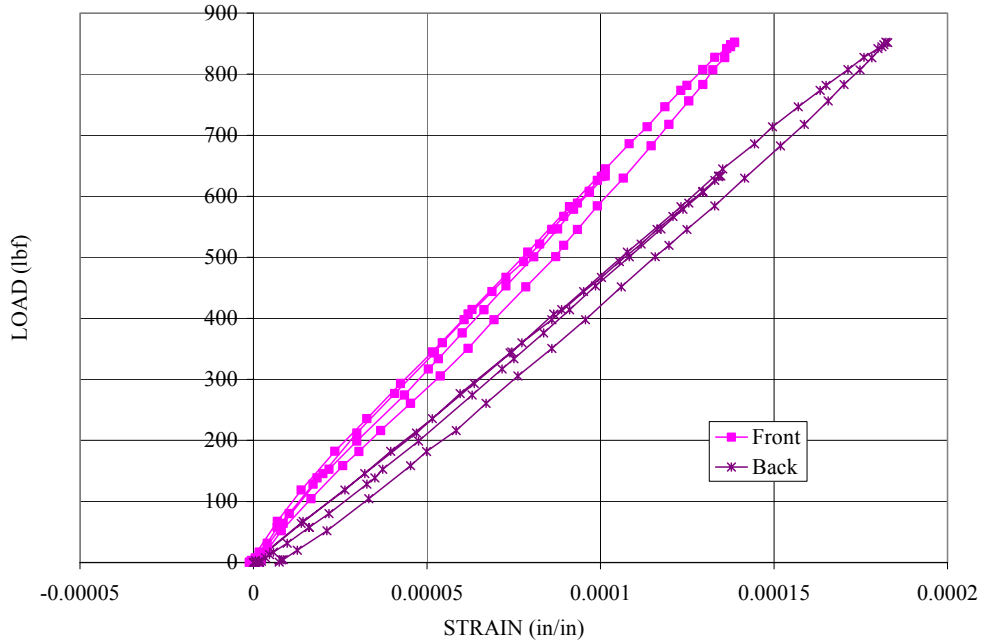

Figure 4.1.16: Load vs. Strain Data for SCG-8; Calibration

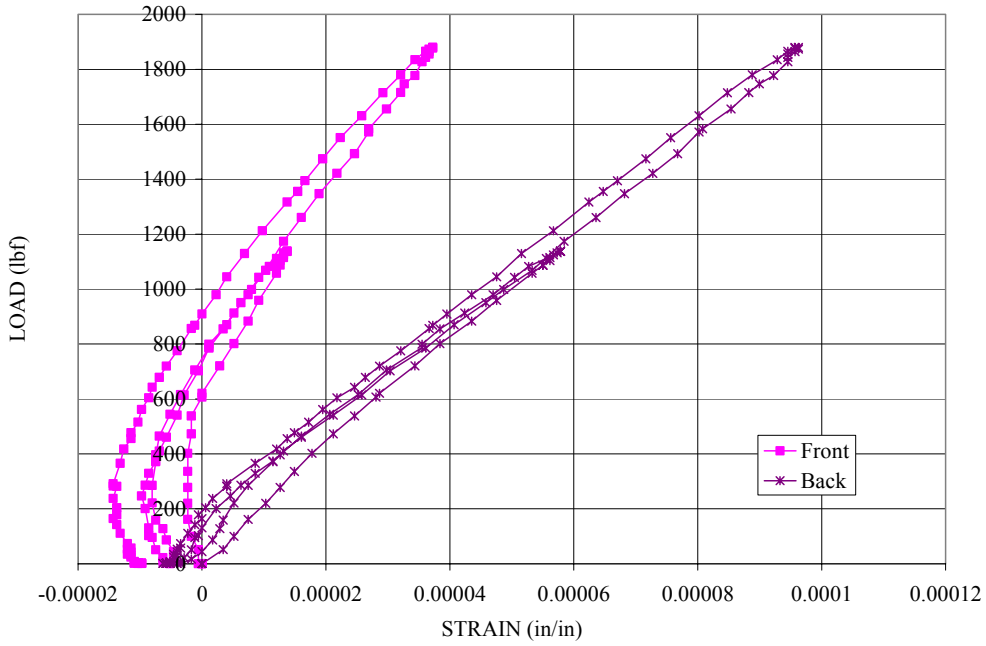

Figure 4.1.17: Load vs. Strain Data for SCG-8; 0 Cycles

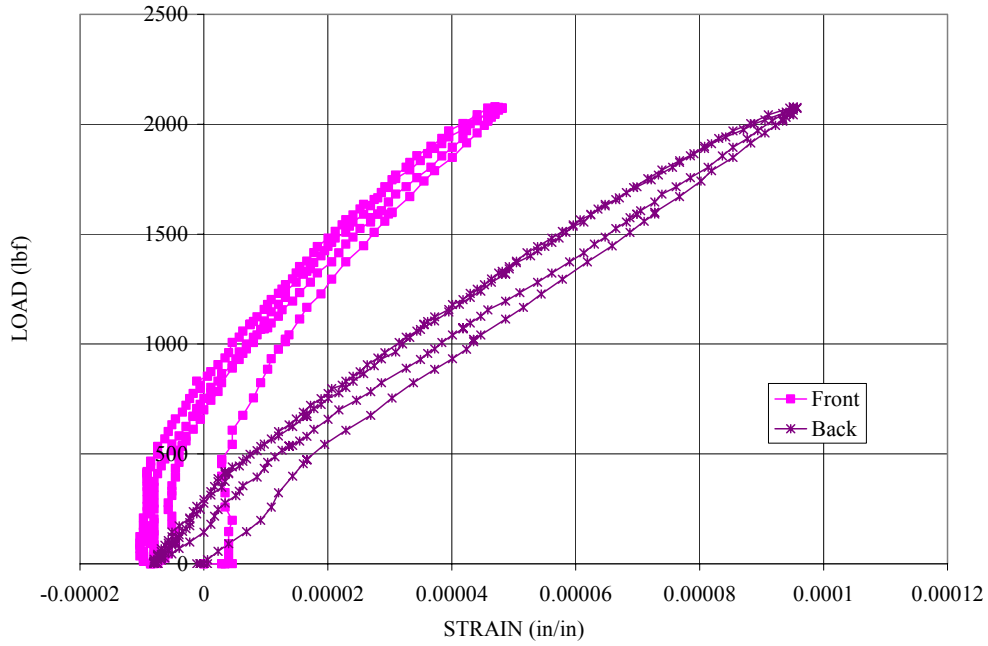

Figure 4.1.18: Load vs. Strain Data for SCG-8; 325K Cycles

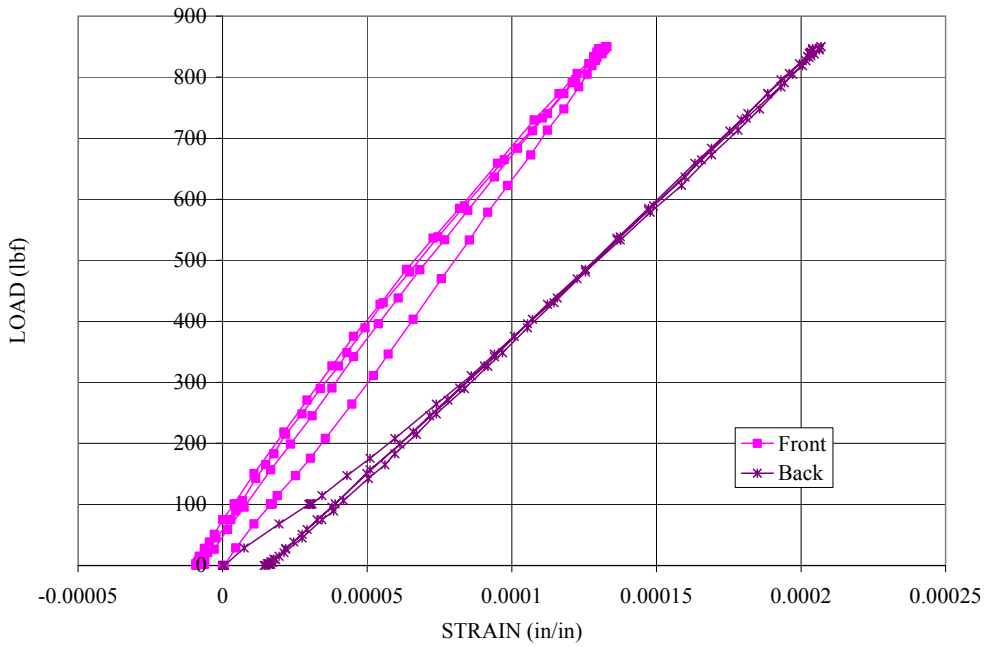

Figure 4.1.19: Load vs. Strain Data for SCG-9; Calibration

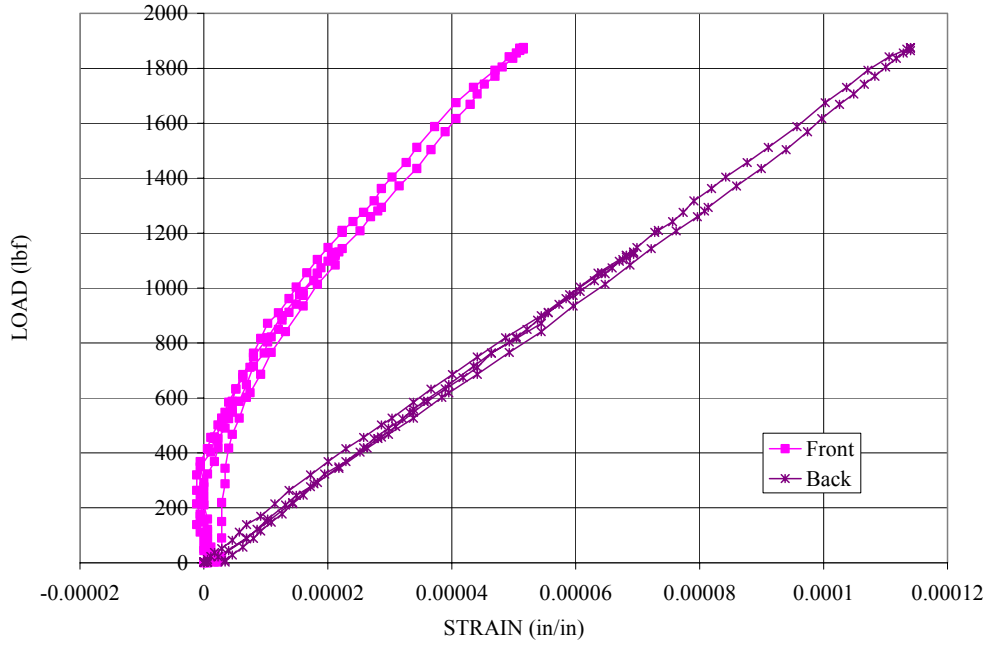

Figure 4.1.20: Load vs. Strain Data for SCG-9; 0 Cycles

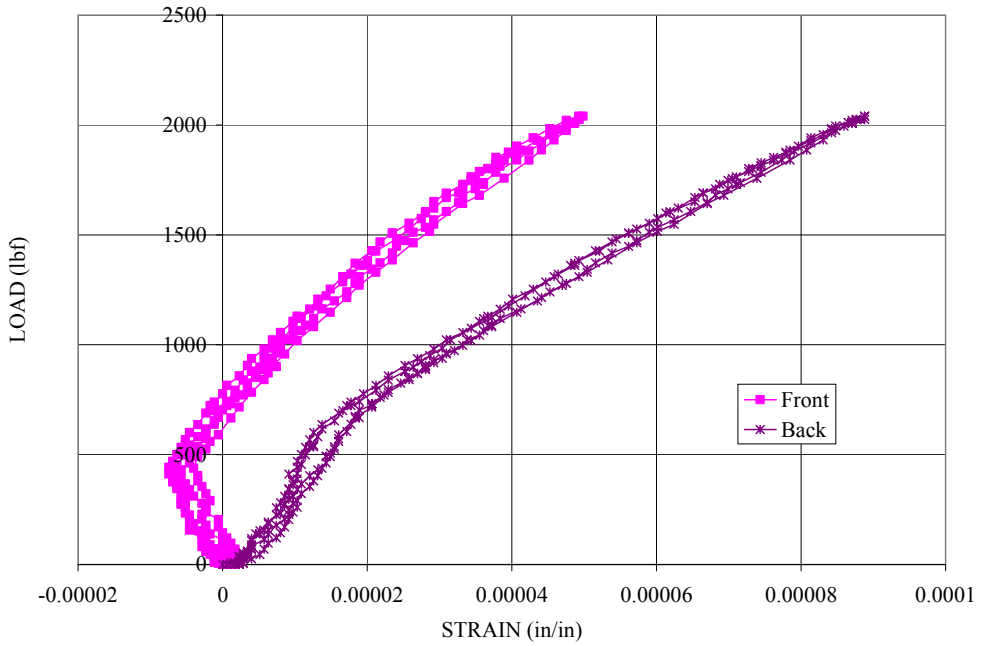

Figure 4.1.21: Load vs. Strain Data for SCG-9; 1.1M Cycles

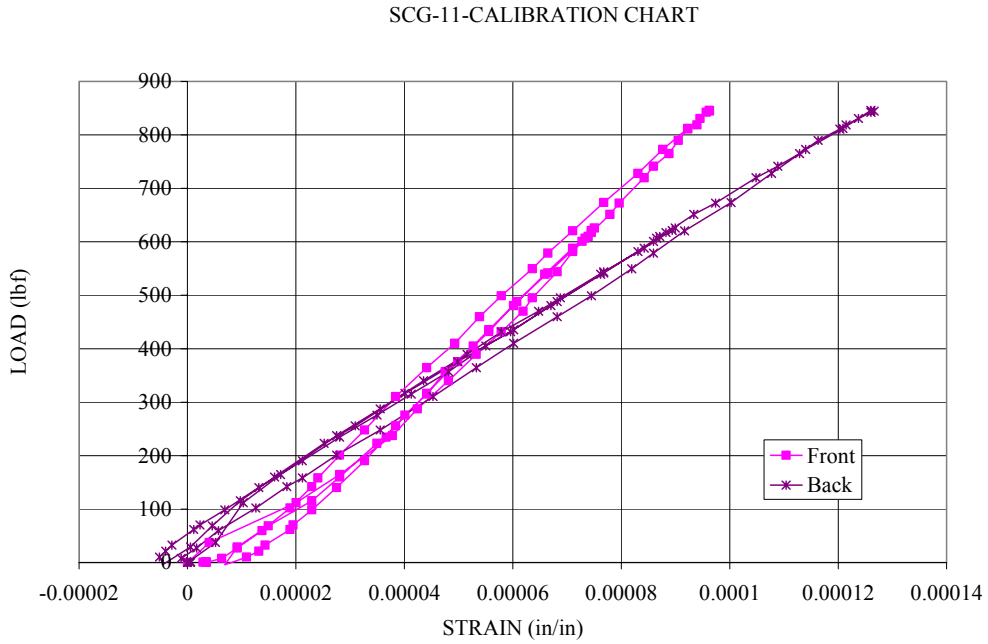

Figure 4.1.22: Load vs. Strain Data for SCG-11; Calibration

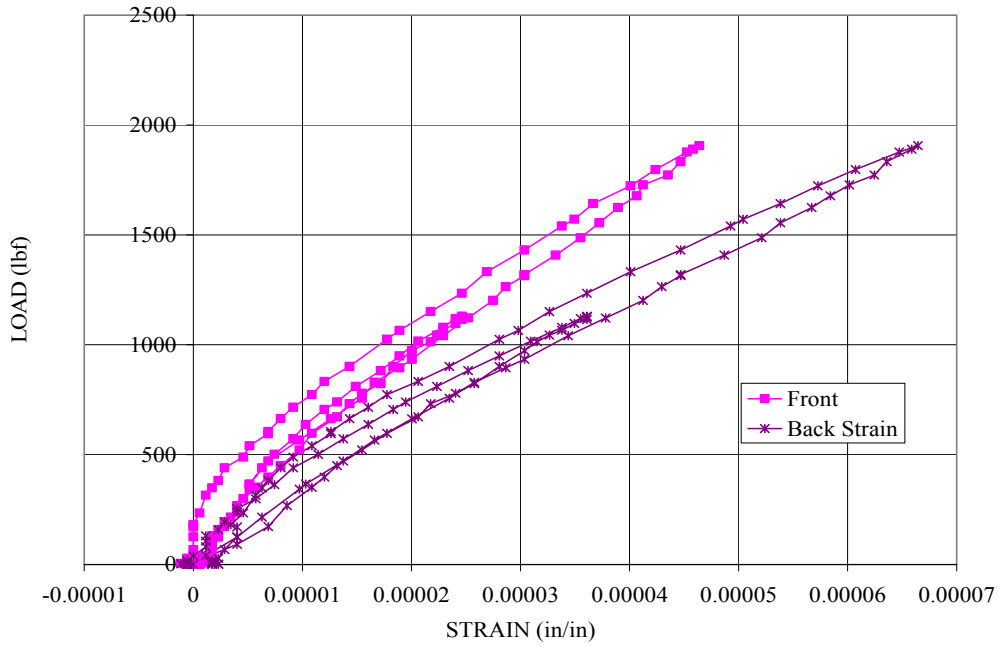

Figure 4.1.23: Load vs. Strain Data for SCG-11; 0 Cycles

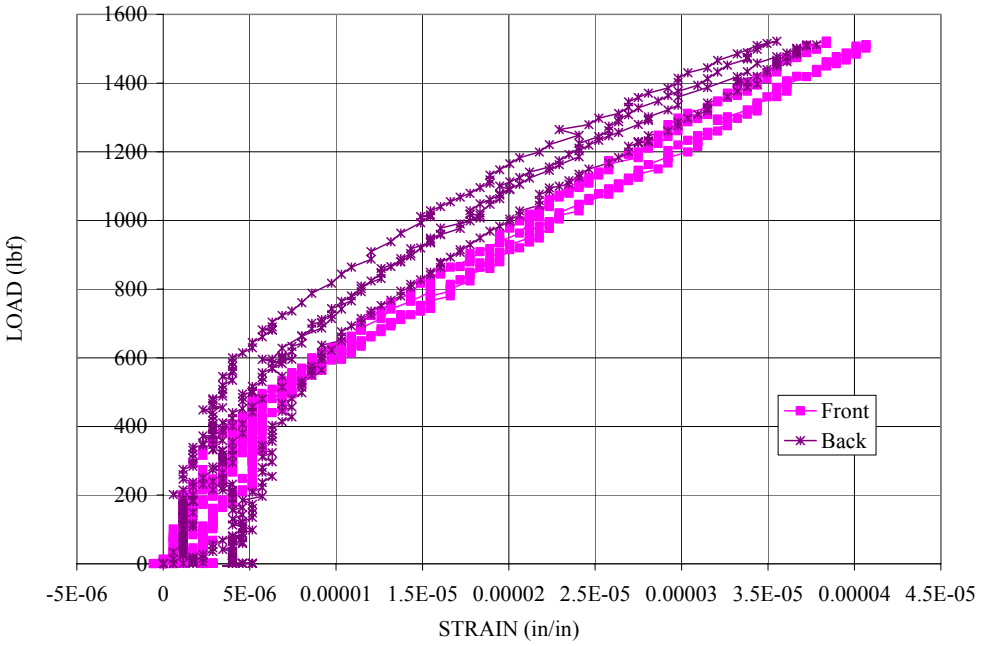

Figure 4.1.24: Load vs. Strain Data for SCG-11; 50K Cycles

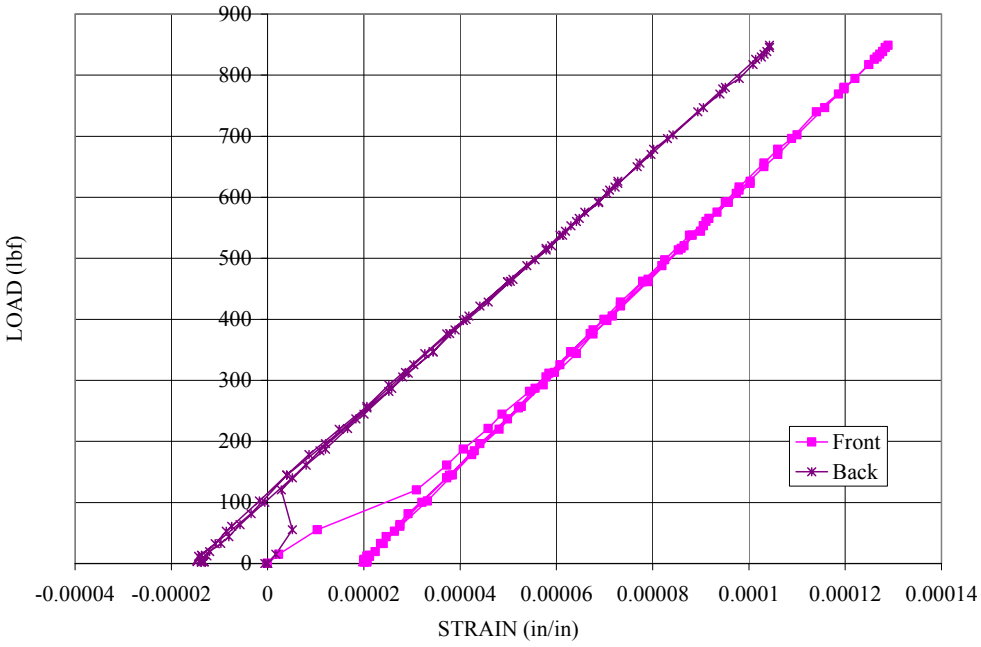

Figure 4.1.25: Load vs. Strain Data for SCG-12; Calibration

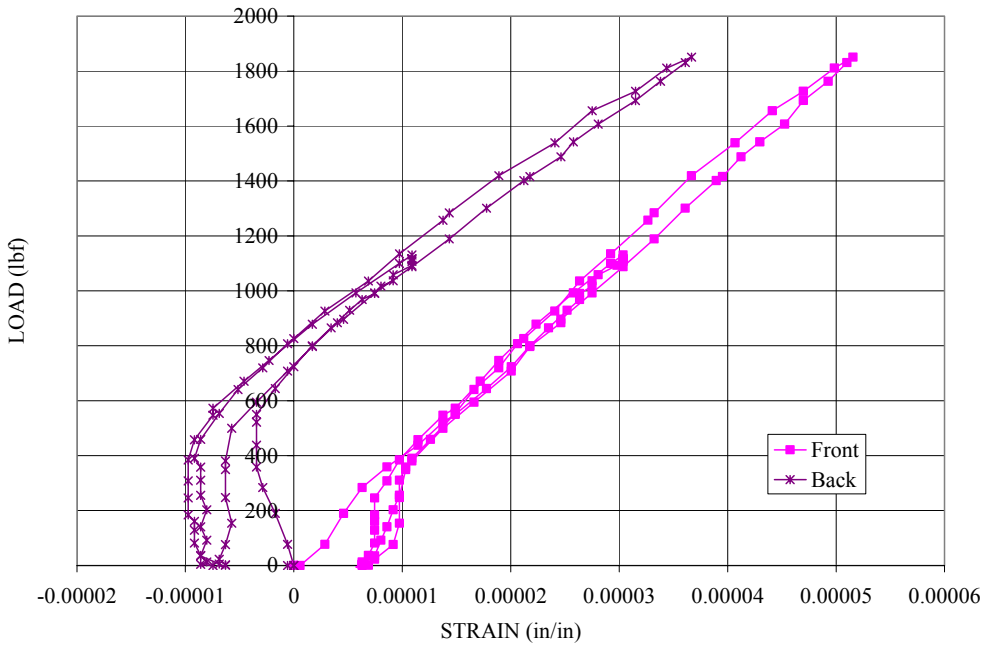

Figure 4.1.26: Load vs. Strain Data for SCG-12; 0 Cycles

4.2. Load Transfer

The load transfer rates for various joint configurations were calculated from experimental strain data. To calculate the rates of load transfer, only the plotted regions with linear relations were used. The data on calibration specimens showed that the rate of load transfer in those joints was 100 percent. This was used as the basis to estimate the loads transmitted in test specimen joints. The load transfer rate F* is given by

$$F^* = 200AESc/P \qquad (2)$$

Where F* is the percent load transfer rate, A is the cross section area of the doubler, E is the elastic modulus of the doubler material, Sc is the measured strain at applied load P. The calculated load transfer rates are shown in Table 4.2. Ideally, the load transfer rates should be the same for each joint type. Due to variations in transfer loads, the average values of the load transfer rates were calculated for each joint type as shown The average values may be a better estimate of load transfer rates. However due to large variations and limited data from small number of specimens, the given values should be further refined. It was observed that the experimental load transfer rates increase with the increasing number of load cycles. This is probably due to the time taken by the joint to stabilize. The results show that the experimental load transfer rates for steel doublers are lower than the values used in the initial test plan for the program based on predictions by finite element methods.

Table 4.2 Load Transfer For Joints with Various Doublers

Spec. No.	Doubler		Load Transfer (Percent)	
Group	Material	Thickness	Initial	Average For.
1S	2024-T3 Al	0.063 in.	(a)	18.4
2			20.2/15.0	
3S			(a)	
4S			(a)	
5			20.0	
6	2024-T3 Al	0.125 in.	22.0	22.0
7			21.0	
8			21.0	
9			24.0	
11	4130 Steel	0.063 in.	22.0/15.0	18.5
12			21.0/16.0	
13S			(a)	
14S			(a)	

(a) Strain data nonlinear and non-symmetric during crack growth tests

4.3. Crack Growth and Residual Strength

The crack growth data for all specimens is summarized in Table 4.3.1. The variation in cyclic life from initial crack to final crack length for specimen's 1S, 2 and 5 with .063 aluminum doublers is normal as shown in Figure 4.3.1. The lower number of crack growth cycles in specimen 2 is partially due to the fact that the initial crack was longer than the planned length of .003 in. The difference is nearly the same as the number of cycles it took specimen 1S or 5 to grow from .0079 in. to .062 in. The slope for all the three specimens is pretty much the same. The results show that the crack growth rates in pin loaded Group I joint specimens is higher than the open hole specimens 16, 17S under the same loading conditions. The specimen 17 S had prior damage in a previous test. No specimens were available. We continued the test instead of discarding a specimen.

The specimen's 3S and 4S tested under EIFS spectrum were machined from a different batch of material and machined at a different facility and had excessive joint deformation. The crack in specimen 3S was not visible at the start of the test. The first time during inspection, the crack was detected; it was already .015 in. long. For these reasons, the data on these specimens is not considered valid even though the crack growth life for both specimens is very close to each other. This data when plotted with the crack growth data for open hole specimens 18S and 19S showed that this crack rate is not reliable because they tend to show the opposite trend. It should be noted however that in these plots, the number of cycles are not on a logarithmic scale but on a linear scale and the number of life cycles differ only by 50 percent which is with in the typical crack growth life scatter band.

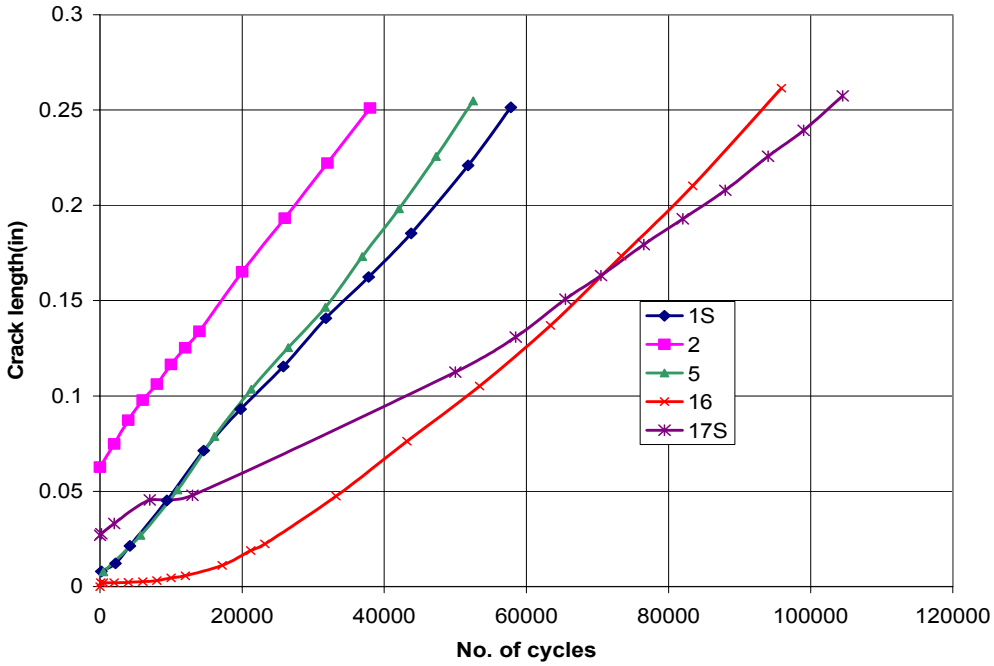

Figure 4.3.1: Crack Growth in specimens with .063 Al. Doublers and Open Hole Specimens (16,17S) Under Marker Loads (15 Ksi max)

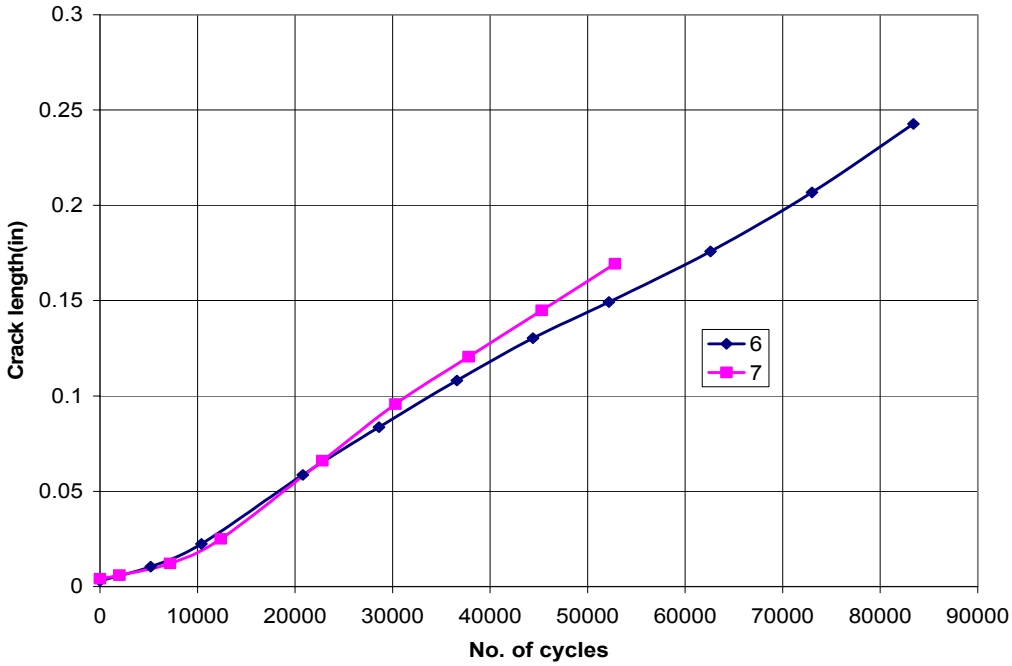

Figure 4.3.2: Crack Growth in specimens with .125 Al. Doublers Under Marker Loads (12.5 Ksi max)

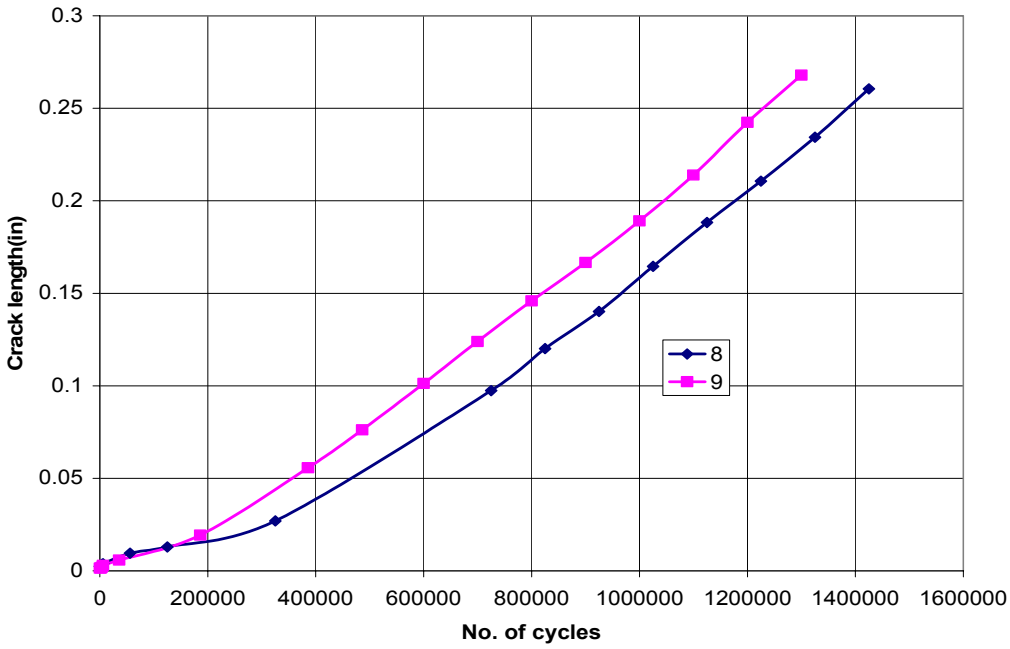

Figure 4.3.3: Crack Growth in specimens with .125 Al. Doublers Under EIFS Spectrum Loads (13.4 Ksi Peak)

The crack growth at the holes in specimens with thick aluminum doublers under marker band loads is also reasonably good data as shown in Figure 4.3.2. The number of fatigue cycles for specimen number 7 is less than those for specimen 6 because the test was stopped at .168 in. of crack length as the crack started to grow at the opposite end of the hole. Based on the crack growth rate in specimen 6 over the crack length from .168 in. to .250 in., it is estimated that the specimen 7 would have reached a .250 inch length at approximately 80, 000 which is very close to the number of cycles for specimen 6. This is further confirmed by crack growth rates under EIFS spectrum loads in specimens 8 and 9 with same type of doublers and plotted in Figure 4.3.3. Both specimens reached the final crack length after almost the same number of cycles. This is in spite of some variations in strain readings in the upper and lower doublers.

The experiments on specimens with steel doublers forming dissimilar material joint were not so successful during strain surveys. The crack growth data for these specimens is presented in Figure 4.3.11 and 4.3.12. The crack growth under marker band specimens in specimens 11 and 12 show that the crack growth rate is slower than originally predicted. For specimen's 13S and 14 tested under EIFS spectrum loads applied at 20 kips/second, there is considerable variation in data. The initial crack in specimen 13 S could not be detected and showed no crack at the hole even after 204 K EIFS load cycles.

Table 4.3.1 Crack Growth Test Results

Spec. No.	Load Type	Max/Peak Stress (Ksi)	Crack Length		No. Of cycles
			Initial	Final	
1S	Marker Band	15	.0079	0.023	57,800
2	Marker Band	15	0.0626	0.251	38,000
(a)					
3S	EIFS	15.8	0.0148	0.261	1,500,000
(b)					
4S	EIFS	15.8	0.0058	0.247	1,191,000
(b)					
5	Marker Band	15	0.0078	0.253	52,500
6	Marker Band	12.5	0.0030	0.242	83,400
7	Marker Band	12.5	0.0041	0.168	52,800
(c)					
8	EIFS	13.4	0.0025	0.260	1,425,000
9	EIFS	13.4	0.0029	0.267	1,300,000
11	Marker Band	10	0.0024	0.266	160,000
12	Marker Band	10	0.005	0.258	165,000
13S	EIFS	11	0.016	0.245	1,761,000
(b)					
14S	EIFS	11	0.026	0.289	16,700,000
(b)					
16	Marker Band	15	0.004	0.262	95,900
17S	Marker Band	15	0.0269	0.258	104,500
18S	EIFS	16	0.006	0.250	975,000
19S	EIFS	15.8	0.015	0.252	900,000
20	Const. Amp.	15.8	0.002	0.760	126,562
(d)					
21	Const. Amp.	15.8	0.002	0.680	152,216
(d)					

(a) Initial crack size longer (b) Invalid test (c) Small crack developed at opposite side of hole (d) Crack growth test to failure

This was because the specimen was accidentally loaded beyond the planned maximum load during strain surveys, which may have caused the crack to close and retard the crack growth. To enhance the visibility of the crack or even to form one, constant amplitude cyclic loads at 19 ksi maximum stress (R=0.1) were applied. When the crack was finally detected, the spectrum loading resumed. During tests on specimen 14, it was observed that the specimen had crack growth at both ends of the hole (diametric cracks). These tests are not considered valid and not used in this study.

The crack growth results for open hole specimens SCG-18S and 19S tested under EIFS spectrum loads are presented in figures 4.3.15 and 4.3.16 respectively. The crack measurements data during tests is listed in Appendix-B (Tables B.12 and B13). The small crack effects are more noticeable for specimen 19S. When the crack becomes .05 in long,

the crack growth rates for both specimens are essentially the same. Figures 4.3.17 and 4.3.18 show crack growth behavior of open hole specimens 20S and 21 under constant amplitude loads for comparison with crack growth rates of other specimens for different loading conditions.

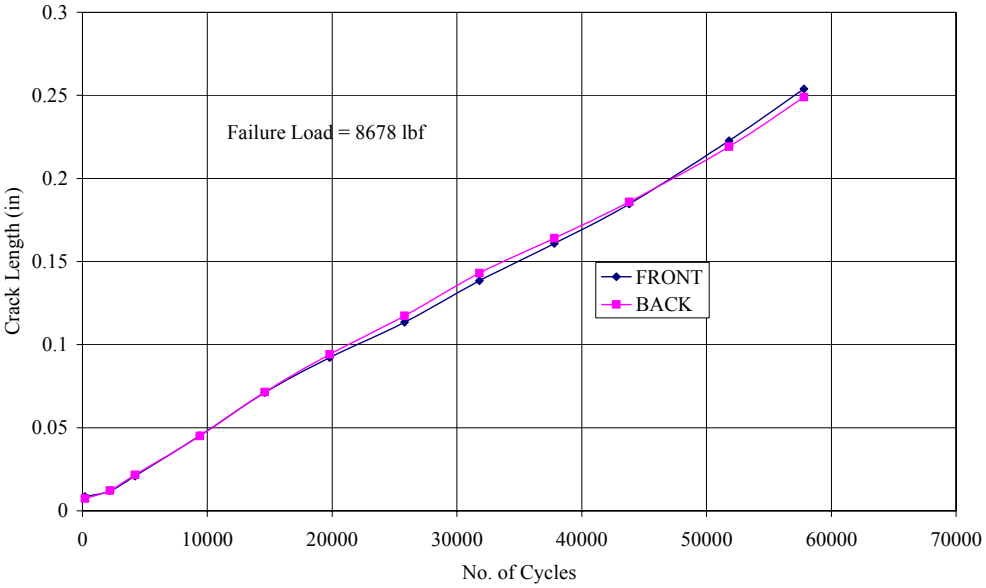

Figure 4.3.4: Crack Length vs. Cycles for SCG-1S

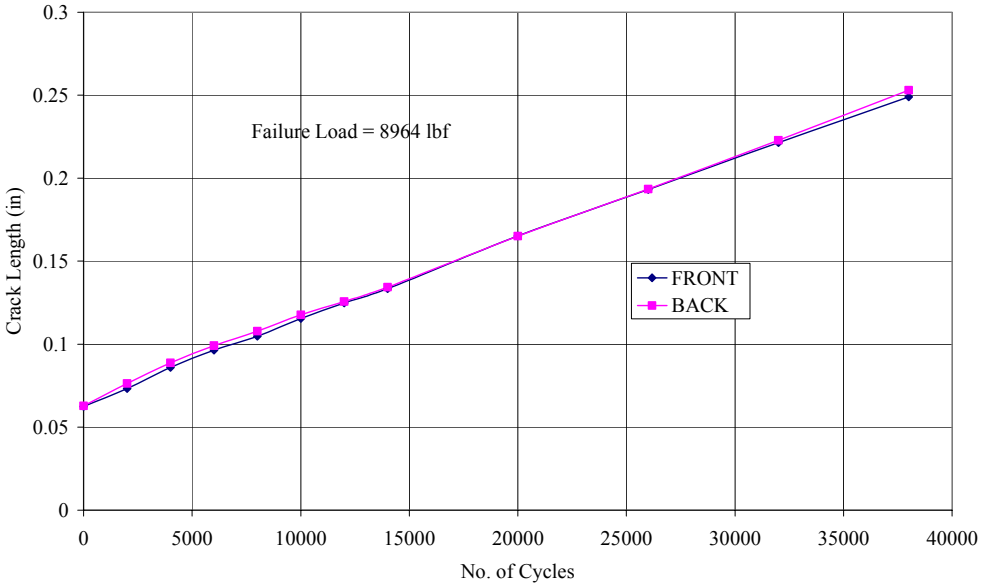

Figure 4.3.5: Crack Length vs. Cycles for SCG-2

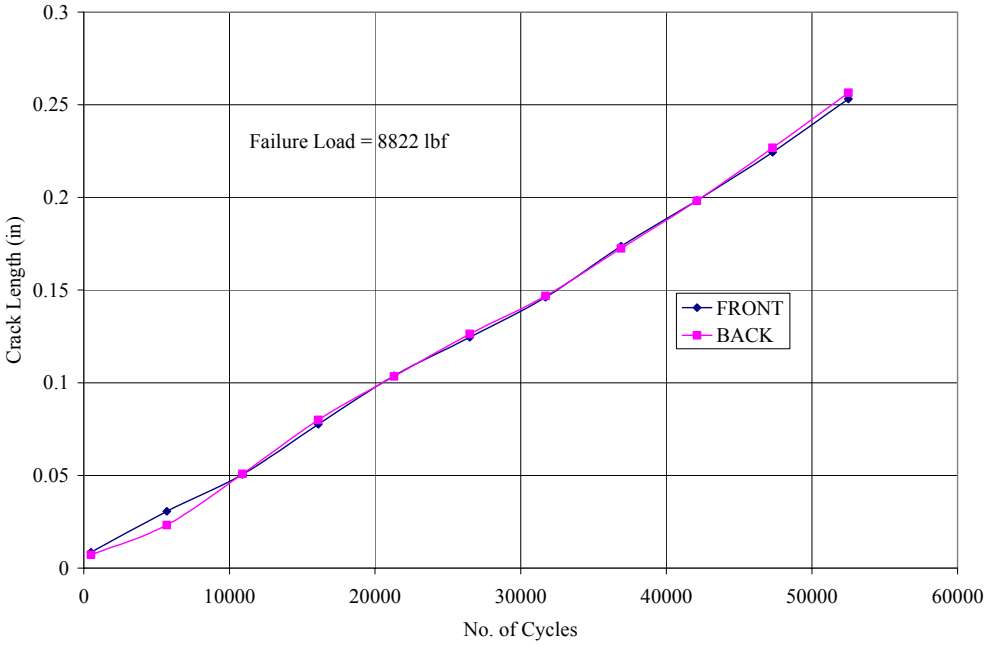

Figure 4.3.6: Crack Length vs. Cycles for SCG-5

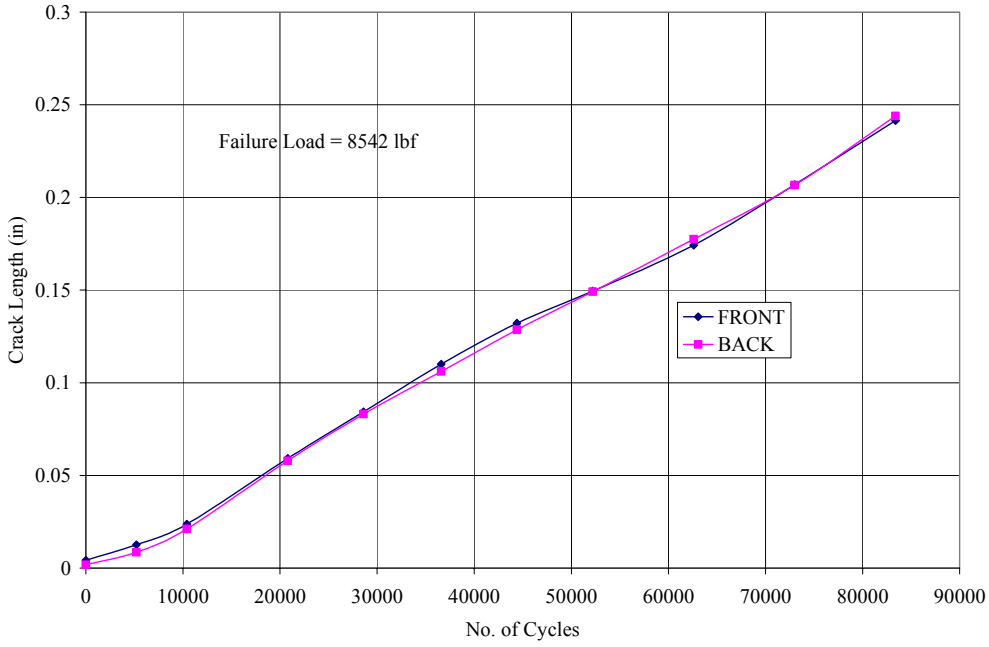

Figure 4.3.7: Crack Length vs. Cycles for SCG-6

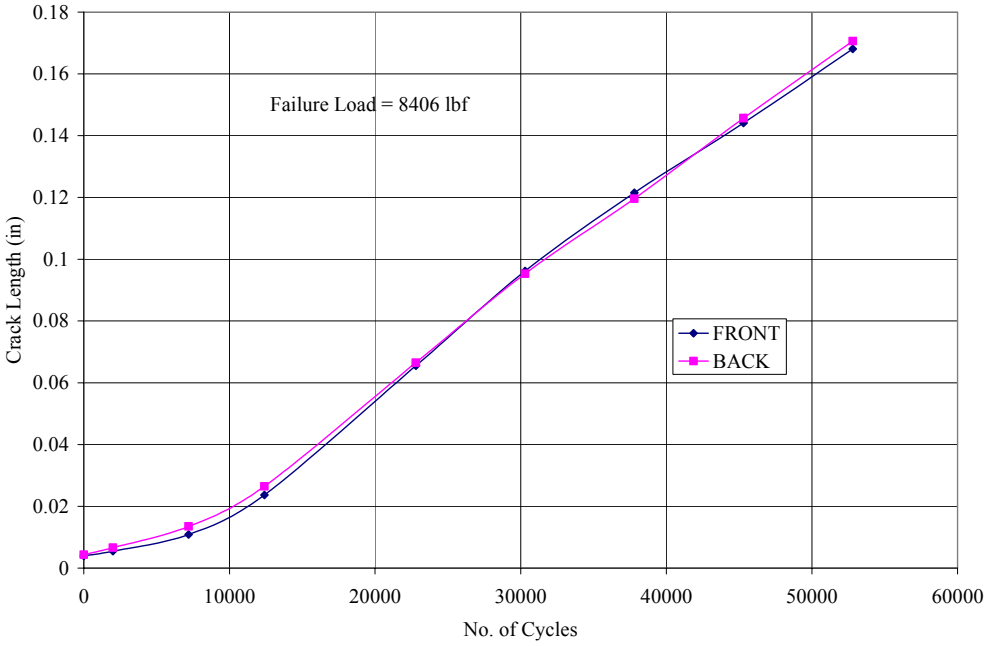

Figure 4.3.8: Crack Length vs. Cycles for SCG-7

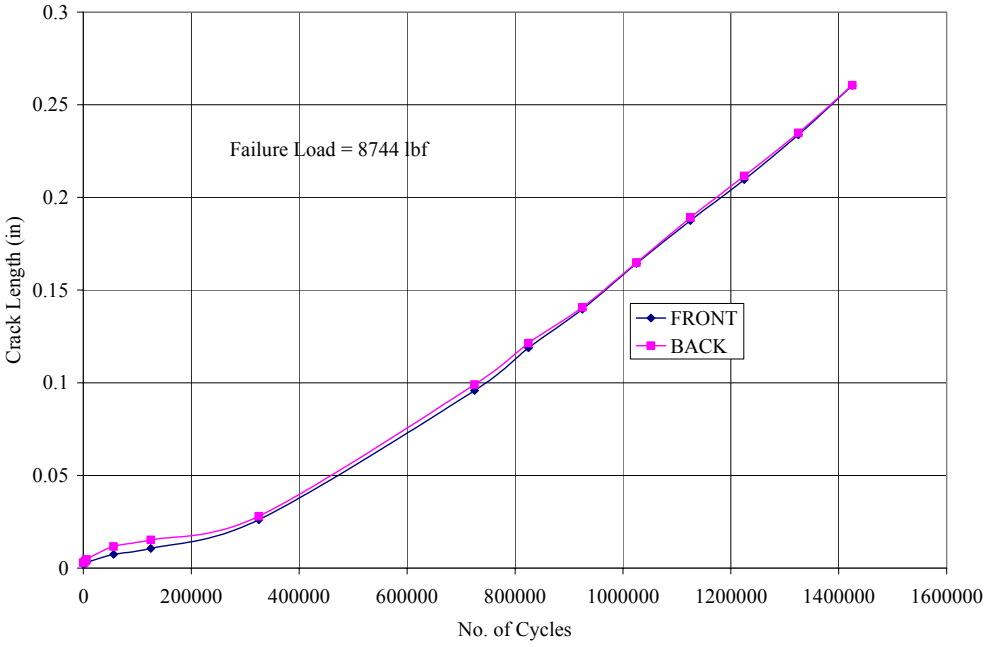

Figure 4.3.9: Crack Length vs. Cycles for SCG-8

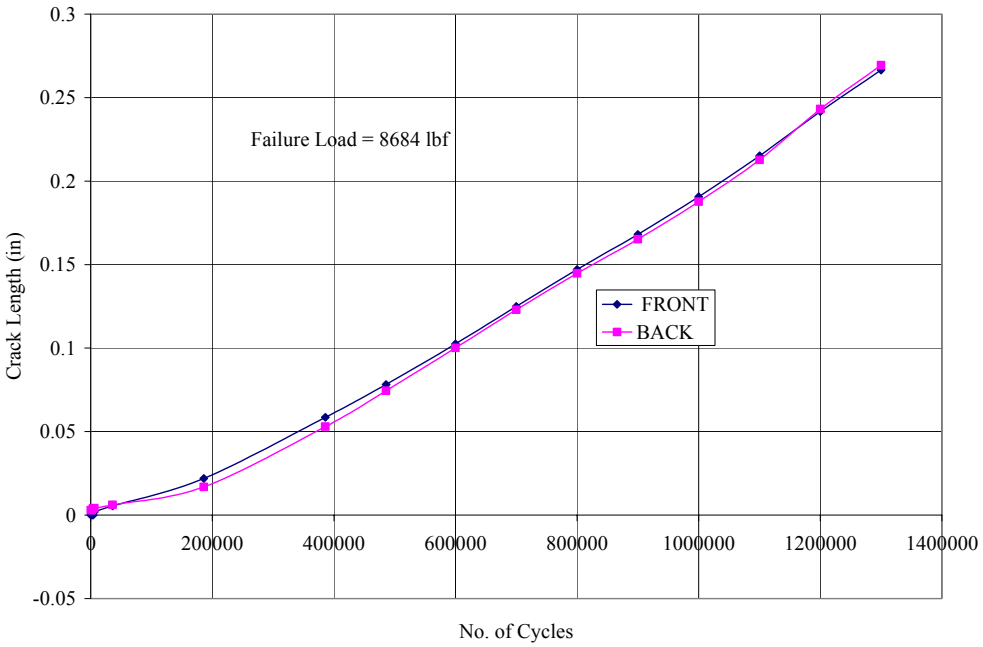

Figure 4.3.10: Crack Length vs. Cycles for SCG-9

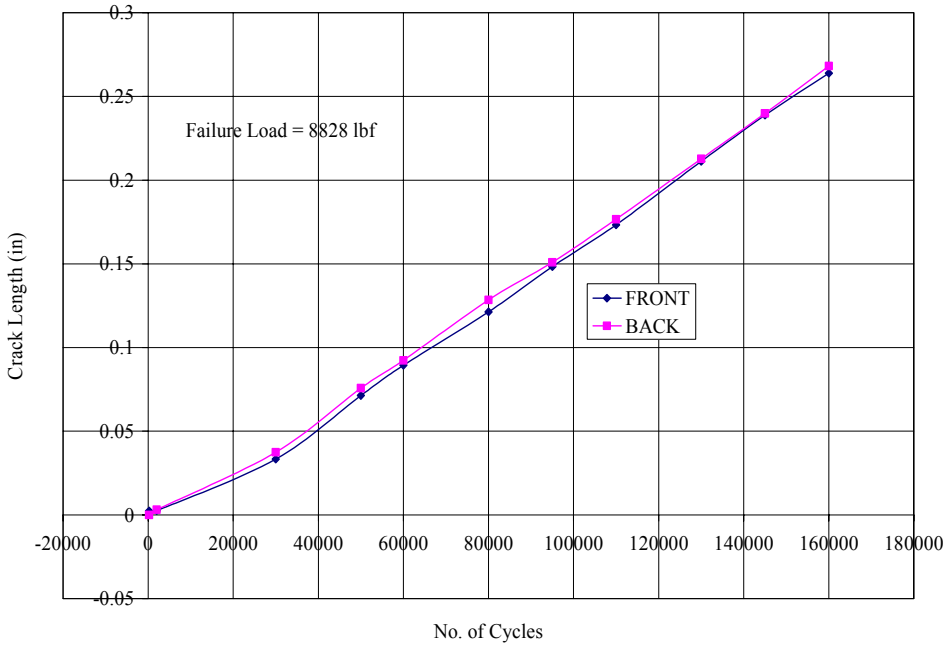

Figure 4.3.11: Crack Length vs. Cycles for SCG-11

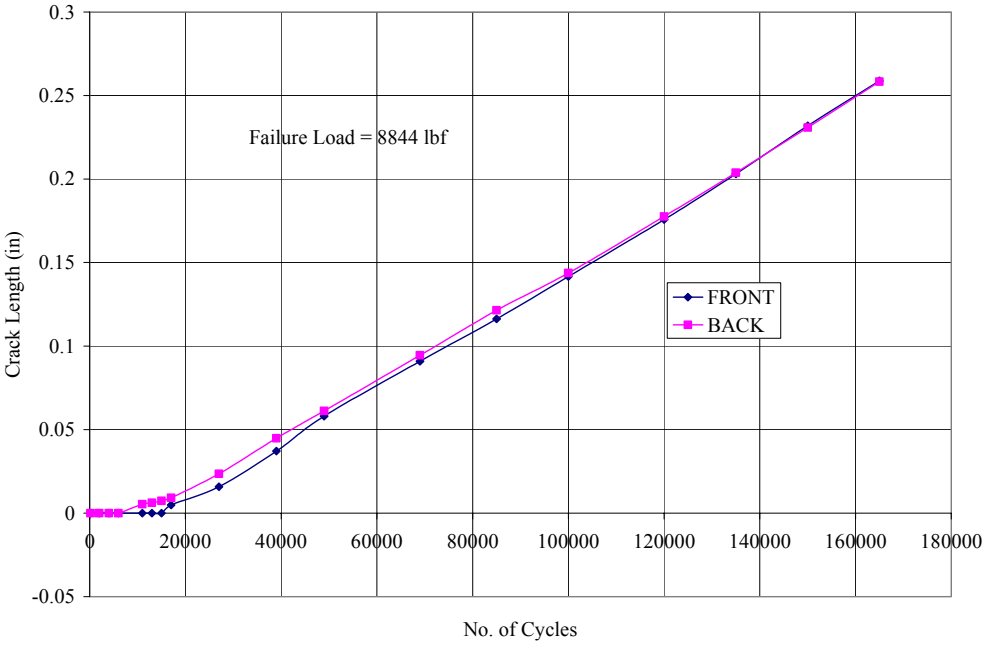

Figure 4.3.12: Crack Length vs. Cycles for SCG-12

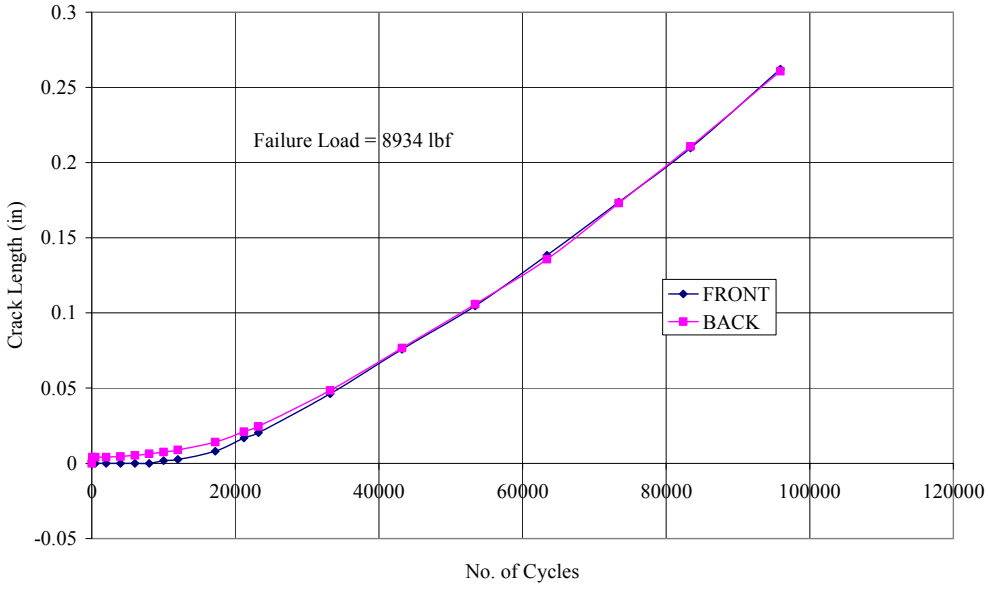

Figure 4.3.13: Crack Length vs. Cycles for SCG-16

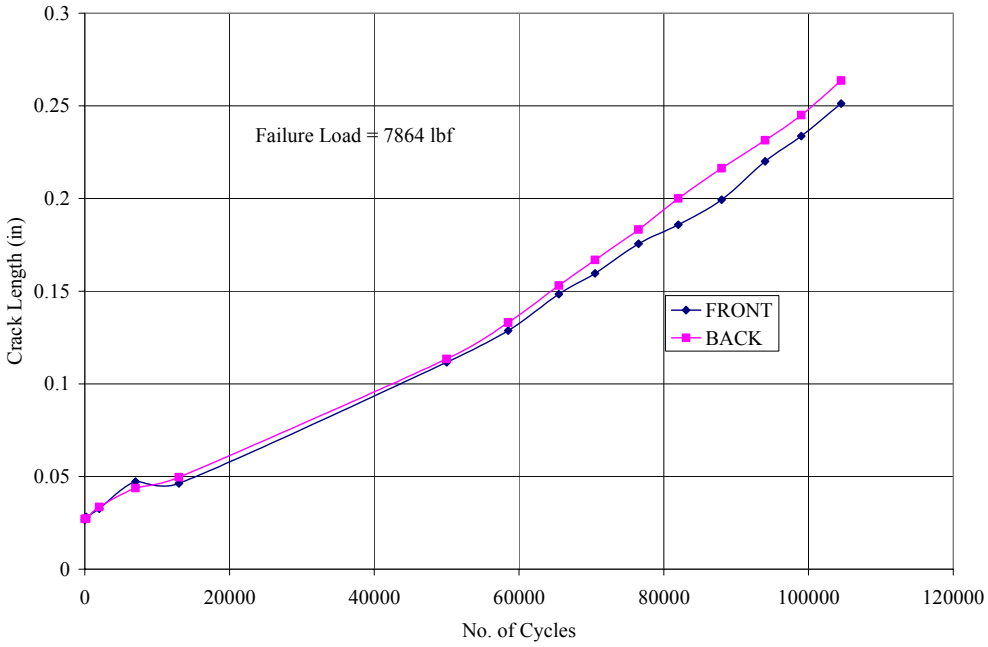

Figure 4.3.14: Crack Length vs. Cycles for SCG-17S

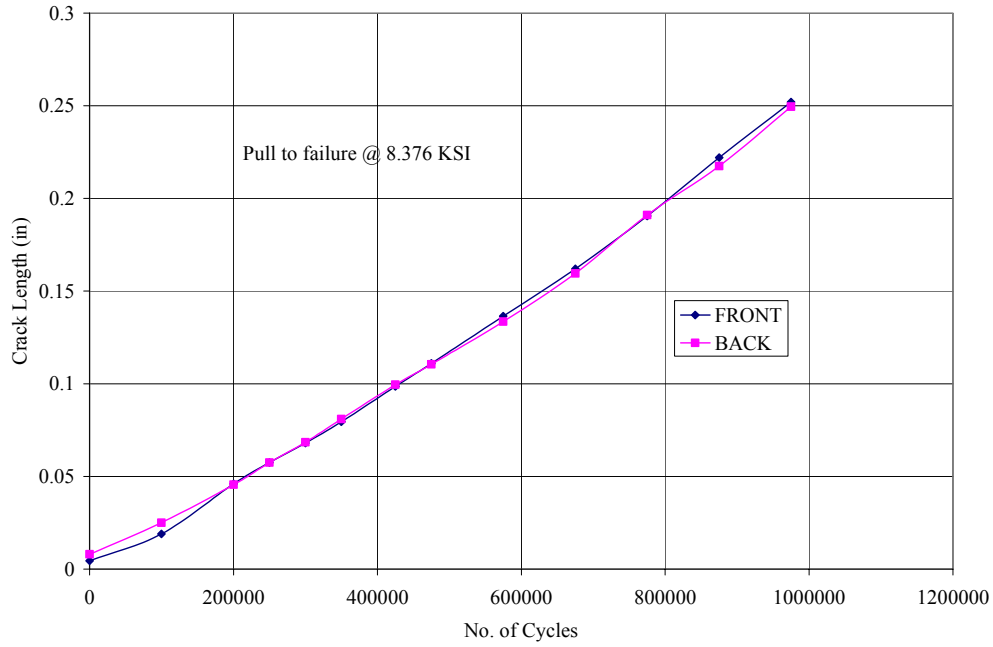

Figure 4.3.15: Crack Length vs. Cycles for SCG-18S

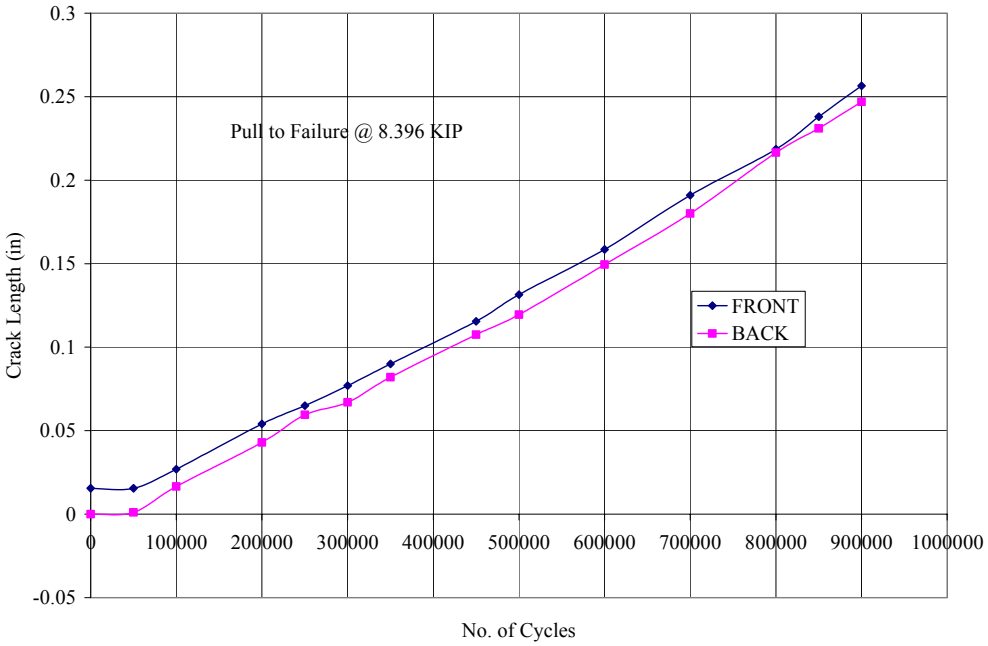

Figure 4.3.16: Crack Length vs. Cycles for SCG-19S

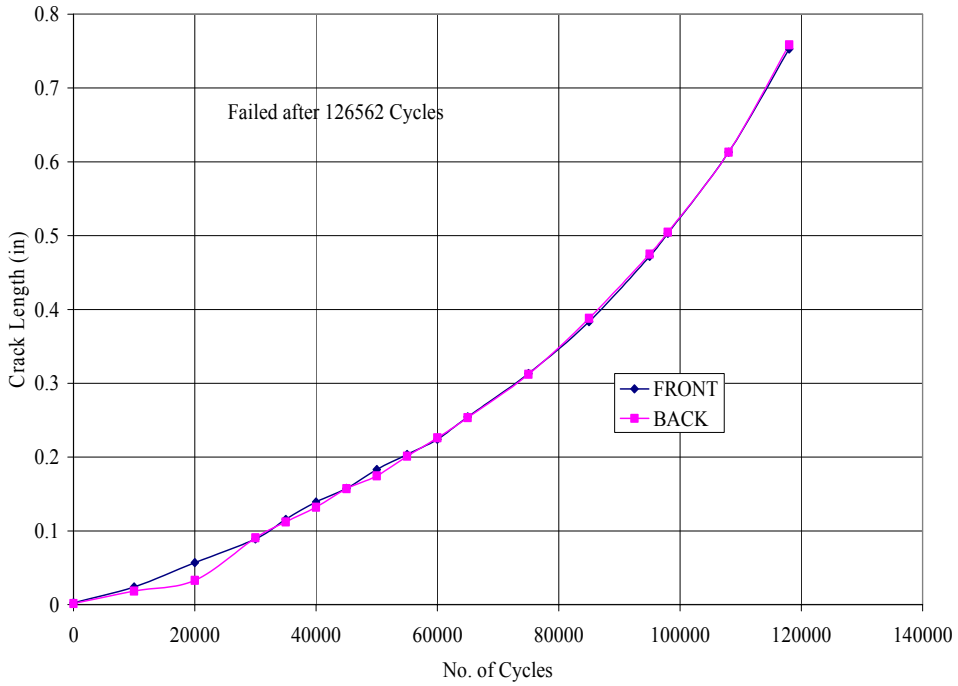

Figure 4.3.17: Crack Length vs. Cycles for SCG-20S

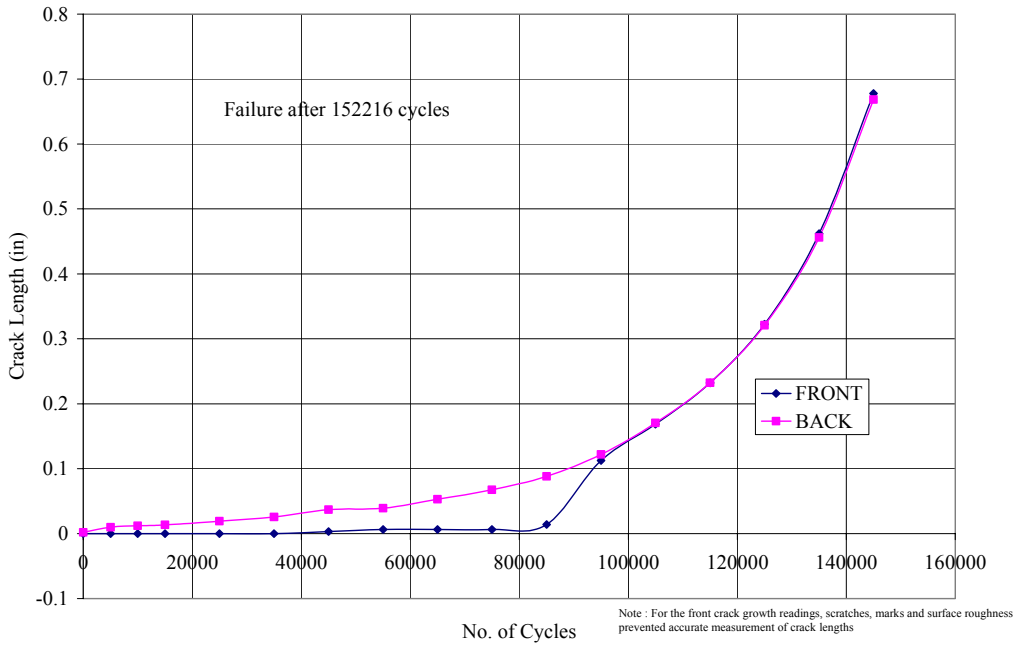

Figure 4.3.18: Crack Length vs. Cycles for SCG-21

4.3.2. Residual Strength

The residual strength (based on gross section area) of all specimens is listed in Table 4.3.2. The average strength is with in 4 percent of 46.5 Ksi. The unexpectedly larger variations are due to the fact that the final crack length was not a controlled variable in the experimental plans. In some specimens, the cracks grew at the opposite end of the hole. The variability is also due to cracks growing in the interior of the specimen and thus surface crack length was smaller than the true crack length as in the case of specimen SCG-7.

Table 4.3.2 Residual Strength Data

Spec. No. Strength	Final Crack Length		Failure Load (Kips)	Residual (Ksi)
	Front	Back		
1S	0.254	0.249	8.68	46.3
2	0.249	0.253	8.96	47.8
3S	0.262	0.261	8.54	45.6
4S	0.247	0.247	8.62	46.0
5	0.253	0.256	8.82	47.0
6	0.241	0.244	8.54	45.6
7	0.168	0.171	8.41	44.9
8	0.260	0.261	8.74	46.6
9	0.266	0.269	8.68	46.3
11	0.264	0.268	8.83	47.1
12	0.259	0.258	8.84	47.1
13S	0.241	0.250	7.69	41.0(a)
14	0.297	0.283	7.86	41.9(a)
16	0.262	0.261	8.93	47.6
17S	0.251	0.264	7.86	41.9(a)
18S	0.252	0.250	8.38	44.7
19S	0.257	0.247	8.40	44.8
20	0.753	0.759	-	(b)
21	0.678	0.669	-	(b)

Note: (a) cracks formed at opposite ends of hole (b) failure due to unstable crack

4.4 SEM Analysis

The fracture surfaces of all specimens were observed under scanning electron microscope for possible correlations with the crack length measured during tests. The SEM data was also used to establish final crack lengths and to determine the sizes of the initial cracks at the hole. The measurements were taken according to section 8.2.2 of ASTM E-399 for a three point through thickness crack curvature (crack tunneling). The fracture surface measurements data is summarized in table 4.4.1.

The fracture surfaces did not reveal distinct striations. The marker bands were visible on surfaces of some specimens. Figure 4.4.1 shows the fracture surface of specimen 1S with random marker bands. The marked bands do not relate to the event described by the end of each block of load cycles (5200 cycles). The crack growth between the marker bands seems to correspond to inspection intervals during the testing program. No such markings on the fracture were found for specimens tested under EIFS spectrum loads.

The final crack lengths on the fracture surfaces (Table 4.4.1) were longer than the measurements during tests and varied from 0.241 inch to 0.312 inch. The corresponding crack lengths from test data are -.168 inch and 0.289 inch respectively. These crack lengths represent the averages calculated according to ASTM standard E-647, which

references ASTM E-399. The crack tunneling was observed for a number of specimens as shown in Figure 4.2.2 through Figures 4.4.5 for specimen's 1S, 2, 6 and 7 respectively. This is a possible explanation why the total length of the crack could not be visible by visual and optical measurement techniques used during the tests. The specimen SCG-7 had a measured crack length of 0.168 inch but the residual strength was about the same as the other specimen's. The fracture surface revealed that crack tunneling occurred during crack propagation (Figure 4.4.5).

Photographs of fracture surfaces were taken near the holes to observe initial cracks and to measure their crack lengths. The fracture surfaces for specimen's 1S, 2, 5 and 6 are shown in Figure 4.4.6 through Figure 4.4.9 respectively. An initial crack for specimen 1S is quite distinctly visible (Figure 4.4.6). The initial crack length measured on the fracture surface was 0.0106 inch (Figure 4.4.1) compared to 0.0079 inch measured during the tests. The initial cracks on the specimen surfaces were not always visible (Figure 4.4.1) at the start of the test. The initial cracks for specimens 6, 7, 8 and 9 with thick aluminum doublers and 11 and 12 with steel doublers were not visible. It is to be noted that the final hole sizes were enlarged under stack drilling of test specimen assemblies, which included the specimen's, calibration plates and the doublers. The drilling operations may have affected the size and visibility of the single, small radial cracks measured on specimen surfaces.

Table 4.4 Fractographic crack lengths

Spec. No.	Initial mm (inch)	Final mm (inch)
1S	0.27(0.0106)	6.72(0.266)
2	0.335(0.013)	6.12(0.241)
3S	0.441(0.017)	7.941(0.312)
4S	0.085(0.003)	7.504(0.295)
5	0.1213(0.005)	7.325(0.288)
6	-	6.649(0.261)
7	-	6.649(0.261)
8	-	7.113(0.280)
9	-	7.871(0.31)
11	-	7.015(0.276)
12	-	6.816(0.268)
12S	-	6.936(0.273)
13S	0.084(0.003)	6.787(0.267)
14	0.142(0.006)	7.726(0.304)
17	0.500(0.20)	6.691(0.264)

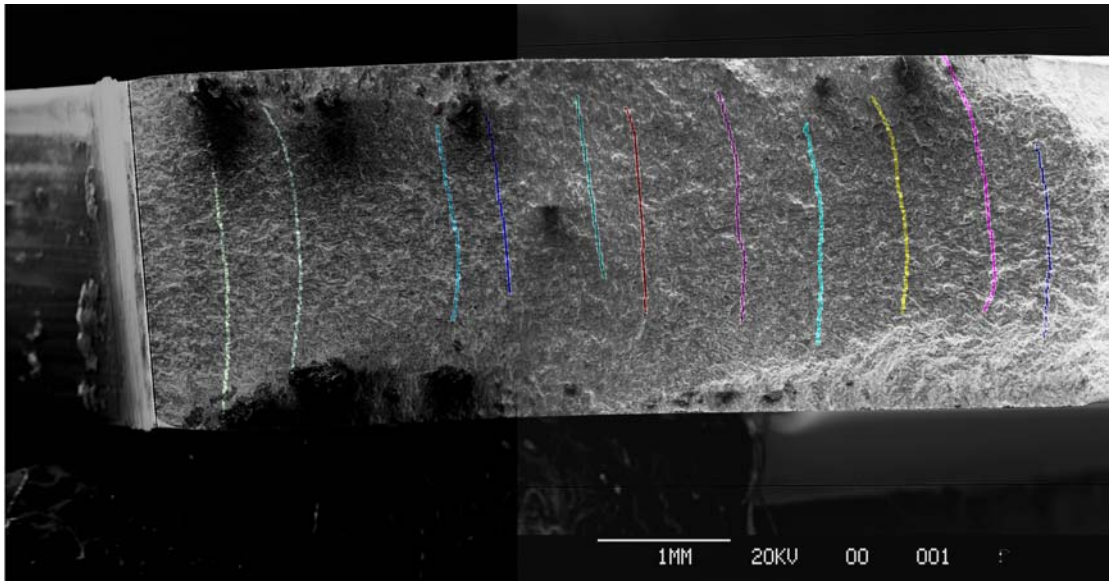

Figure 4.4.1 Fracture surface of specimen 1-S showing random marker bands

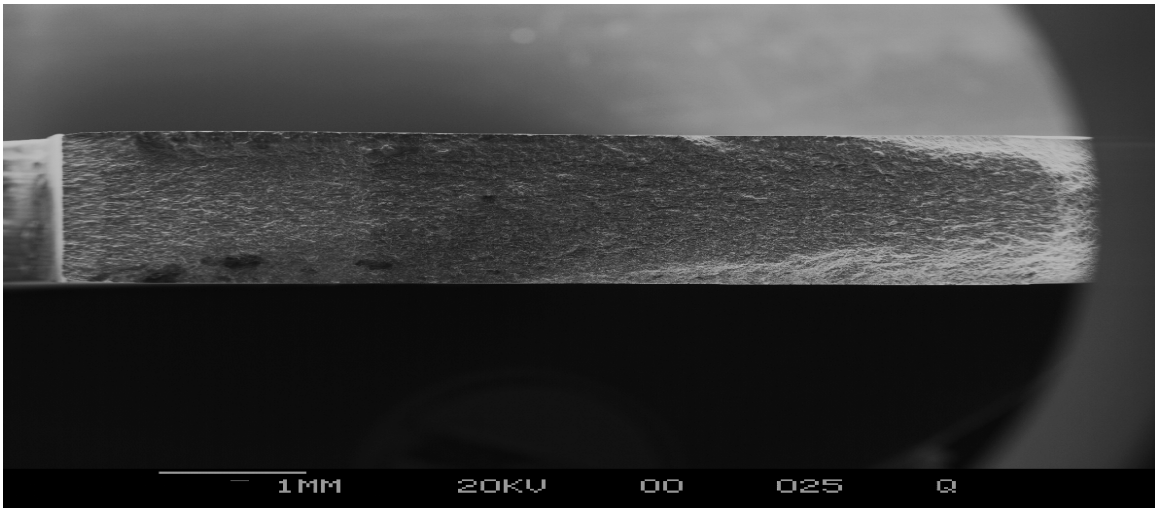

Figure 4.4.2 Fracture surface of specimen 1-S showing entire fatigue area

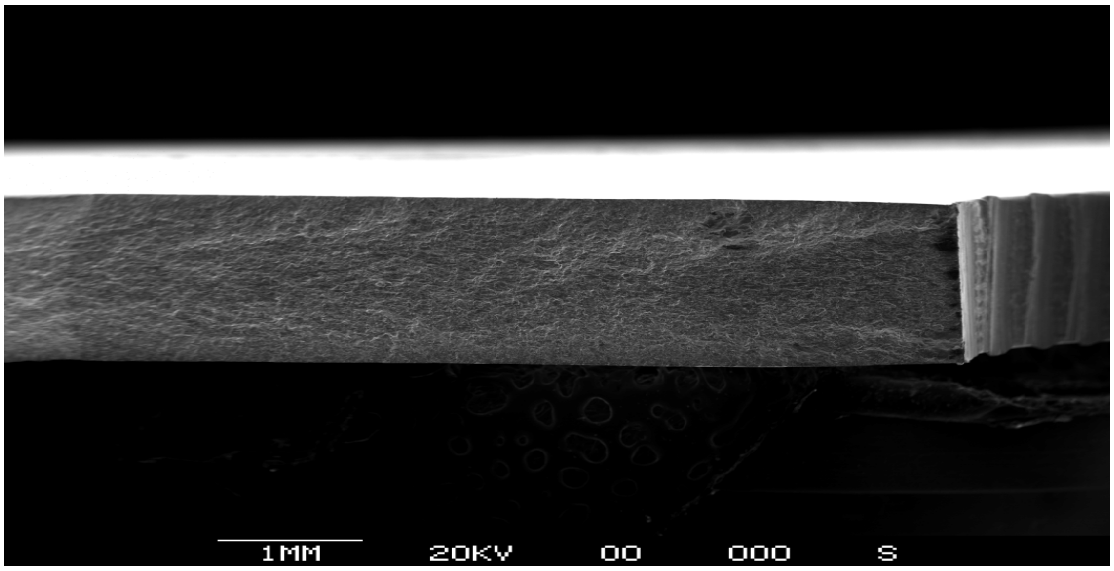

Figure 4.4.3 Fracture surface of specimen 2 showing entire fatigue area

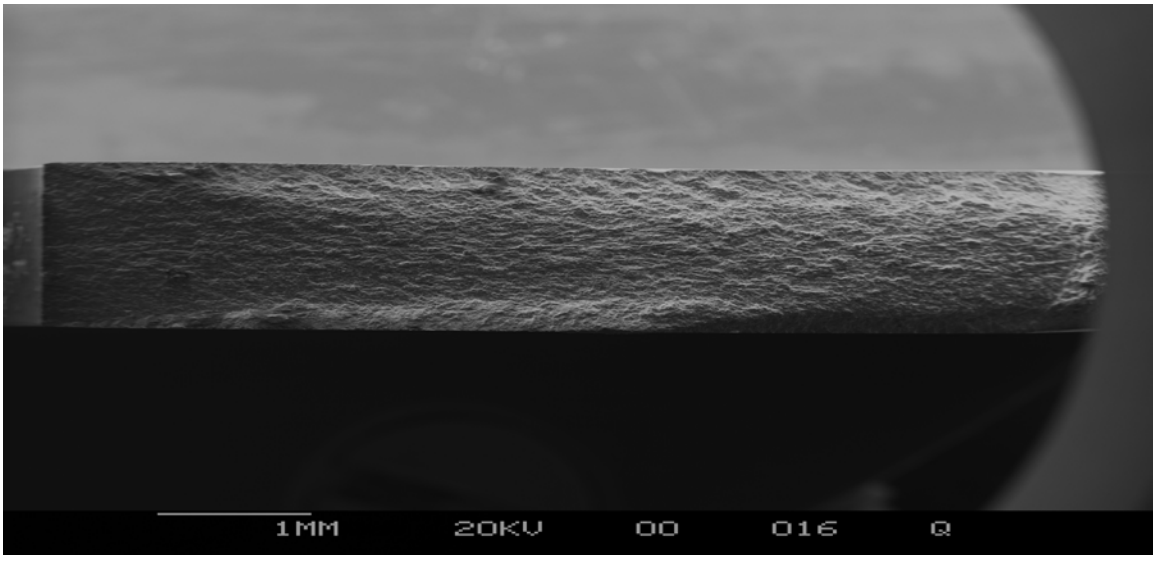

Figure 4.4.4 Fracture surface of specimen 6 showing entire fatigue area

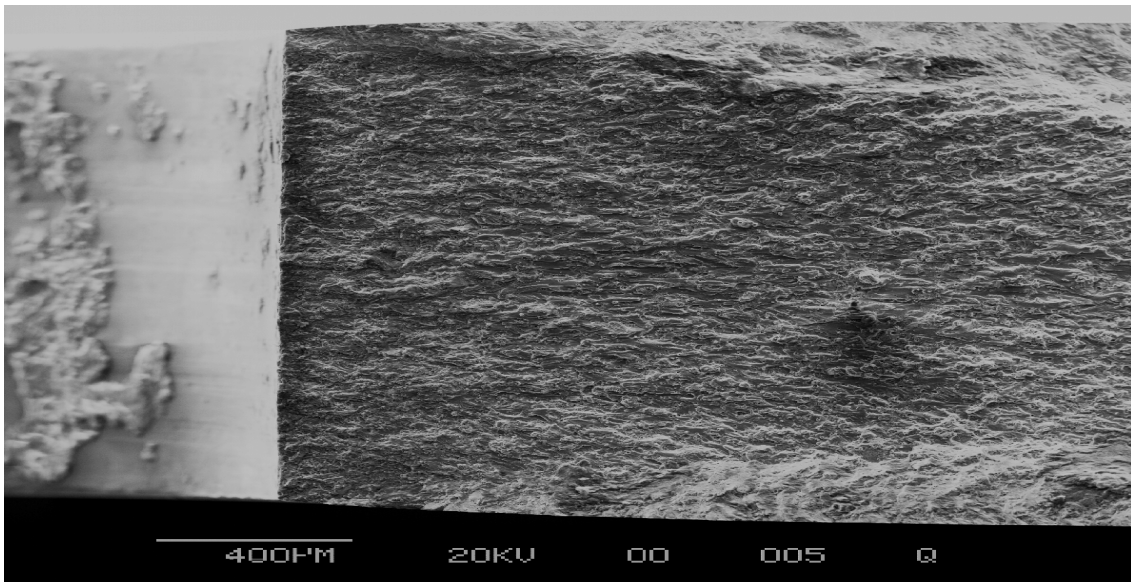

Figure 4.4.5 Specimen No. 7 Crack grew inside and was not visible on the surface after 0.168 inch of growth on surface

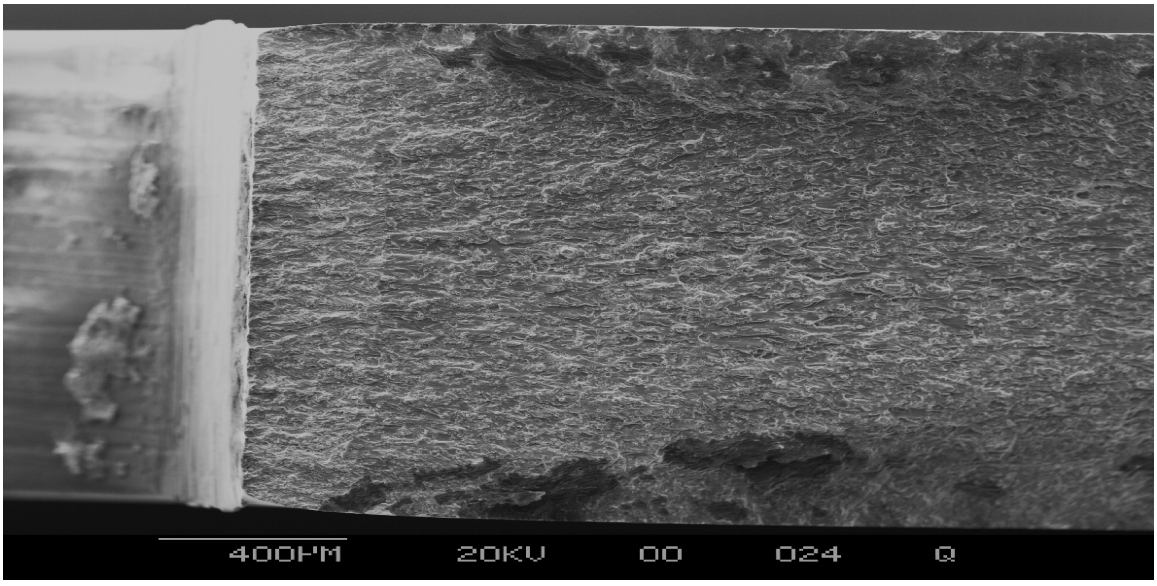

Figure 4.4.6 Fracture surface of specimen 1-S near the hole showing initial crack.

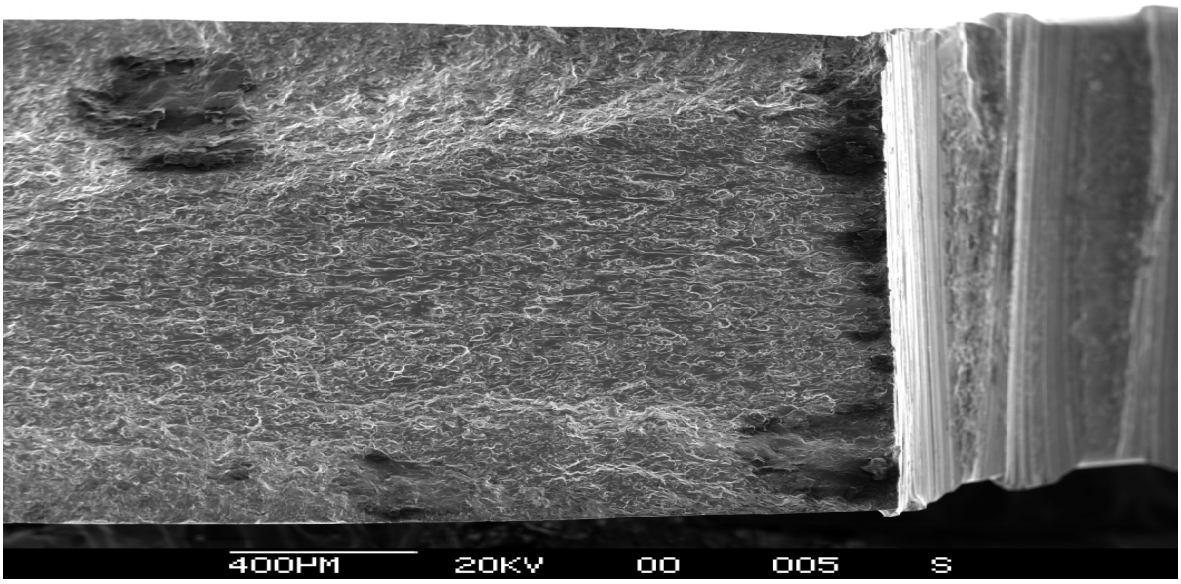

Figure 4.4.7 Fracture surface of specimen 2 near the hole showing initial crack.

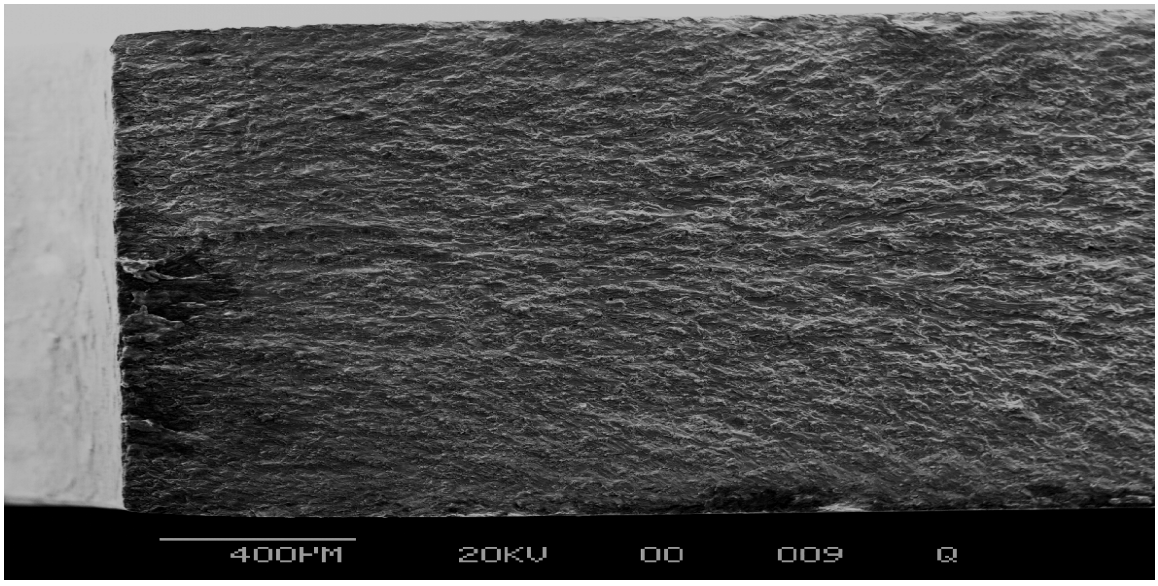

Figure 4.4.8 Fracture surface of specimen 8 near the hole showing initial crack.

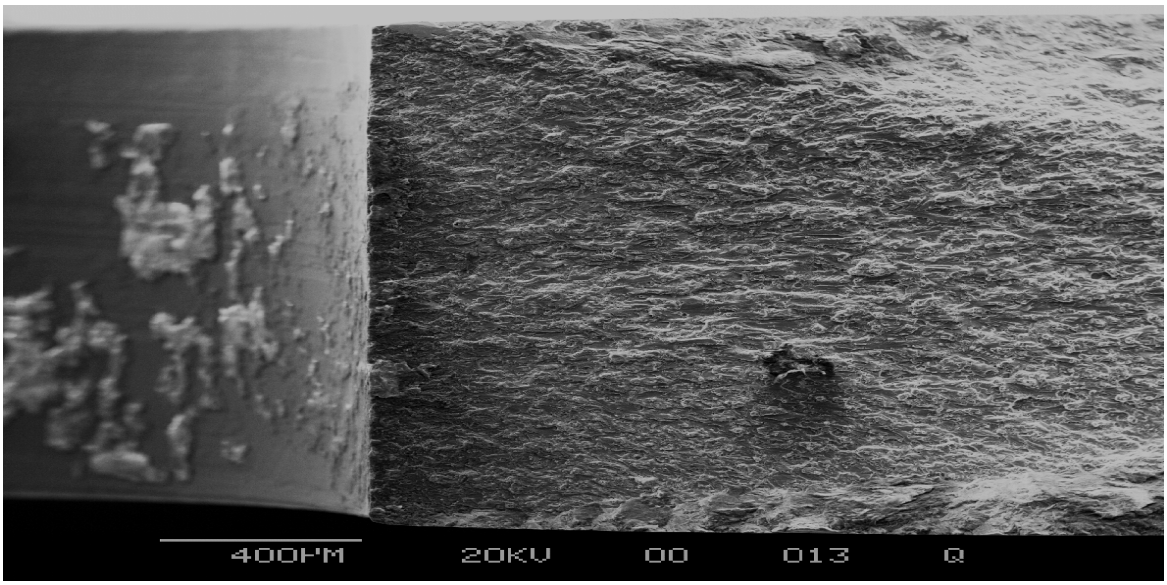

Figure 4.4.9 Fracture surface of specimen 6 near the hole to view the initial crack.

5. Conclusion and Recommendations

5.1. Conclusions

The calibration strain data is in good agreement with analytic predictions assuming a hundred percent load transfer. However, the strains measured for test specimen joints varied significantly. The variations were observed for doublers with different thickness, material and load level changes and number of load cycles. The differences in strains on front and back doublers were observed for specimens with steel doublers and doublers and specimens from machined different batch of material. The strain differences in other specimens were minor. The observed strains behaved nonlinearly at loads well below the proportional limit. This was in spite of the fact that each test joint was custom designed and machined. These variations may have been from various sources. The clearance, interference between the joining members due to machining, assembly and deformations and wear of pin coating and hole surfaces during cycling. The diameters of several fasteners were out of specifications and roundness along their lengths.

Crack growth data for constant amplitude and marker band load tests appear to be with in reasonable scatter bound. The crack growth and life data under EIFS spectrum loads show some variability. The cyclic life for these specimens is several times longer compared to other tests and initial predictions. Long experimental lives are probably due to peak load level changes, pre-cracking effects, crack orientation and accidental overloads by test operators.

Residual strength data varies within 4 percent due to variations in final crack lengths and variations in specimen widths and thickness. Observations of fracture surfaces under SEM revealed marker bands on some specimens. They seem to correlate with the various inspections conducted during the tests. The striations were not found on the surfaces for any meaningful correlation with the experimental crack growth rates. It was a difficult task to design test joints for tight tolerances between the pins and the fastener holes and meet the requirements for an initial crack length of .003 inch of the fatigue crack at the hole. It was difficult to detect the initial crack after hole enlargement when the specimen was assembled.

5.2. Recommendations

1. The load transfer rates and crack growth in joints with dissimilar material doublers under EIFS loads should be further studied.

2. More durable, high strength and stiffness fasteners and their coatings should be used for cyclic load tests.

3. More emphasis should be on development of data in the small crack length and low crack growth rates region. There should be more frequent inspections and shorter intervals during this part of testing.

4. To better understand variability in fatigue life, at least 3 specimens per test condition should be used.

5. The enlargement of hole should be performed in incremental sizes if possible. The residual stresses in the vicinity of initial crack tip should be reduced or measured and accounted for in the analysis.

6. There should be more in-depth surface analysis under scanning electron microscope for all specimens. The test loads should be revised so that striations are formed and can be observed.

7. More reliable methods should be developed and used to detect and measure small crack sizes.
8. Extra precautions are required to conduct small crack growth tests, to handle joint assemblies and obtain data.

6. References

1. Nagar, A. “Small Crack Growth Behavior”, USAF Damage Tolerant Design Handbook: Guidelines for the Analysis and Design of Damage Tolerant Aircraft Structures, AFRL-VA-WP-TR-2003-3002, Section 5.3, 2003.
2. Leis, B.N., Kanninen, M.F., Hopper, A.T., Ahmad, J. and Broek, D., “ Critical Review of the Fatigue Growth of Short Cracks”, Engineering Fracture Mechanics, Vol. 23, 1986.
3. Blom, A.F., et al. “Short Fatigue Crack Growth Behavior in Al 2024 and Al 7475” EGF Publication 1 1986, Mechanical Engineering Publications, London, pp. 37-66.
4. Newman, J.C. “Fracture Mechanics Parameters for Small Cracks”, Small Crack Test Methods, ASTM STP 1149, 1992.
5. Nagar, A., Report, “Small Crack Growth at Pin Loaded Holes”, Air Force Research Laboratory Report, AFRL-VA-WP-TR-2001-3008, to be published.

Appendix A
Load Vs Strain Data

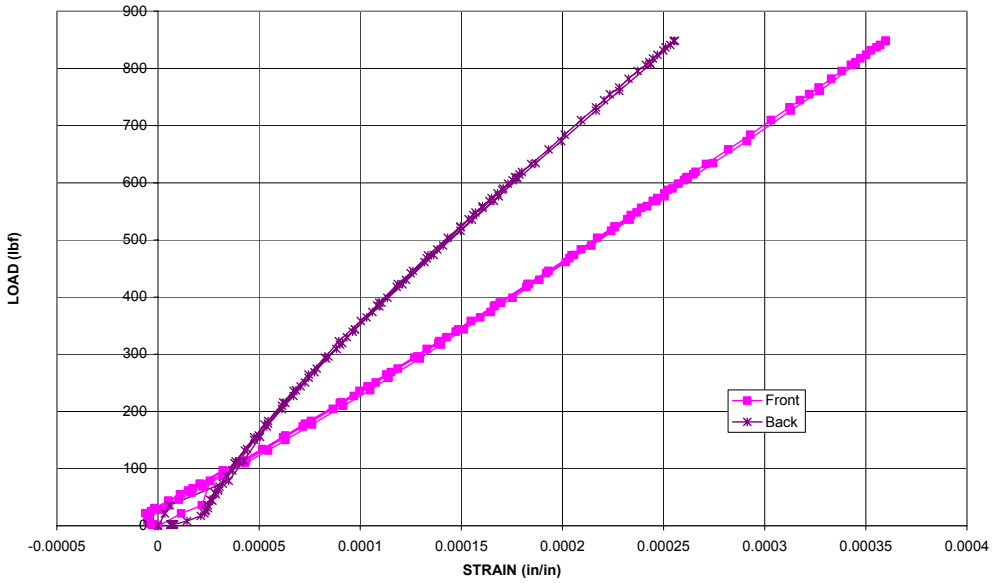

Figure A.1: Load vs. Strain Data for SCG-1S; Calibration

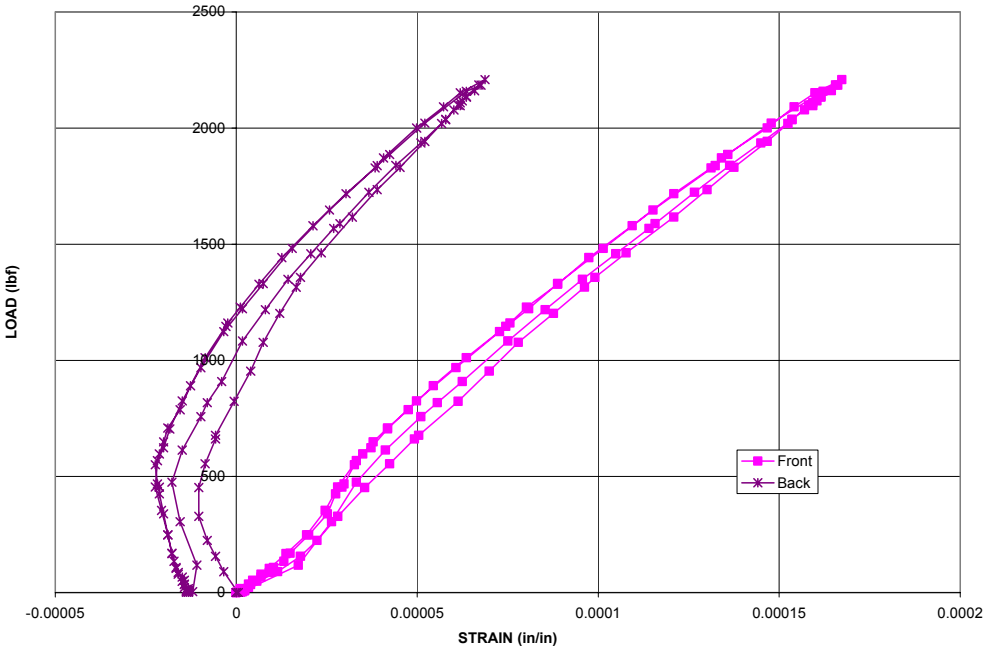

Figure A.2: Load vs. Strain Data for SCG-1S; 0 Cycles

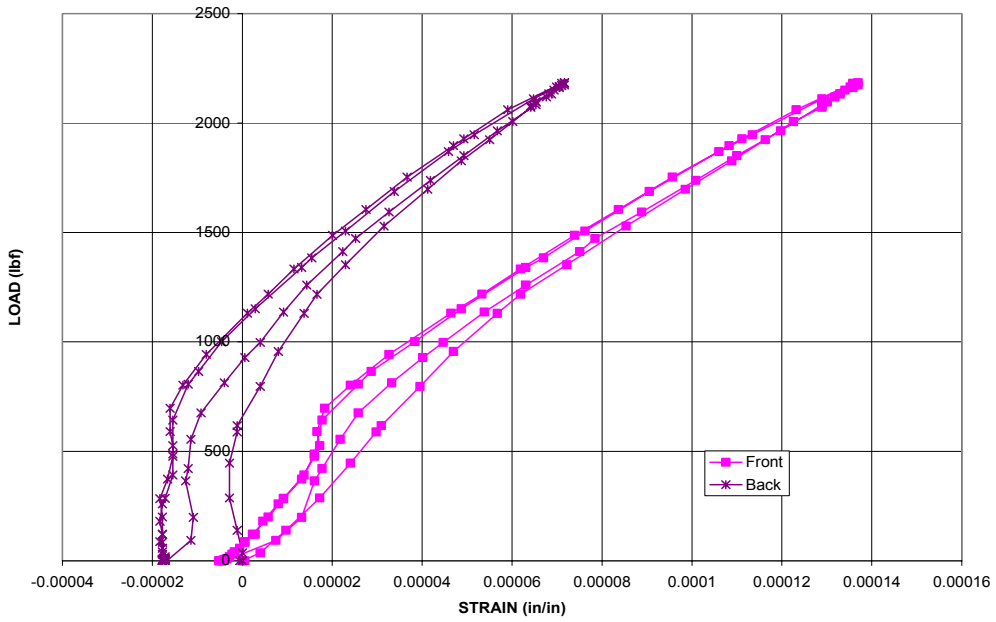

Figure A.3: Load vs. Strain Data for SCG-1S; 2.2K Cycles

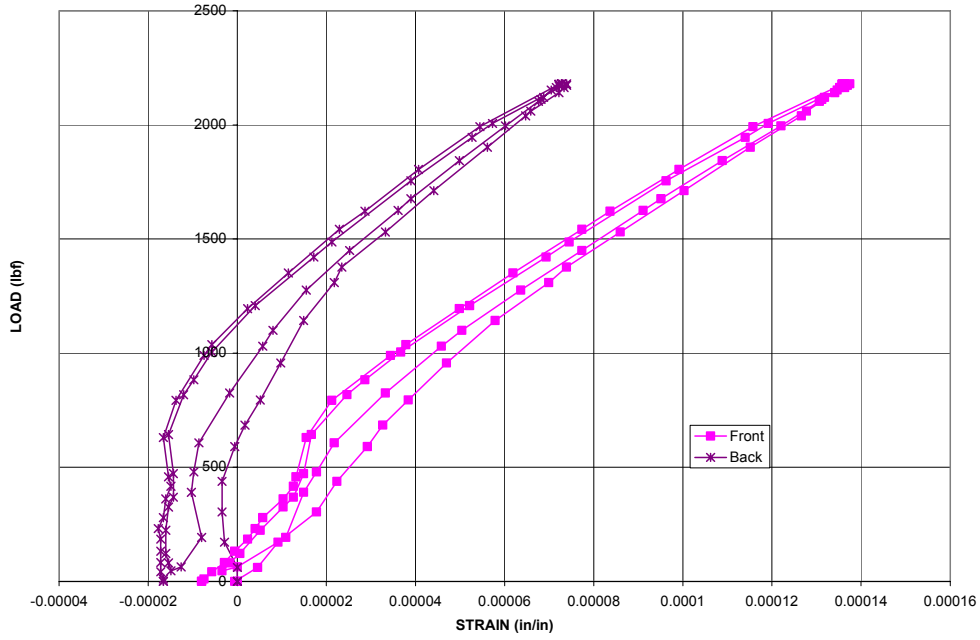

Figure A.4: Load vs. Strain Data for SCG-1S; 4.2K Cycles

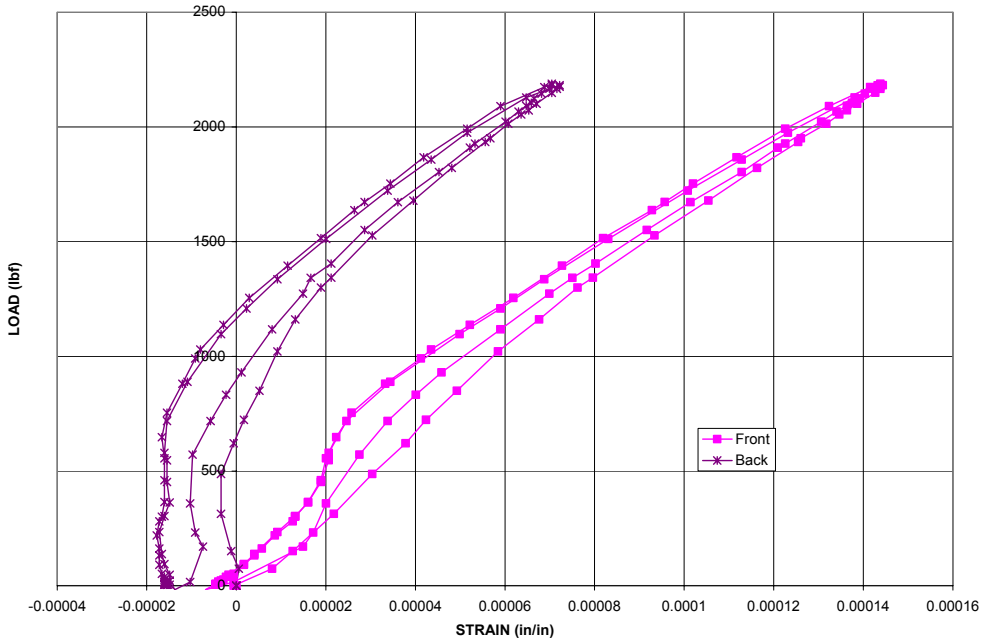

Figure A.5: Load vs. Strain Data for SCG-1S; 9.4K Cycles

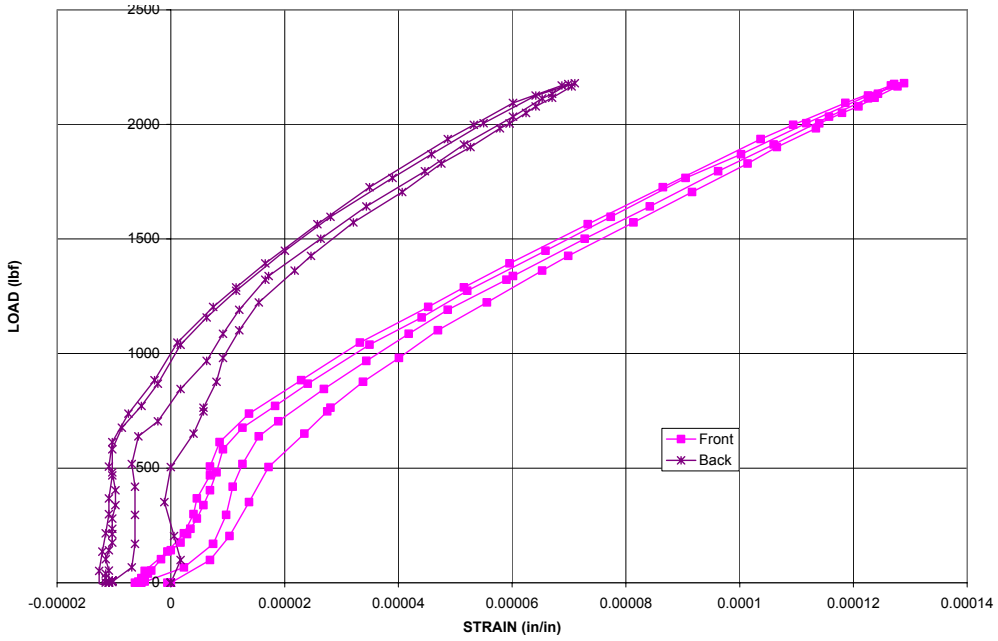

Figure A.6: Load vs. Strain Data for SCG-1S; 19.8K Cycles

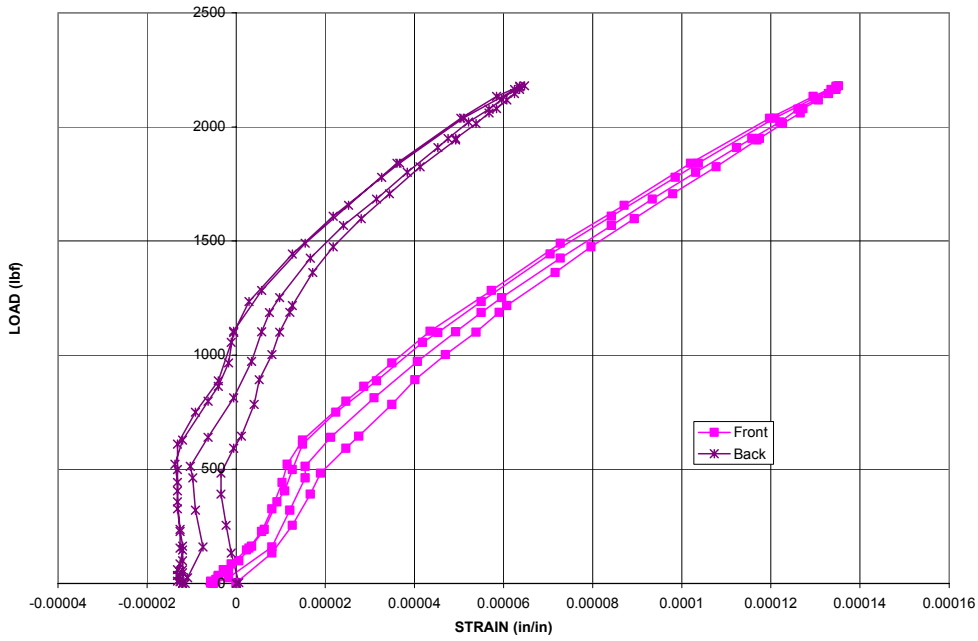

Figure A.7: Load vs. Strain Data for SCG-1S; 25.8K Cycles

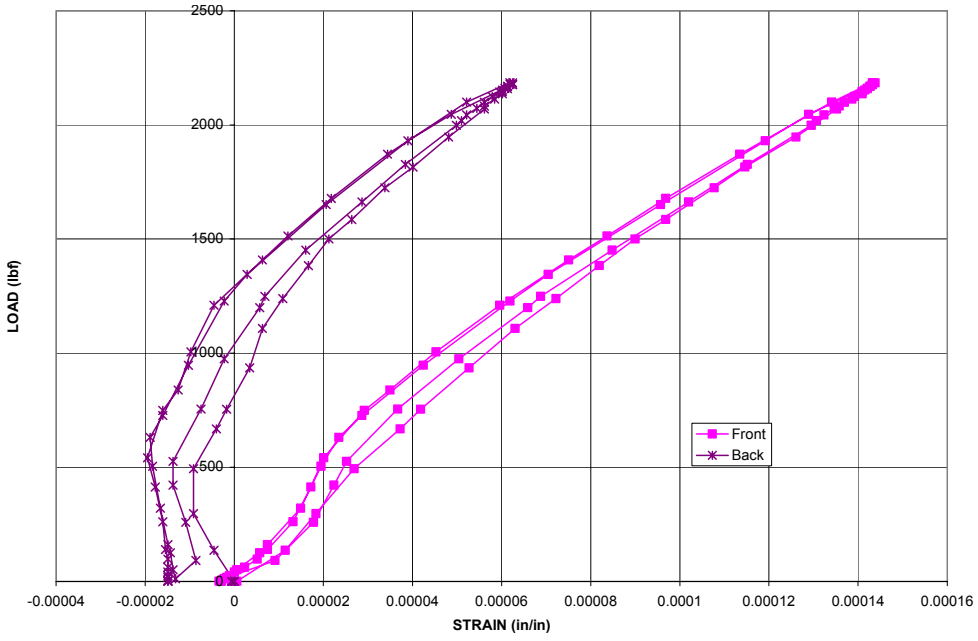

Figure A.8: Load vs. Strain Data for SCG-1S; 31.8K Cycles

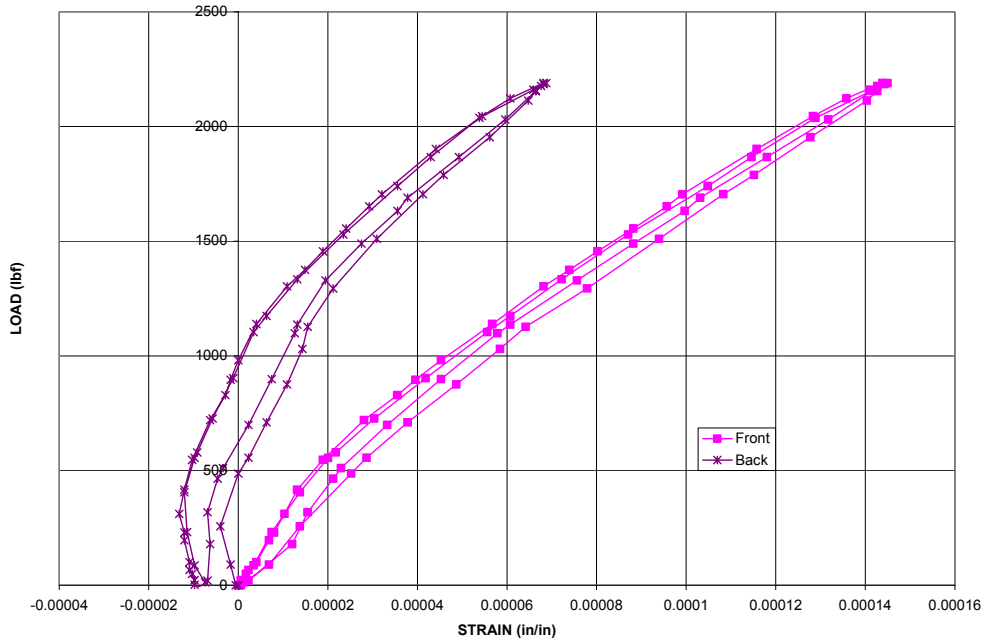

Figure A.9: Load vs. Strain Data for SCG-1S; 37.8K Cycles

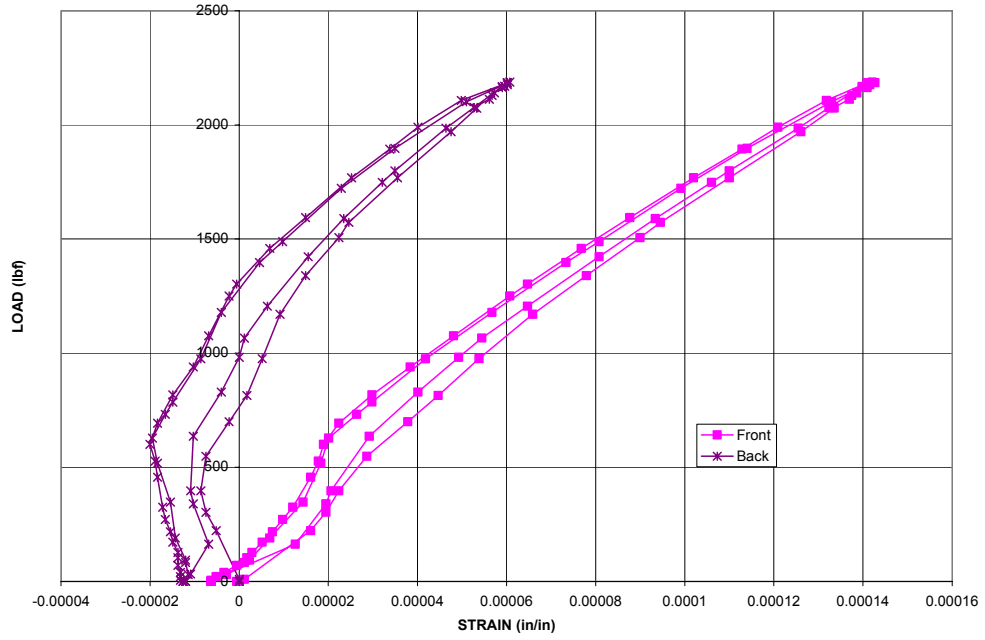

Figure A.10: Load vs. Strain Data for SCG-1S; 43.8K Cycles

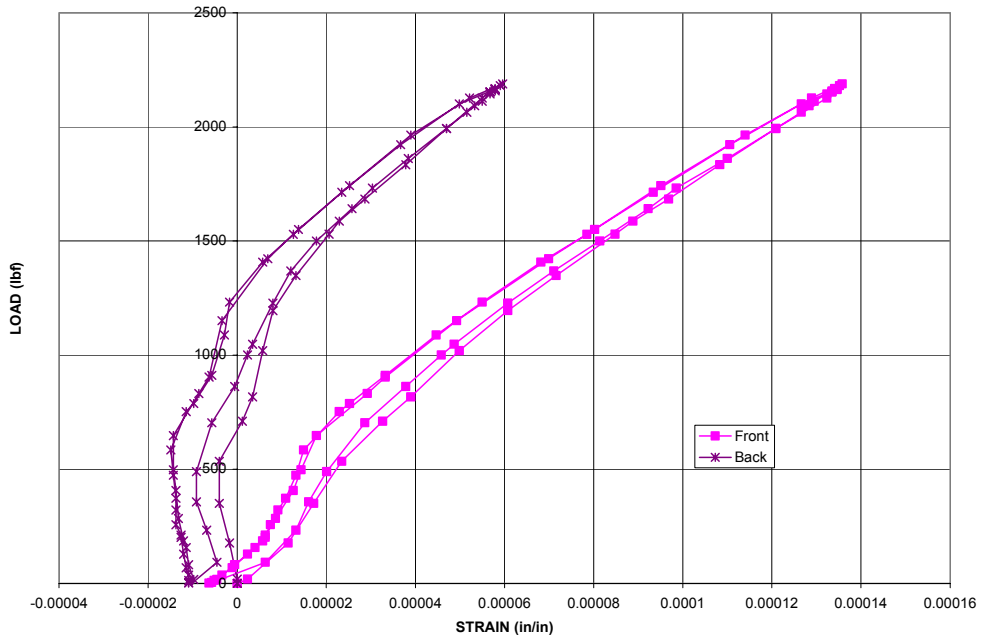

Figure A.11: Load vs. Strain Data for SCG-1S; 51.8K Cycles

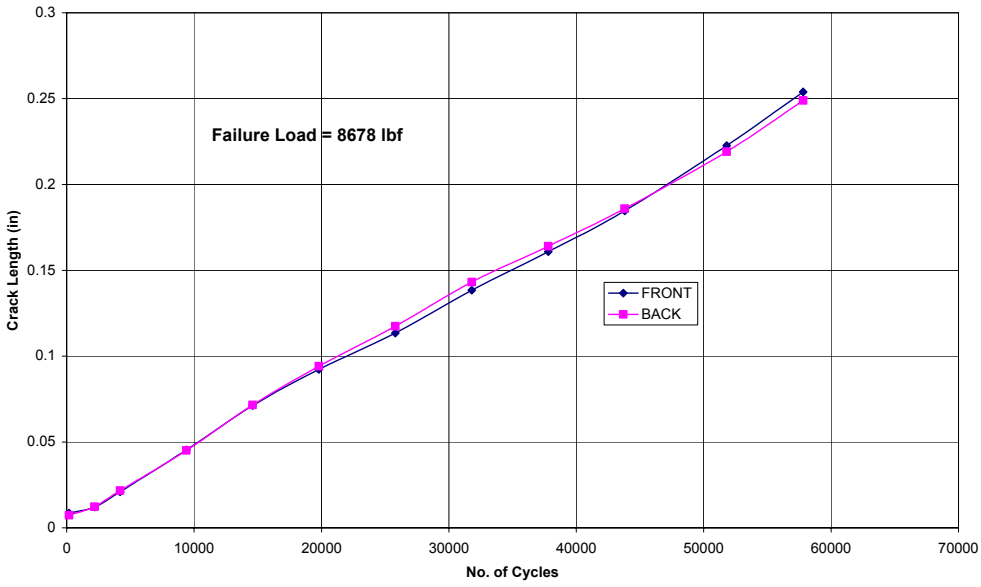

Figure A.12: Crack Length vs. Cycles for SCG-1S

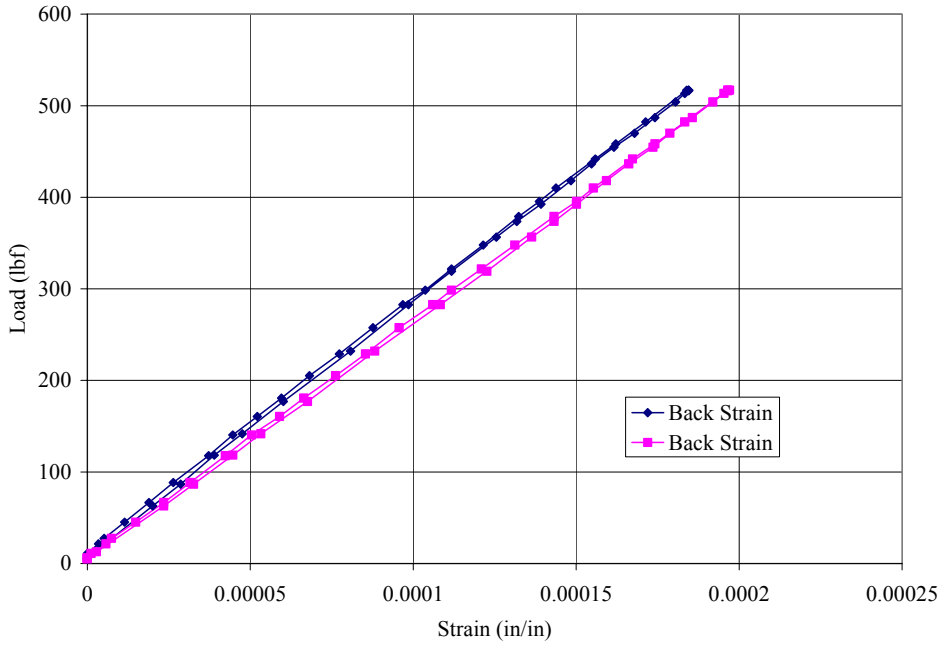

A.13: Load vs. Strain Data for SCG-2; Calibration

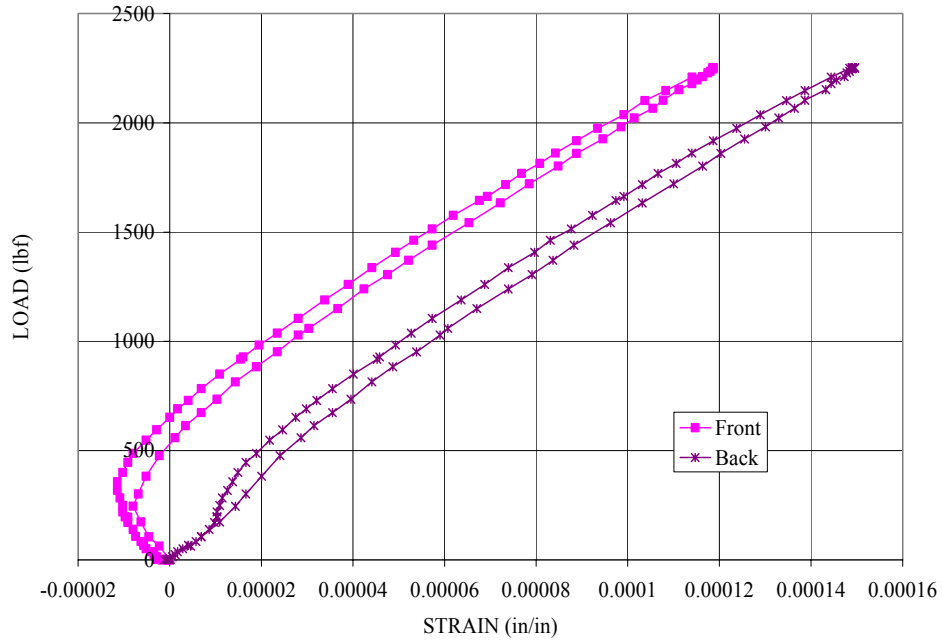

Figure A.14: Load vs. Strain Data for SCG-2; 0 Cycles

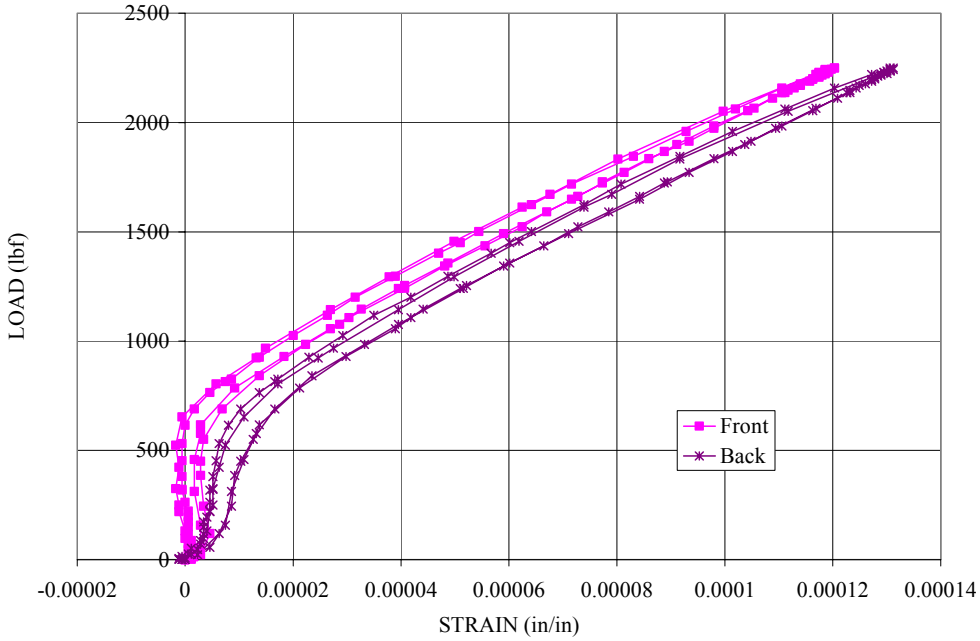

Figure A.15: Load vs. Strain Data for SCG-2; 2K Cycles

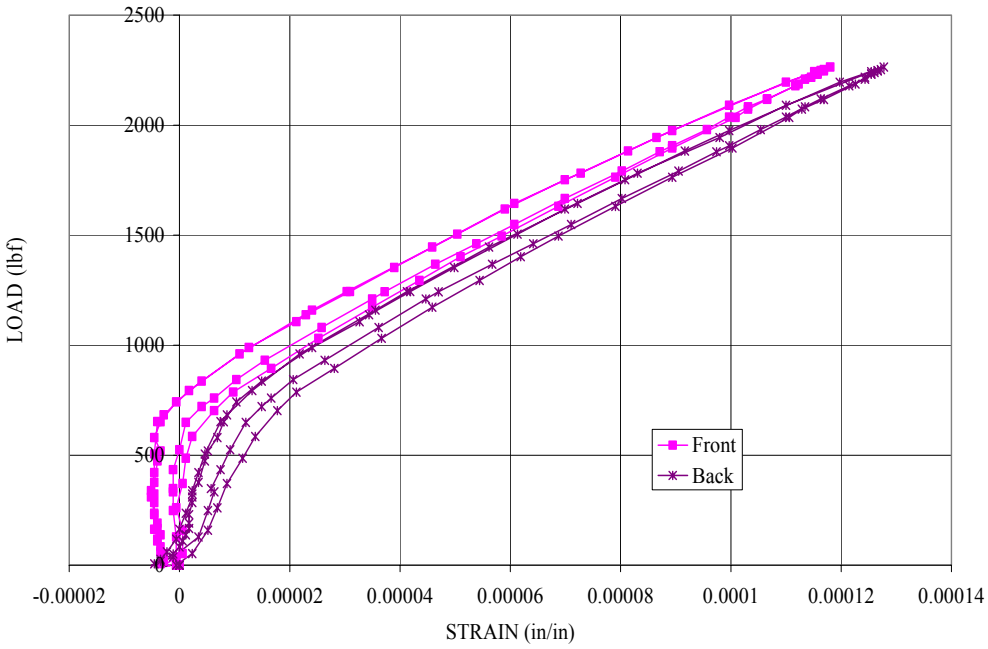

Figure A.16: Load vs. Strain Data for SCG-2; 4K Cycles

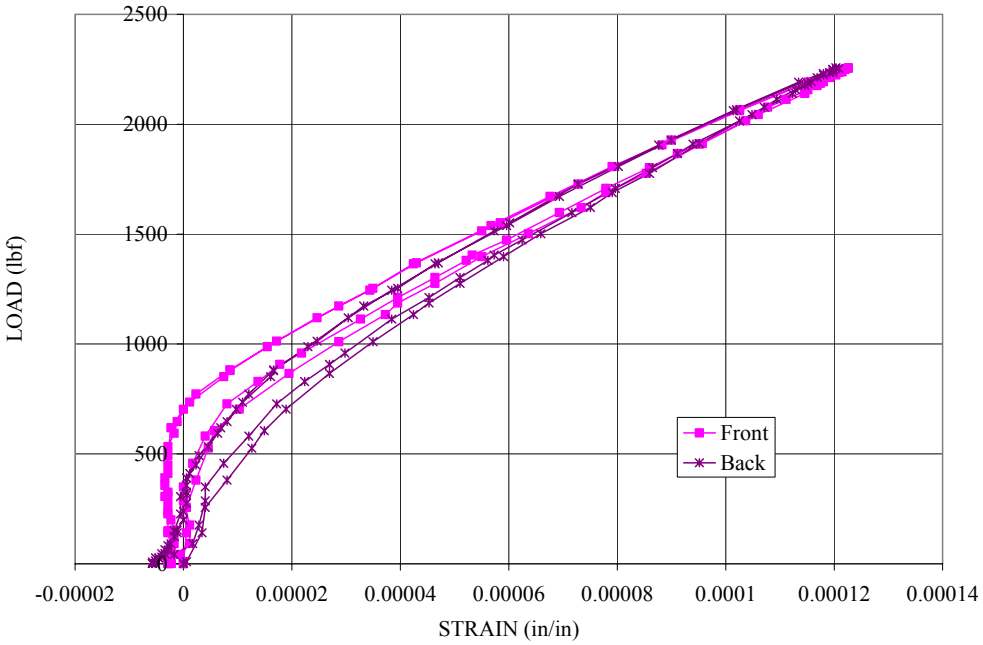

Figure A.17: Load vs. Strain Data for SCG-2; 6K Cycles

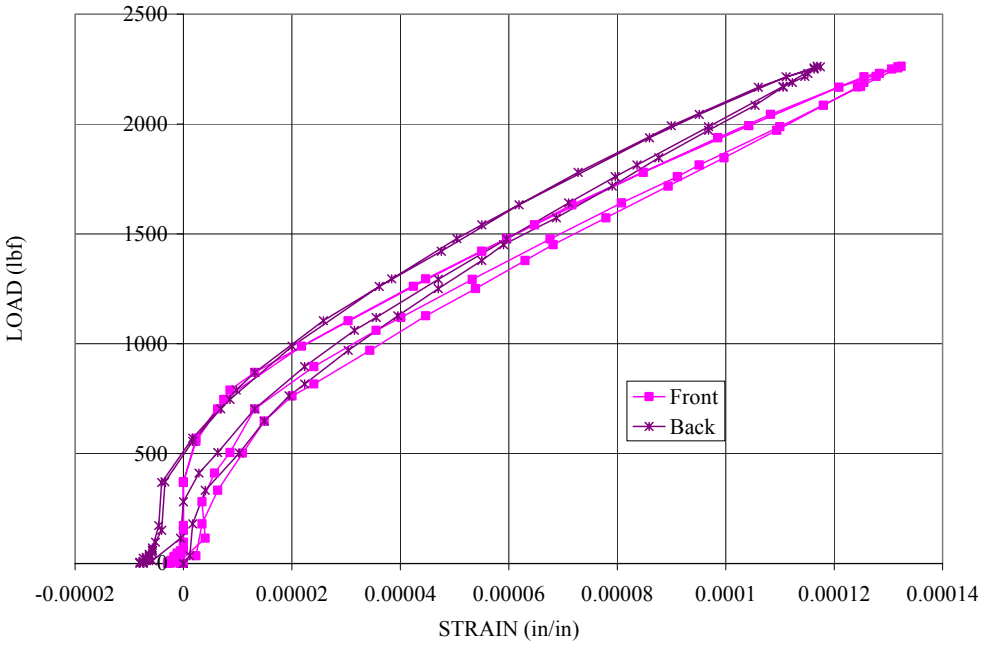

Figure A.18: Load vs. Strain Data for SCG-2; 8K Cycles

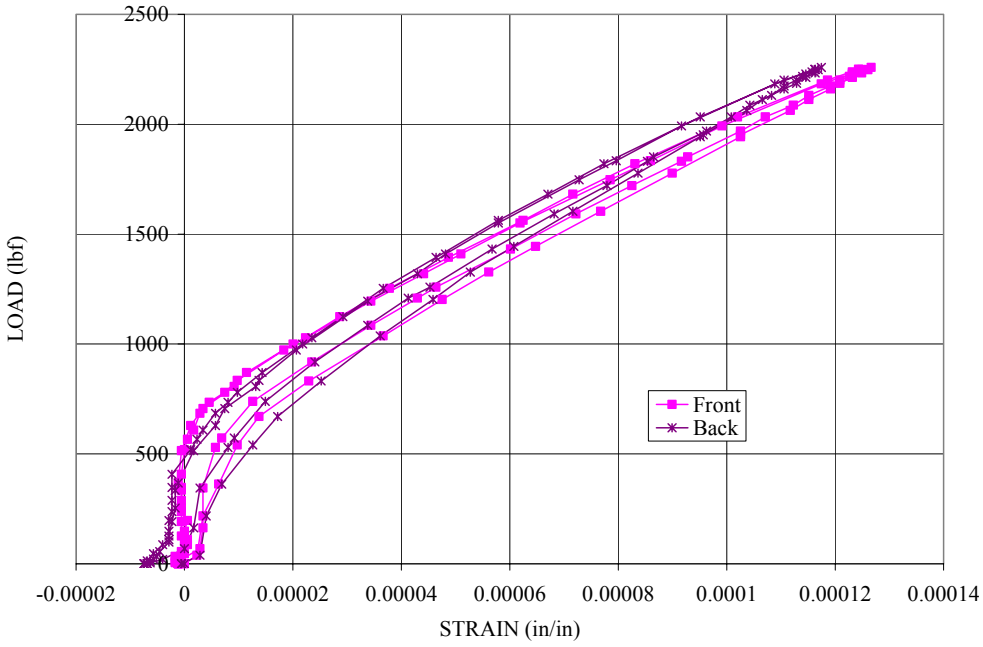

Figure A.19: Load vs. Strain Data for SCG-2; 10K Cycles

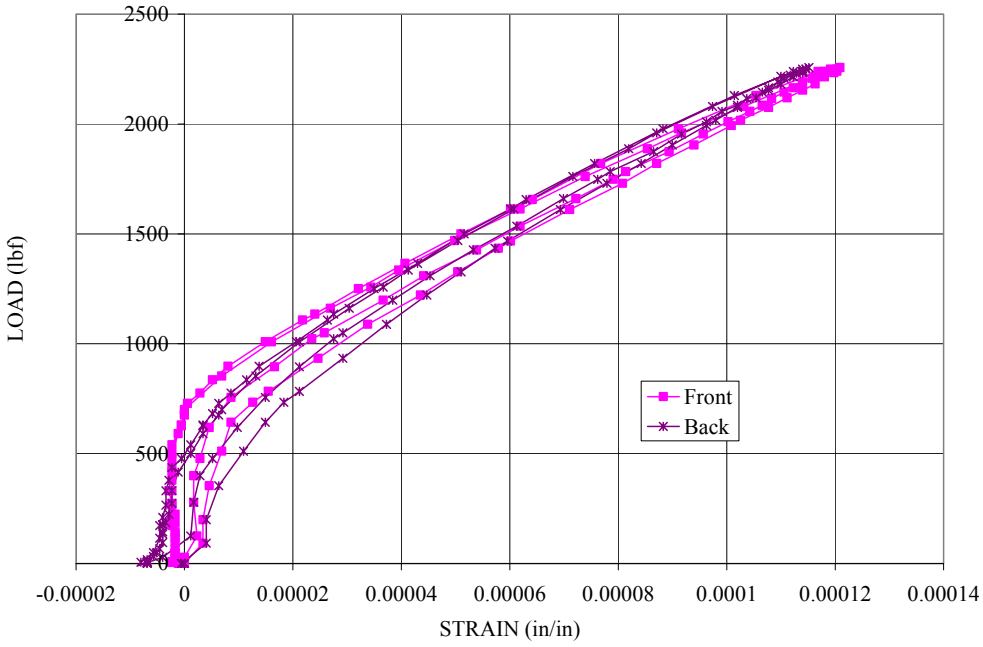

Figure A.20: Load vs. Strain Data for SCG-2; 12K Cycles

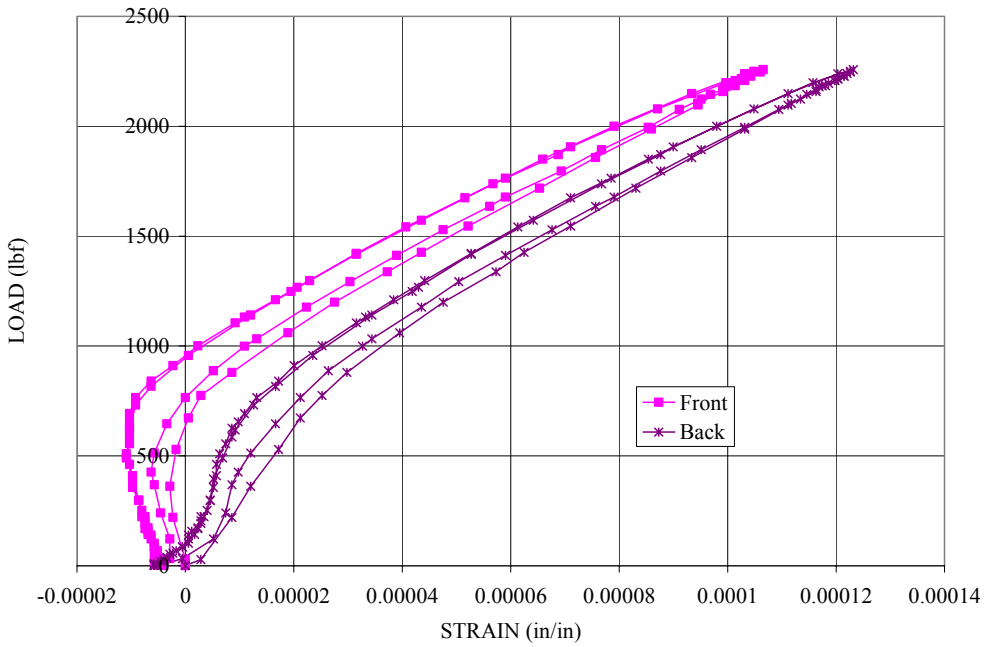

Figure A.21: Load vs. Strain Data for SCG-2; 14K Cycles

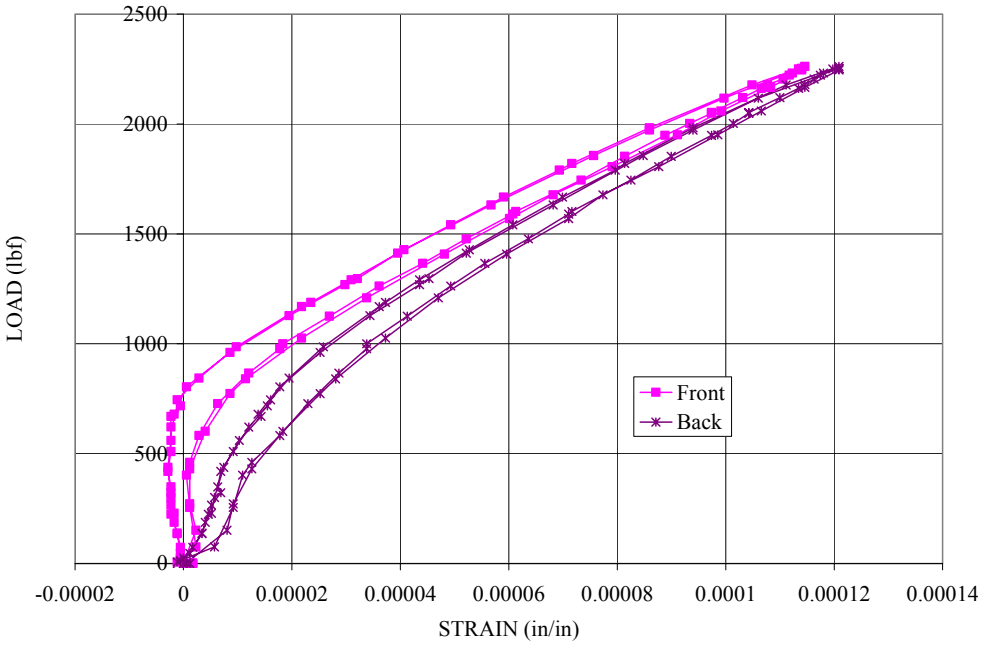

Figure A.22: Load vs. Strain Data for SCG-2; 20K Cycles

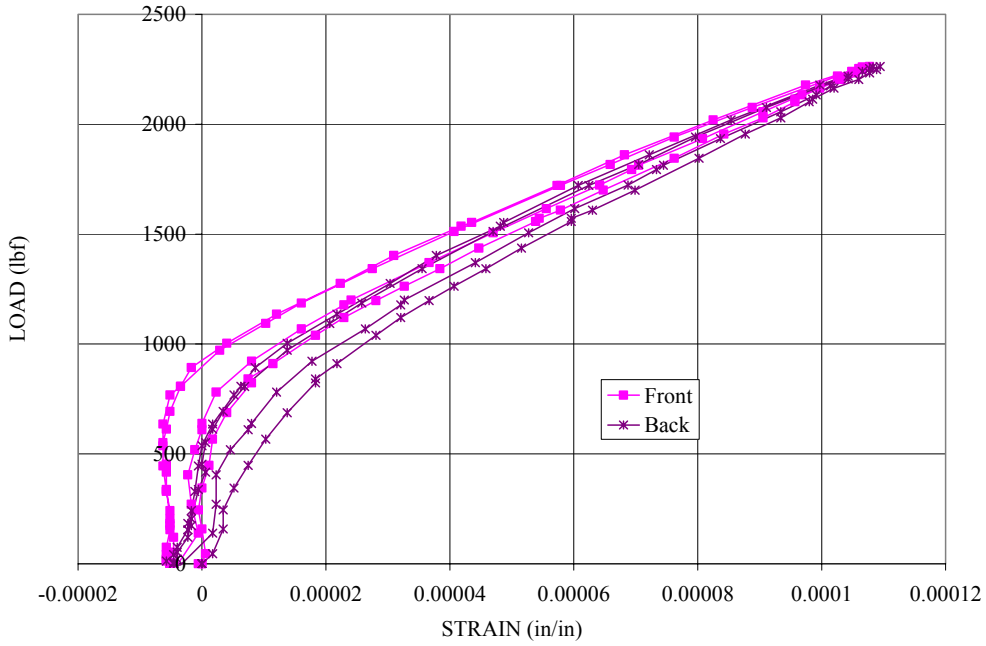

Figure A.23: Load vs. Strain Data for SCG-2; 26K Cycles

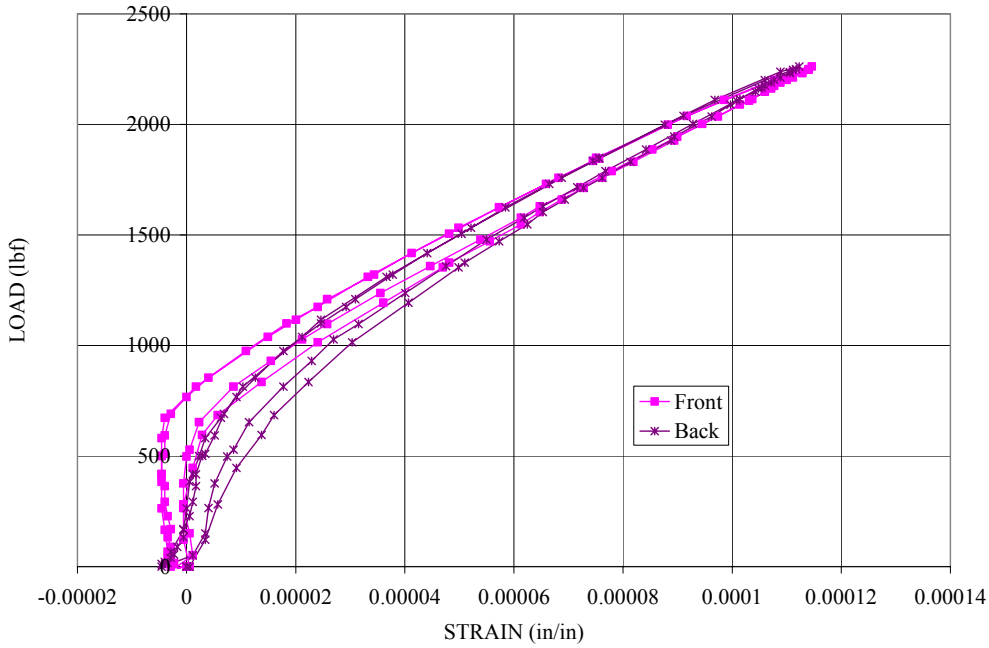

Figure A.24: Load vs. Strain Data for SCG-2; 32K Cycles

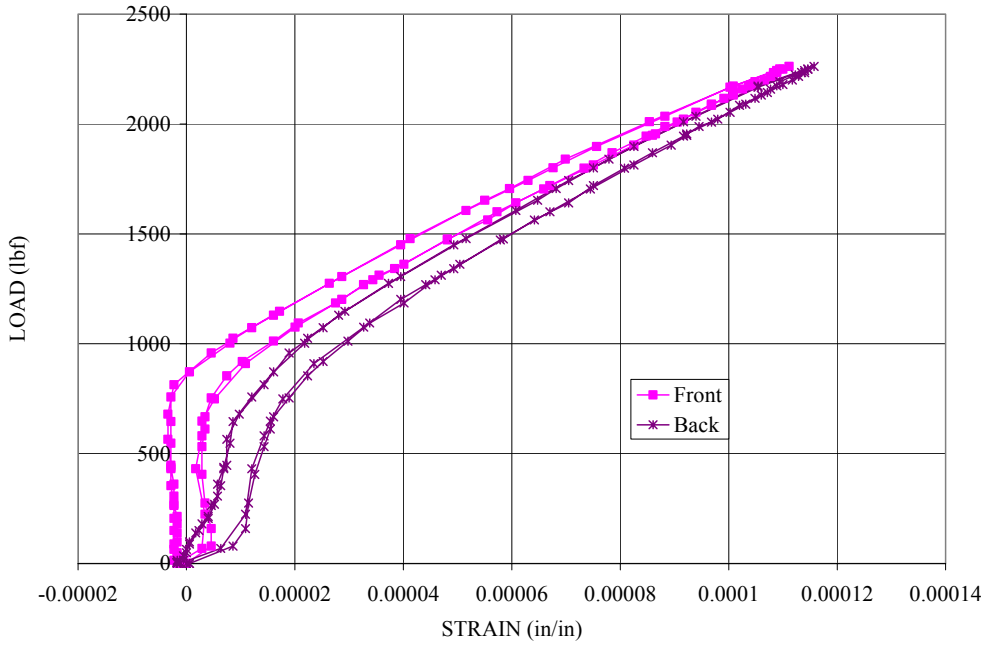

Figure A.25: Load vs. Strain Data for SCG-2; 38K Cycles

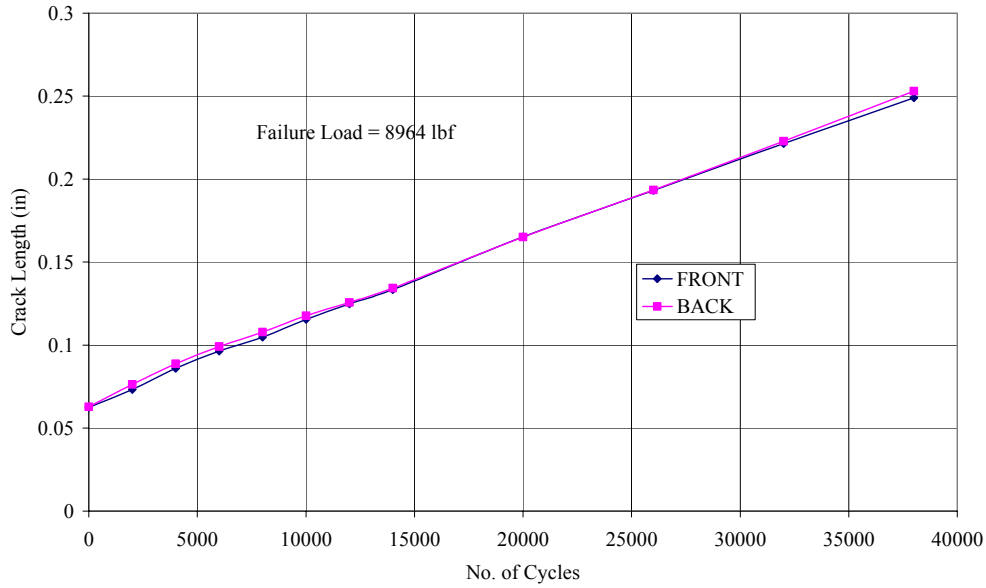

Figure A.26: Crack Length vs. Cycles for SCG-2

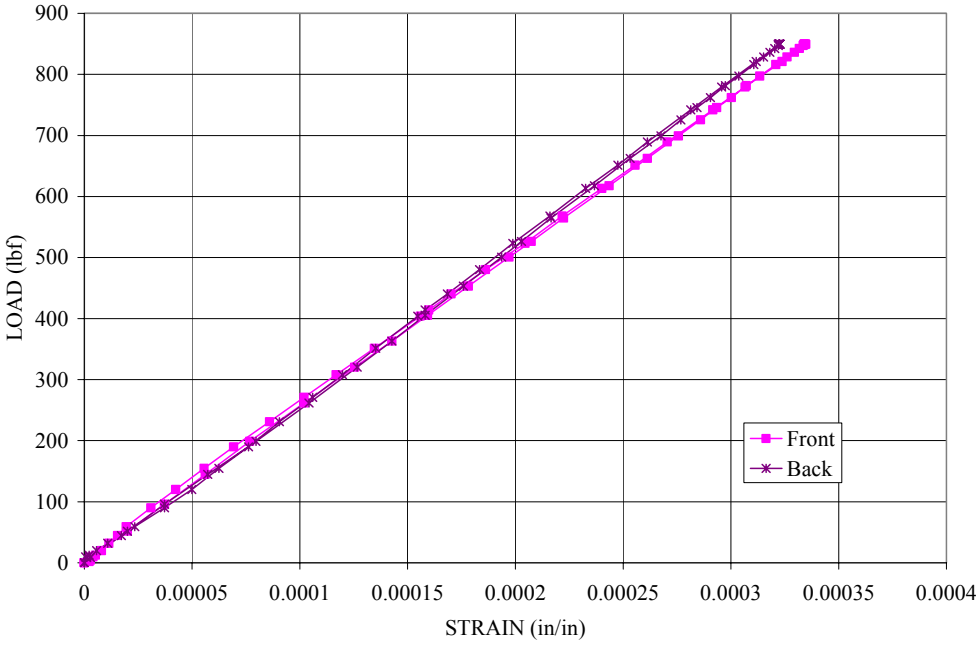

Figure A.27: Load vs. Strain Data for SCG-5; Calibration

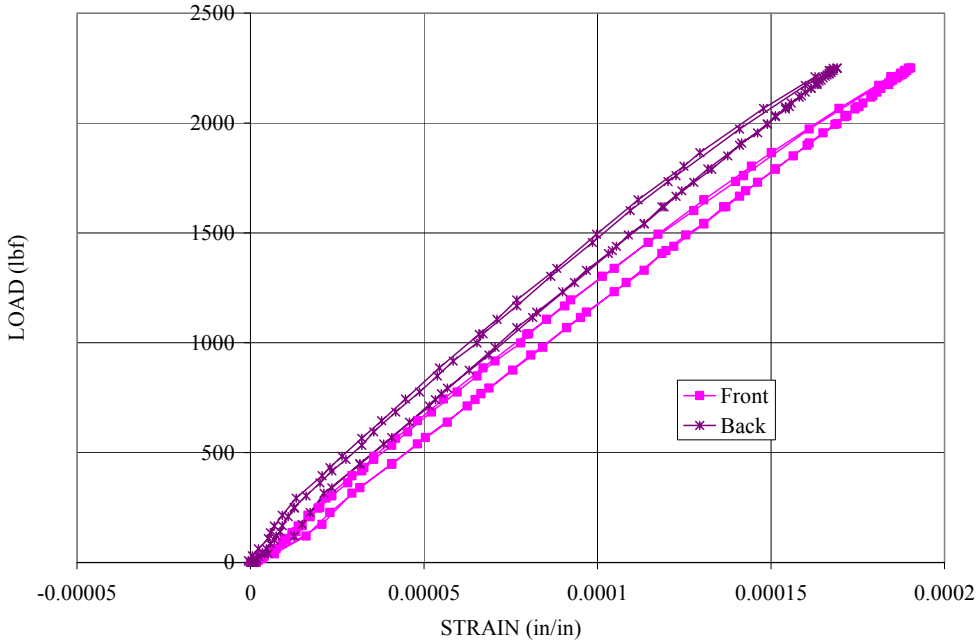

Figure A.27: Load vs. Strain Data for SCG-5; 0 Cycles

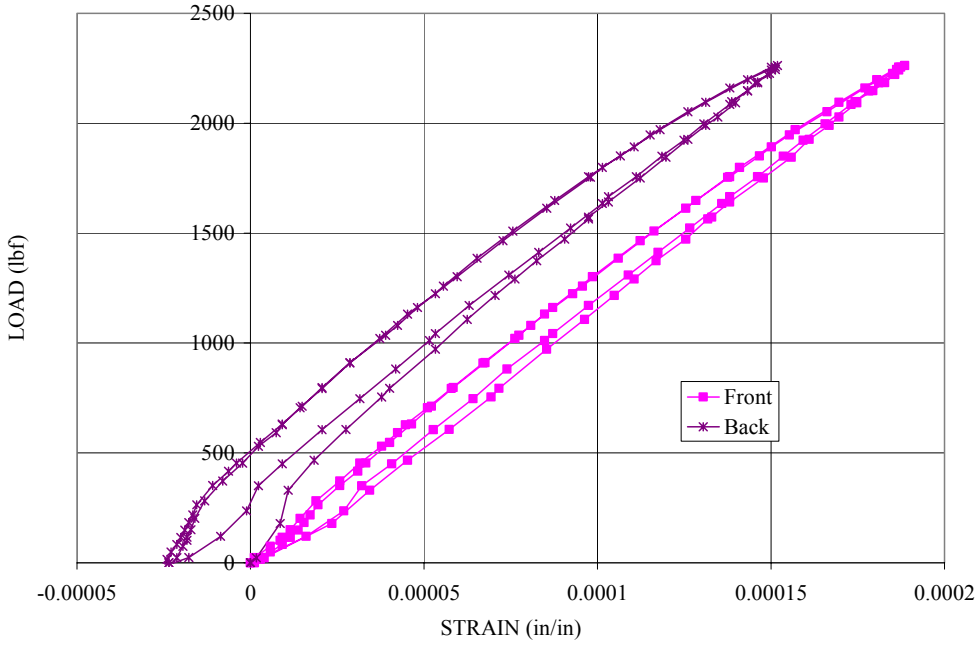

Figure A.29: Load vs. Strain Data for SCG-5; 500 Cycles

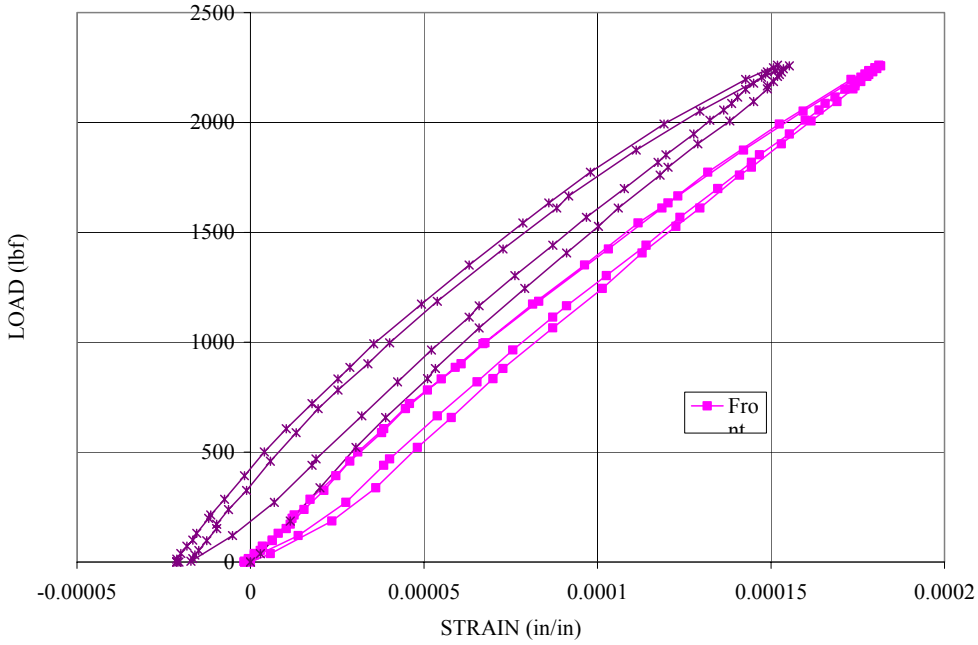

Figure A.30: Load vs. Strain Data for SCG-5; 5.7K Cycles

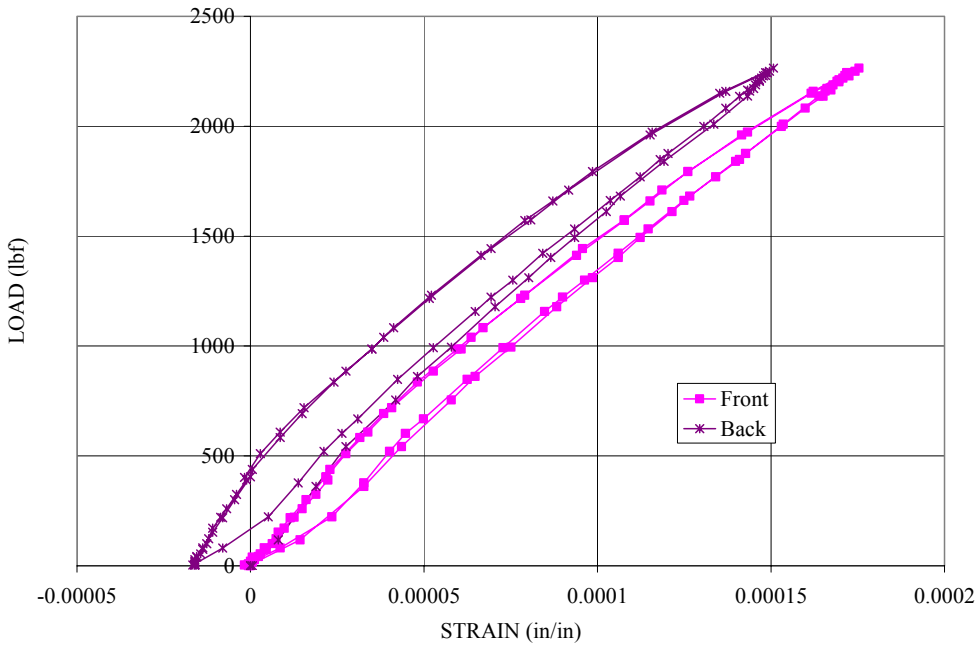

Figure A.31: Load vs. Strain Data for SCG-5; 10.9K Cycles

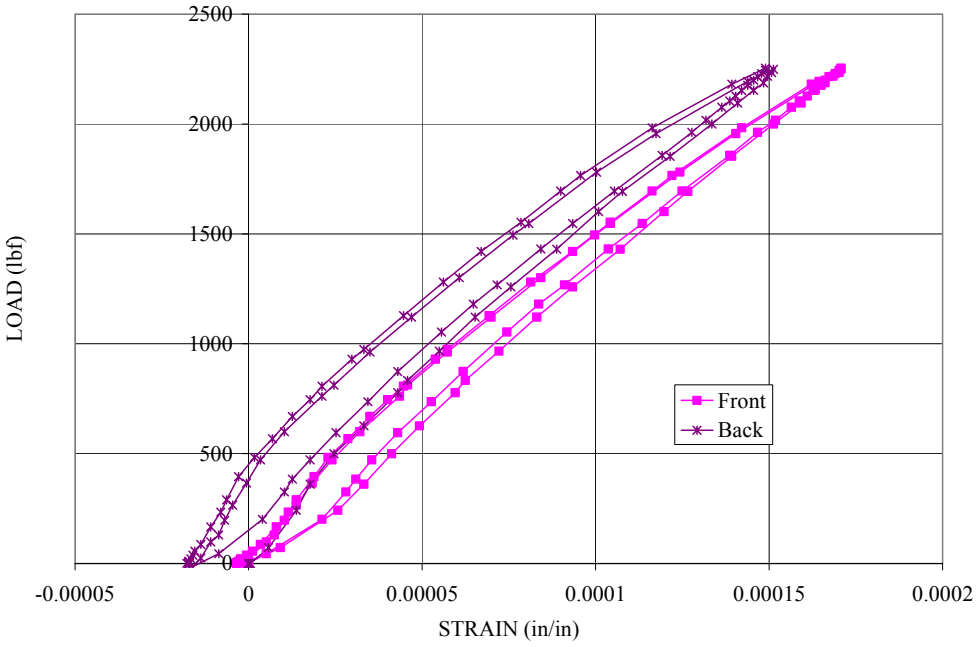

Figure A.32: Load vs. Strain Data for SCG-5; 16.1K Cycles

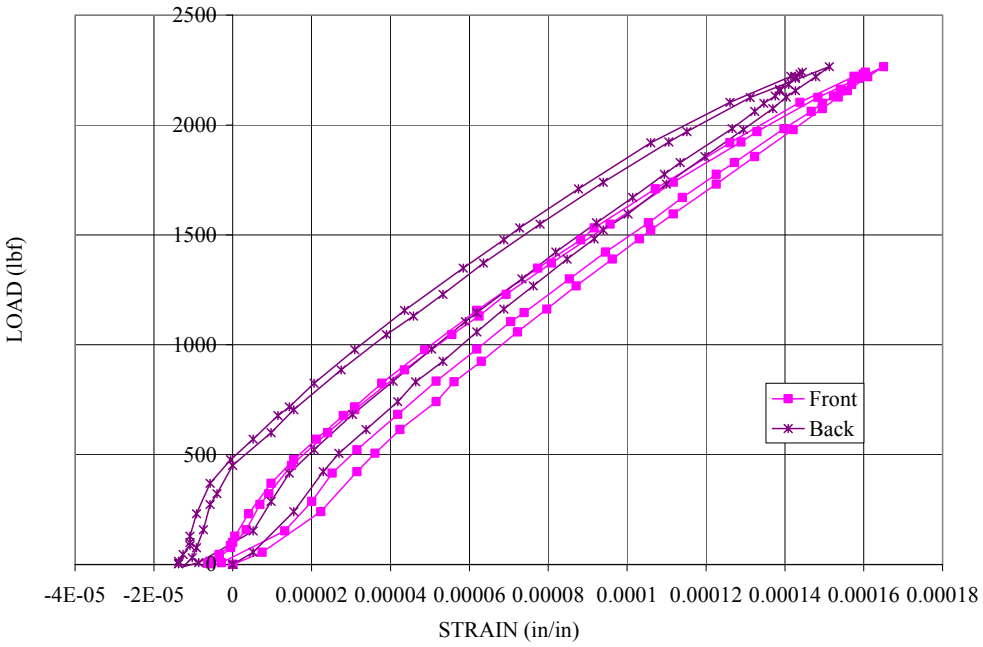

Figure A.33: Load vs. Strain Data for SCG-5; 21.3K Cycles

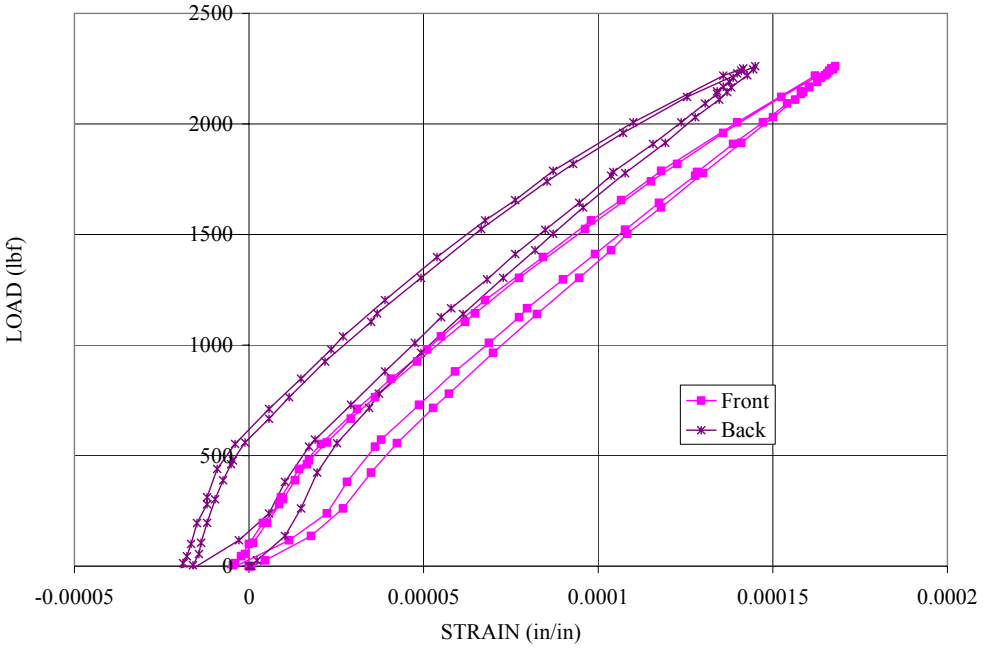

Figure A.34: Load vs. Strain Data for SCG-5; 26.5K Cycles

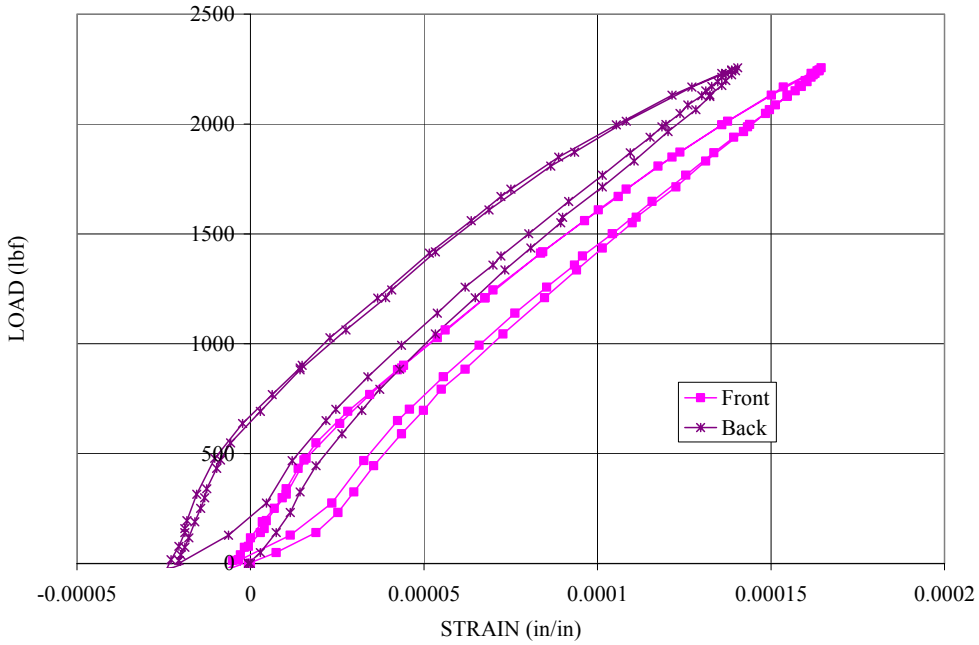

Figure A.35: Load vs. Strain Data for SCG-5; 31.7K Cycles

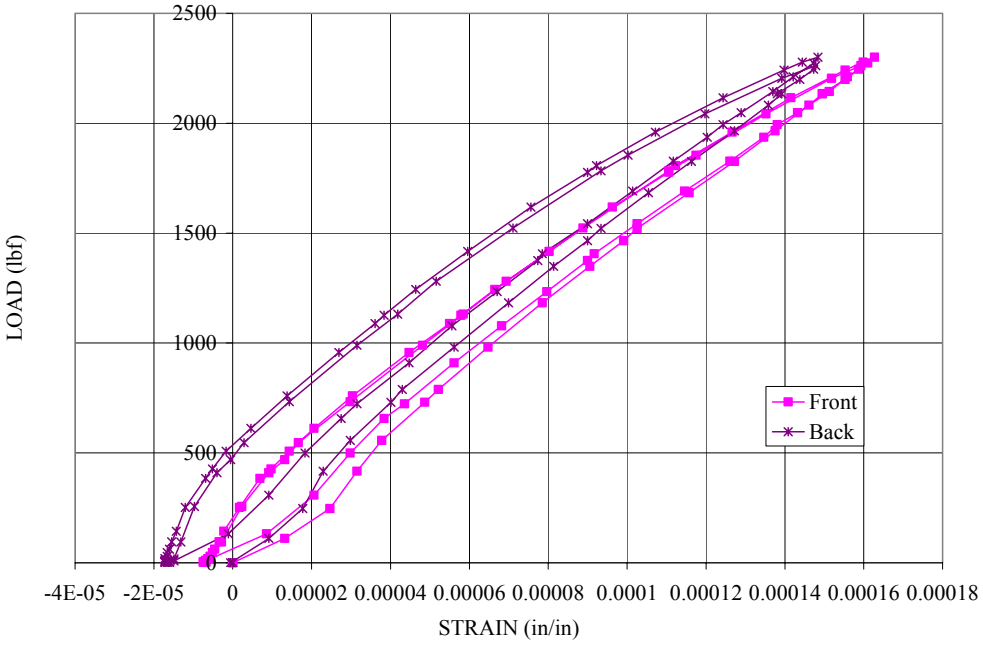

Figure A.36: Load vs. Strain Data for SCG-5; 36.9K Cycles

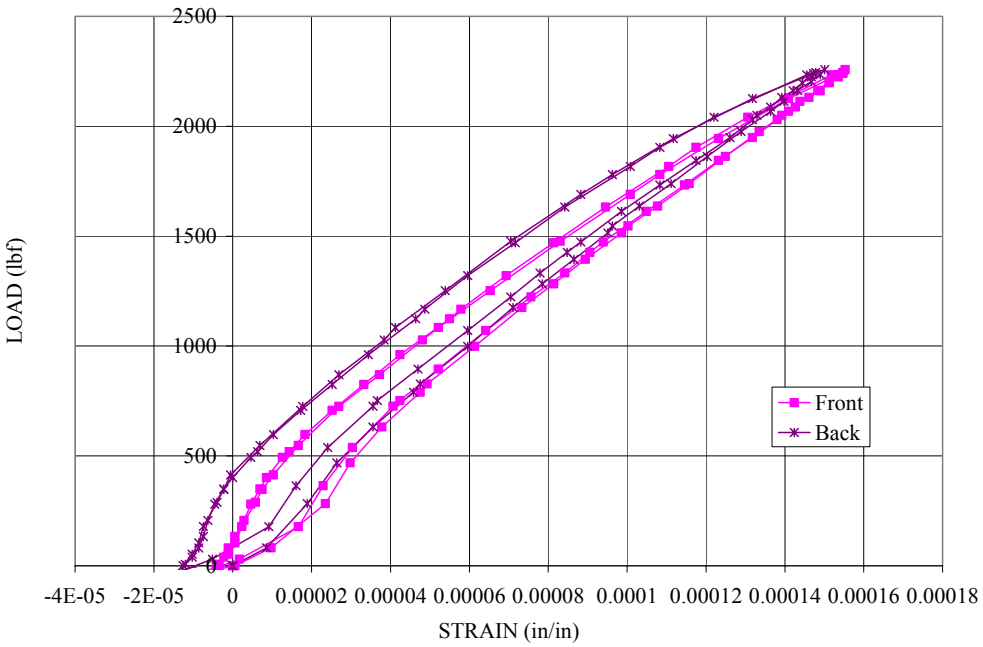

Figure A.37: Load vs. Strain Data for SCG-5; 42.1K Cycles

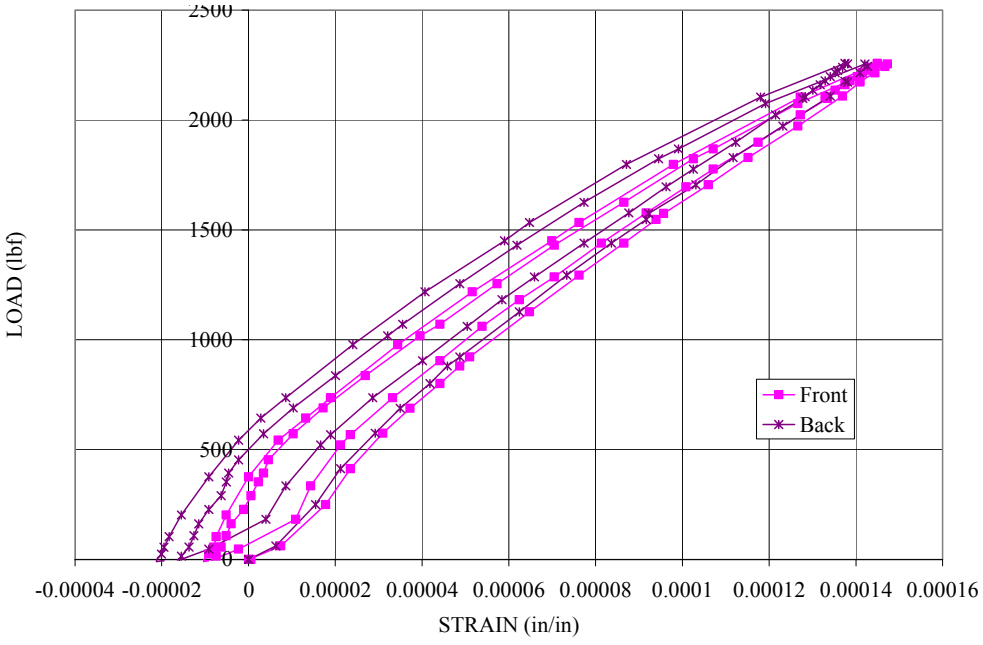

Figure A.38: Load vs. Strain Data for SCG-5; 47.3K Cycles

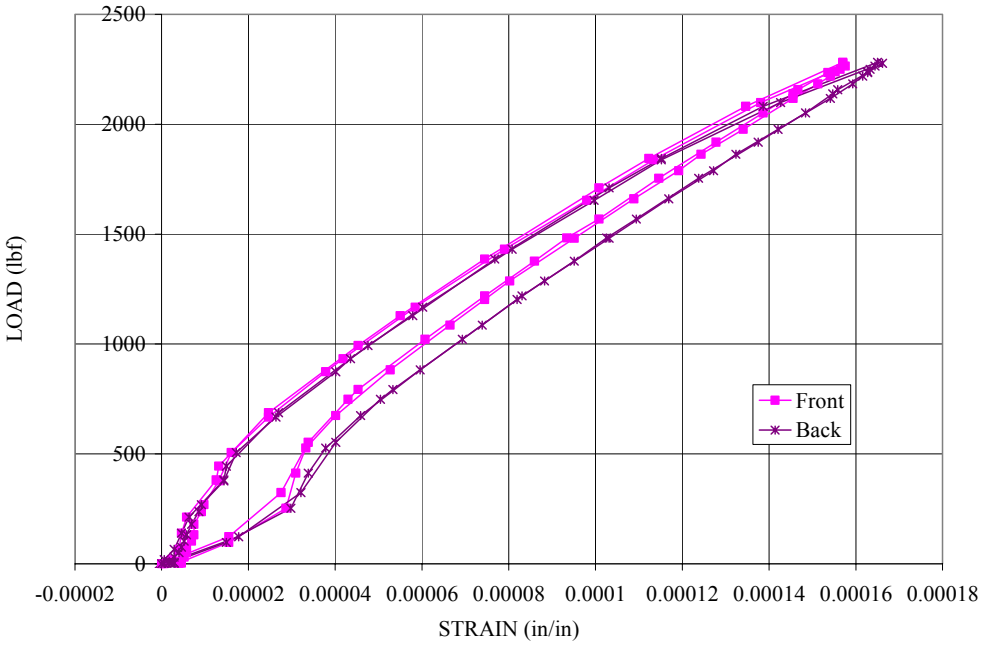

Figure A.39: Load vs. Strain Data for SCG-5; 52.5K Cycles

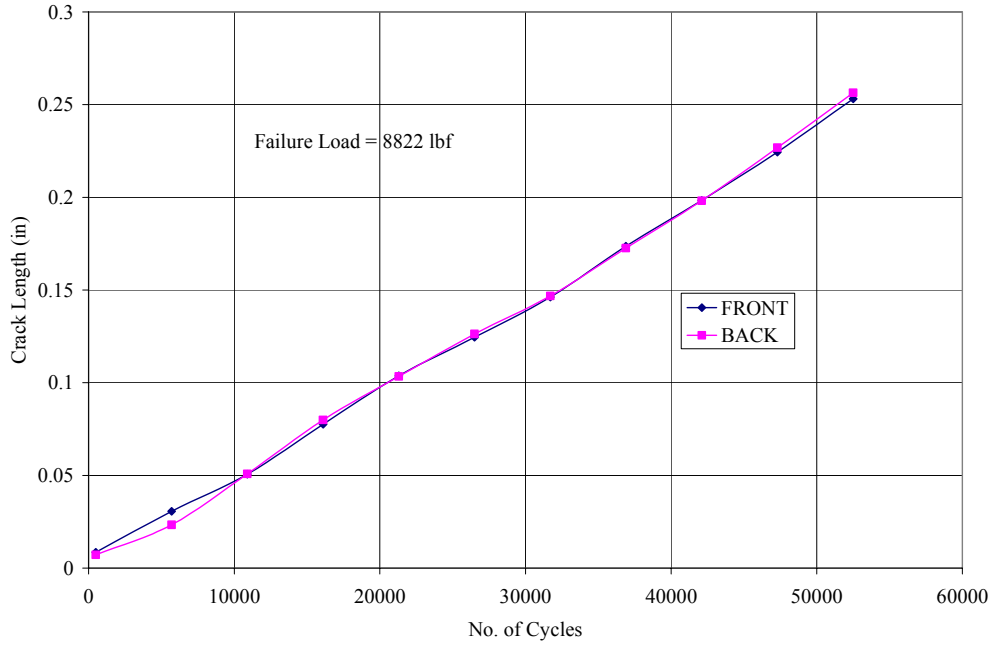

Figure A.40: Crack Length vs. Cycles for SCG-5

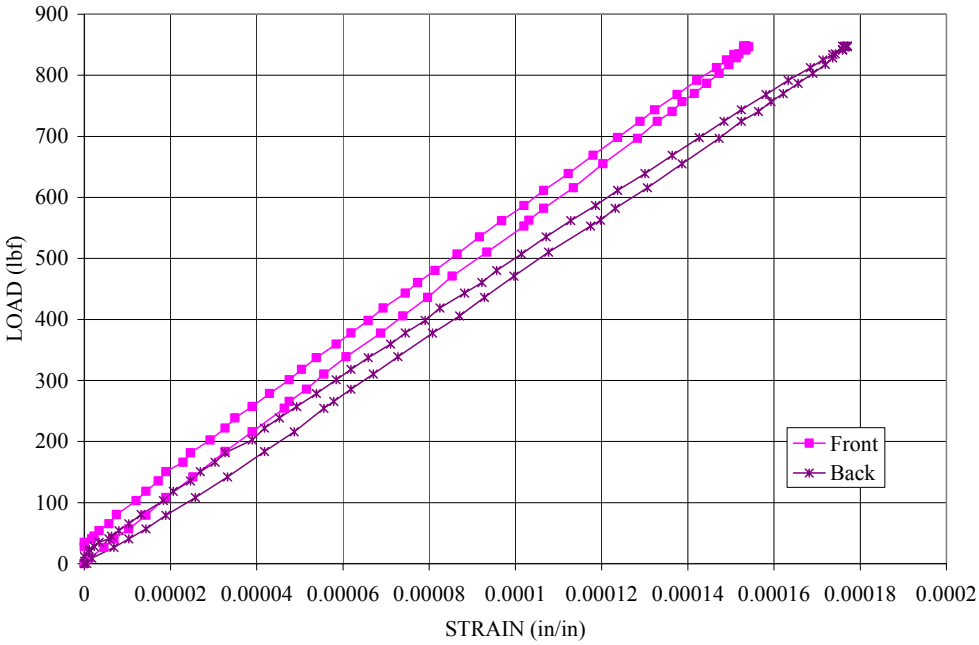

Figure A.41: Load vs. Strain Data for SCG-6; Calibration

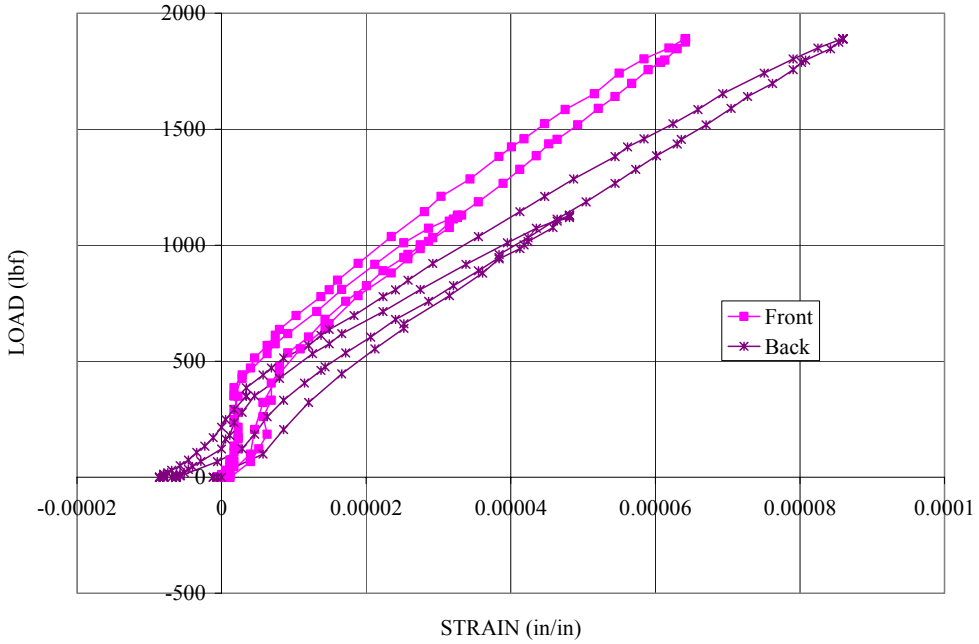

Figure A.42: Load vs. Strain Data for SCG-6; 0 Cycles

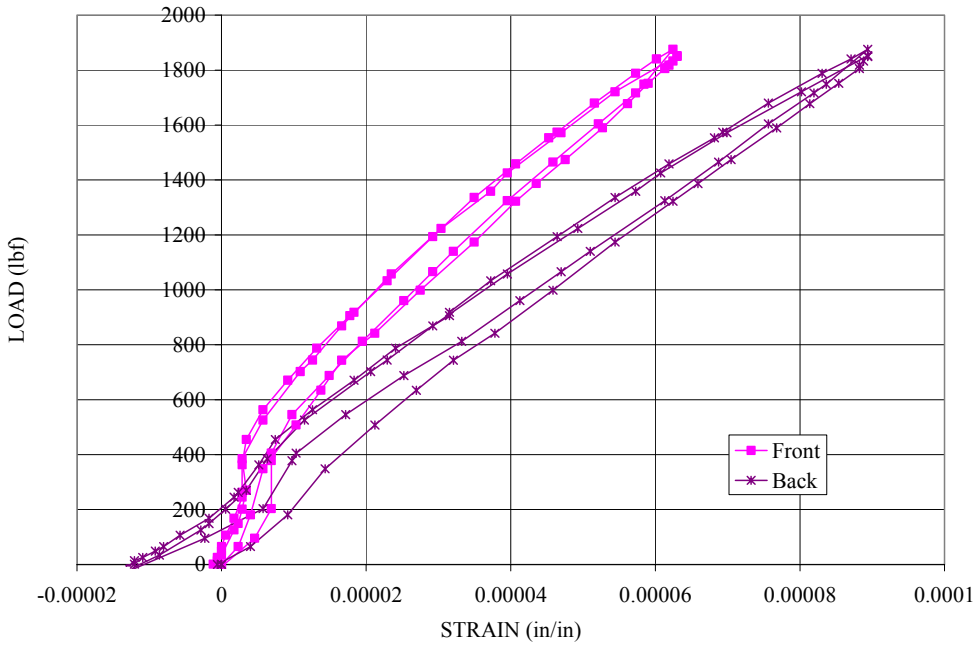

Figure A.43: Load vs. Strain Data for SCG-6; 5.2K Cycles

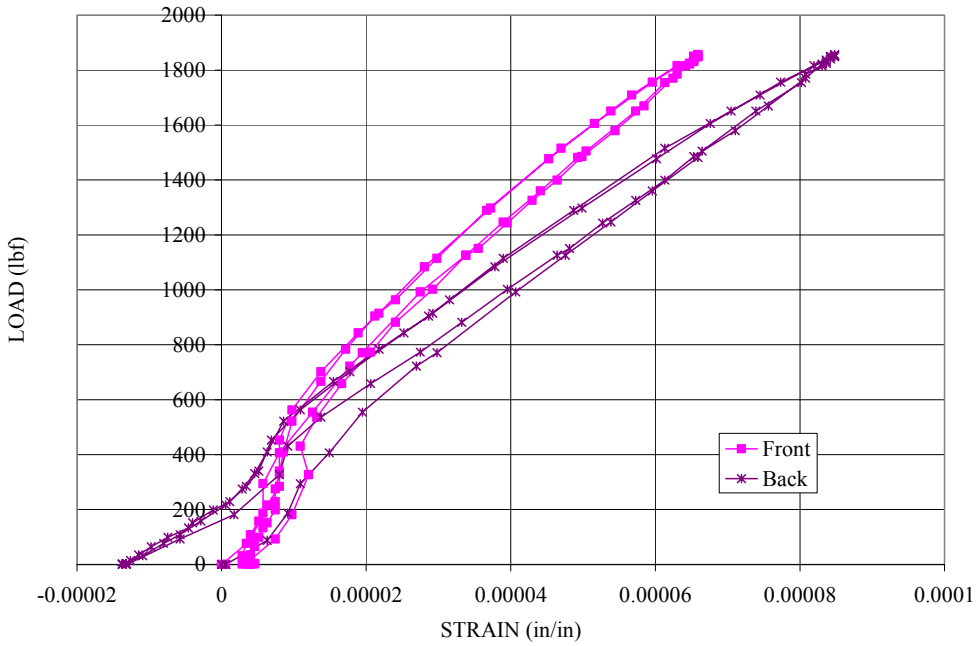

Figure A.44: Load vs. Strain Data for SCG-6; 10.4K Cycles

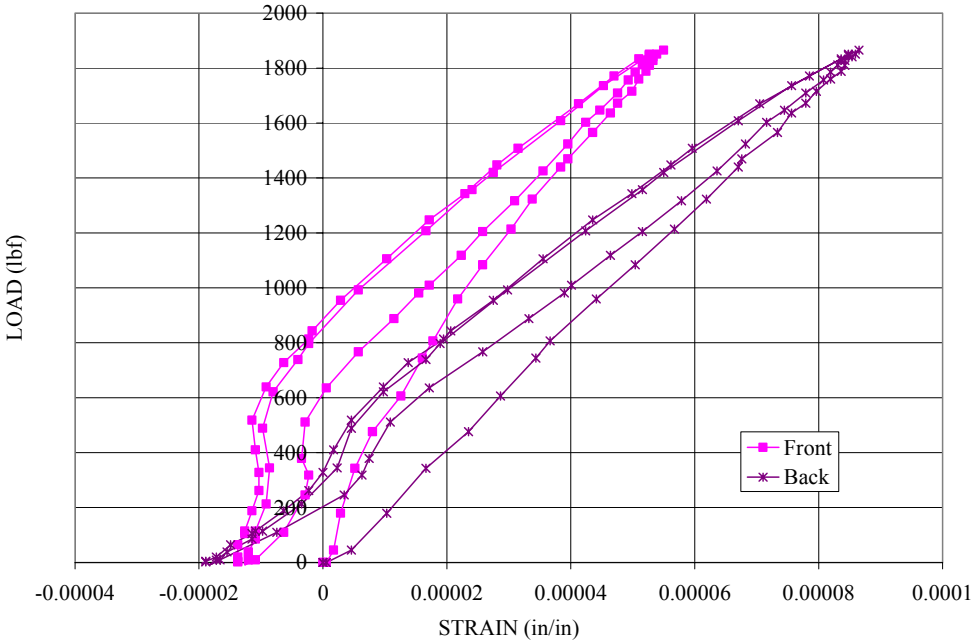

Figure A.45: Load vs. Strain Data for SCG-6; 20.8K Cycles

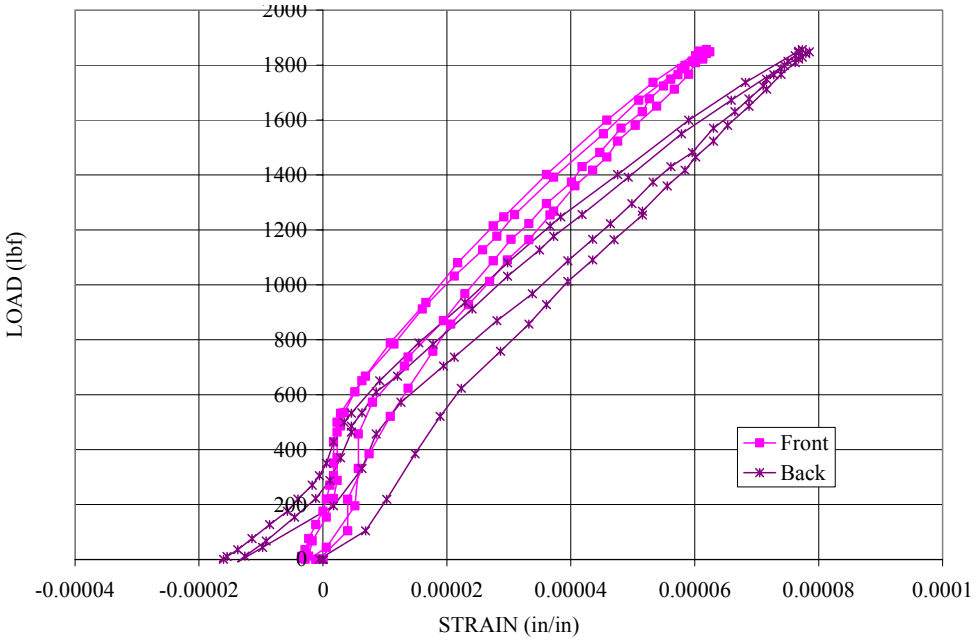

Figure A.46: Load vs. Strain Data for SCG-6; 28.6K Cycles

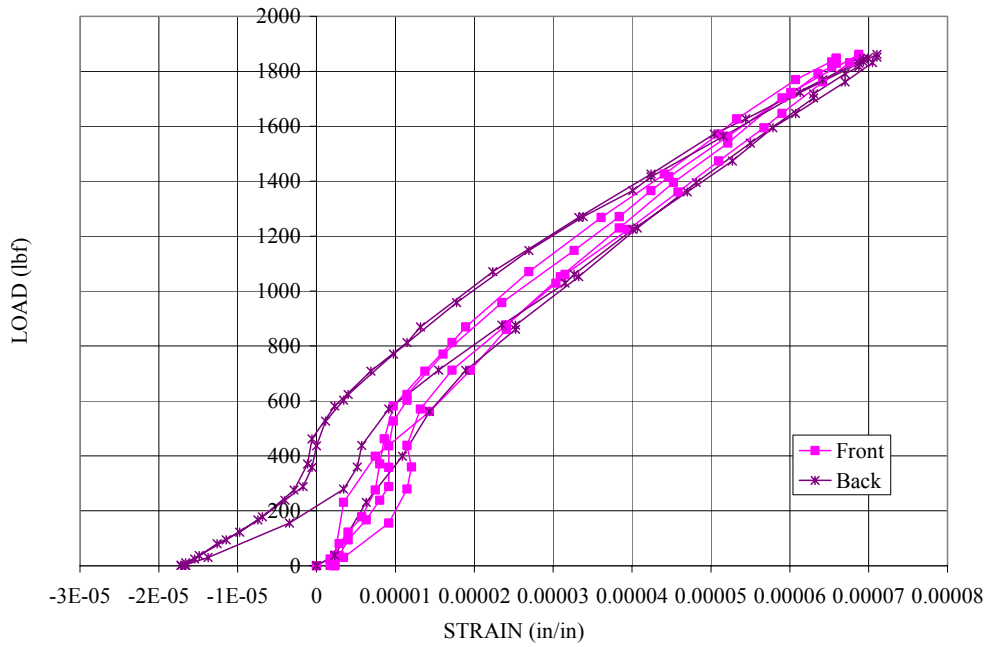

Figure A.47: Load vs. Strain Data for SCG-6; 36.6K Cycles

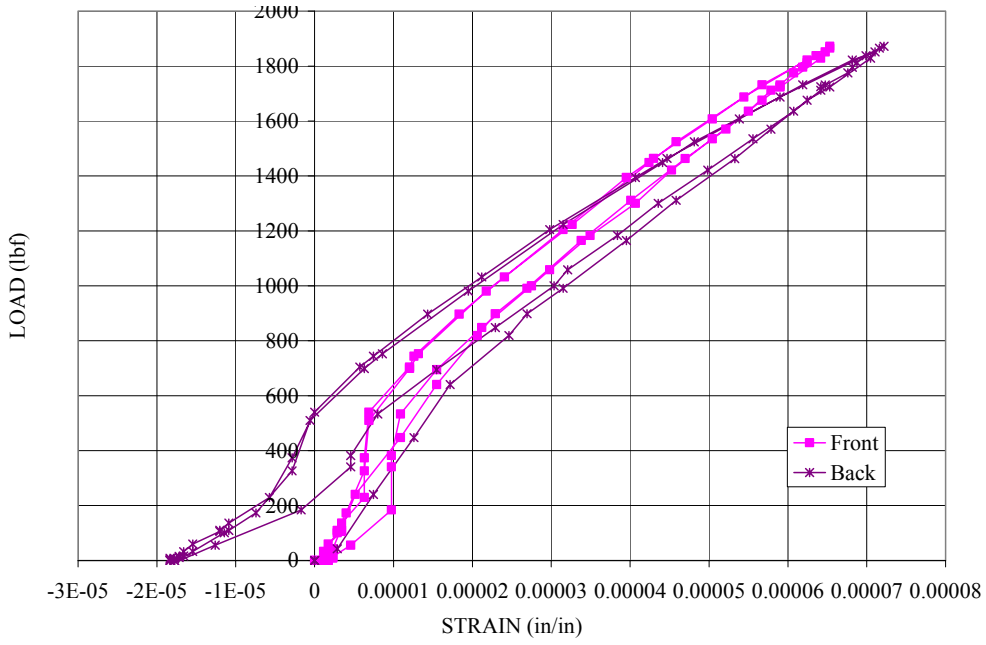

Figure A.48: Load vs. Strain Data for SCG-6; 44.4K Cycles

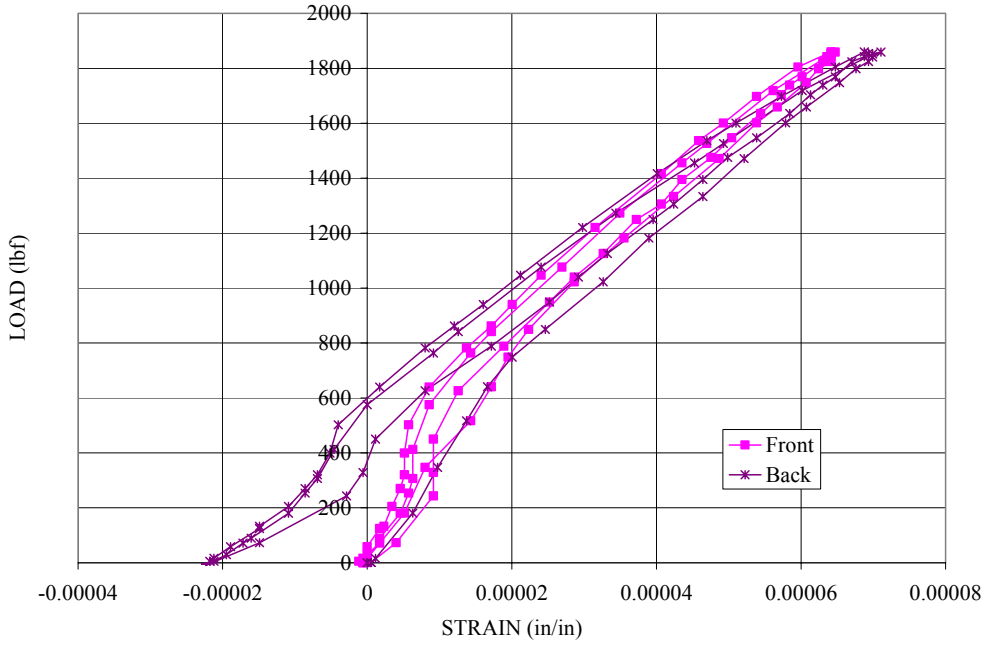

Figure A.49: Load vs. Strain Data for SCG-6; 52.2K Cycles

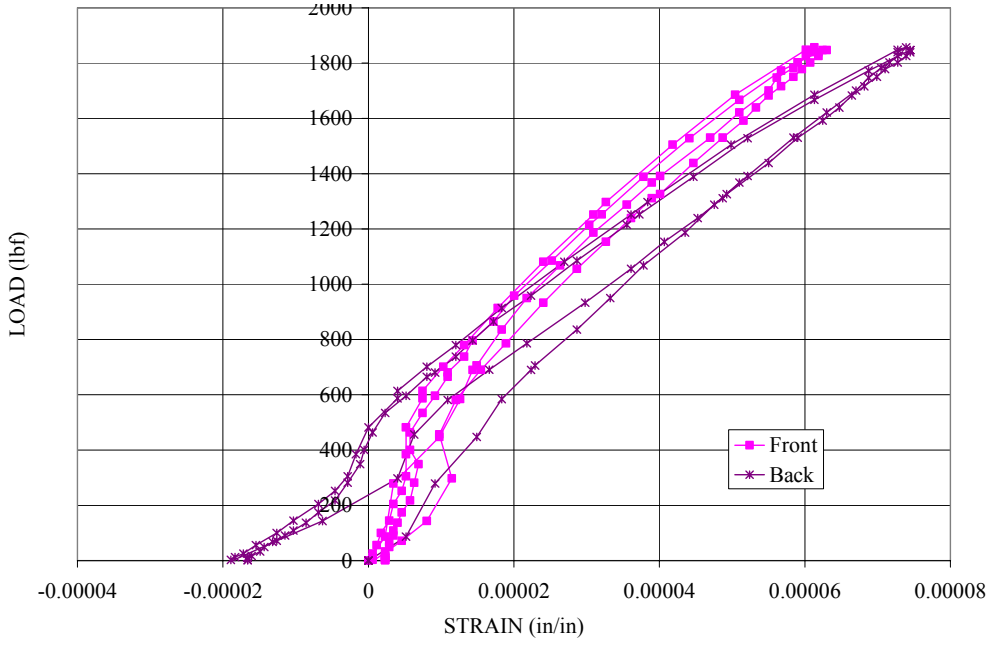

Figure A.50: Load vs. Strain Data for SCG-6; 62.6K Cycles

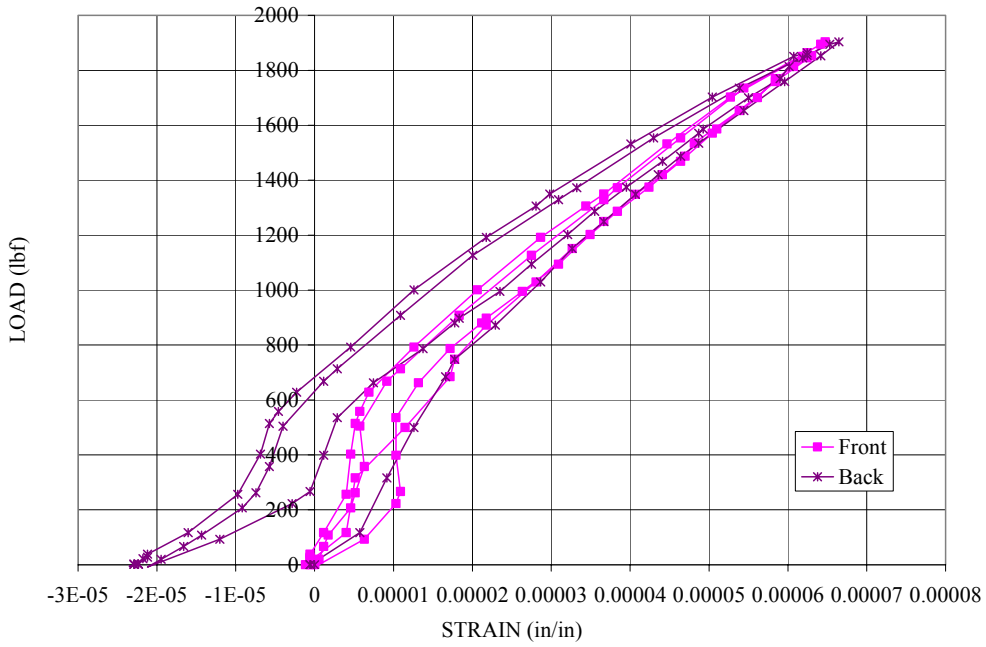

Figure A.51: Load vs. Strain Data for SCG-6; 73K Cycles

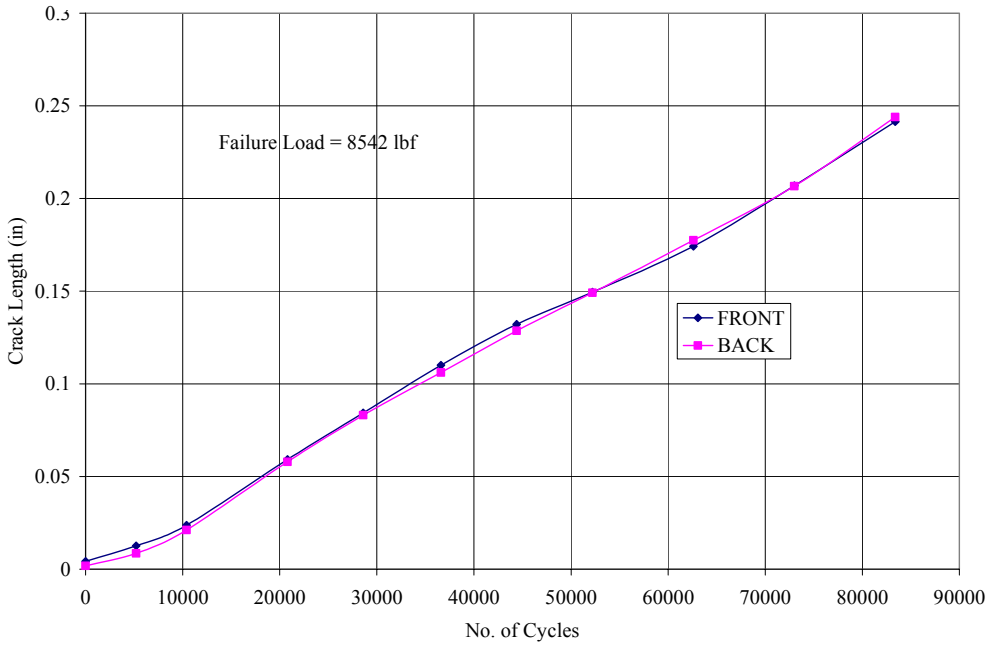

Figure A.52: Crack Length vs. Cycles for SCG-6

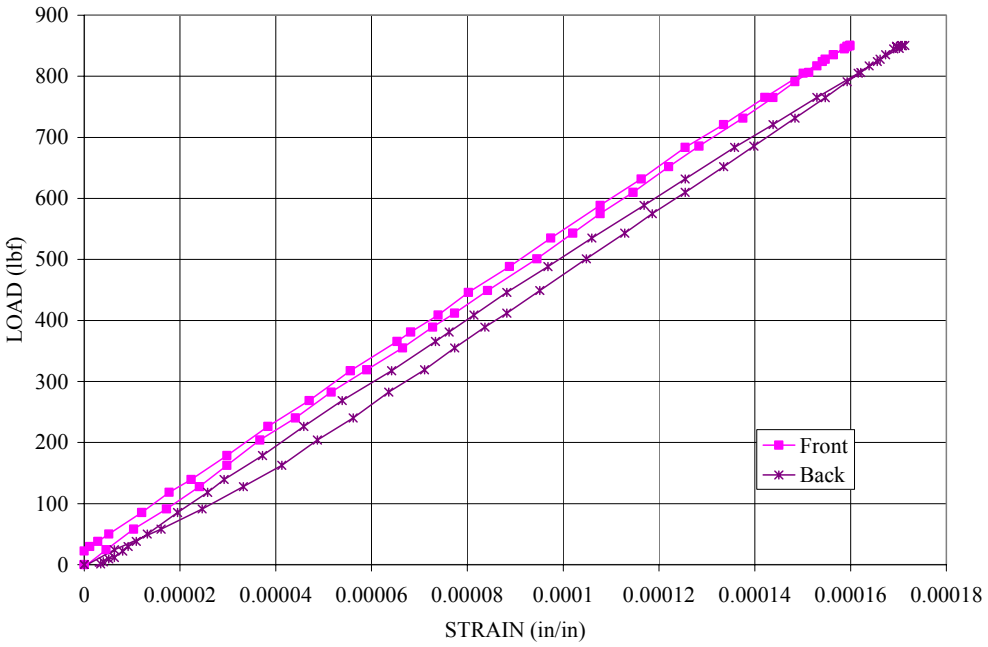

Figure A.53: Load vs. Strain Data for SCG-7; Calibration

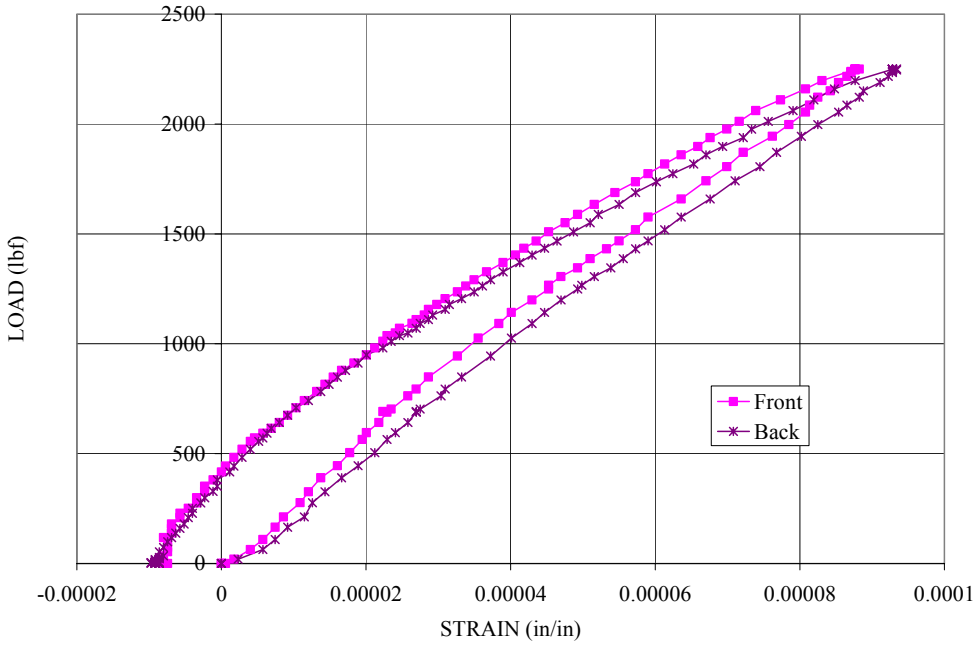

Figure A.54: Load vs. Strain Data for SCG-7; 0 Cycles

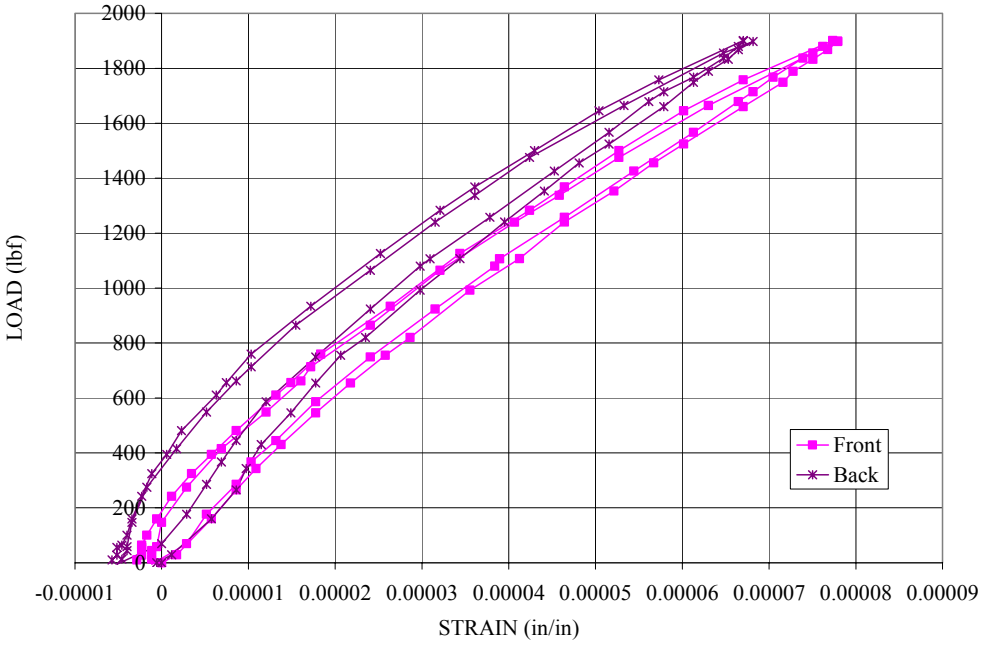

Figure A.55: Load vs. Strain Data for SCG-7; 2K Cycles

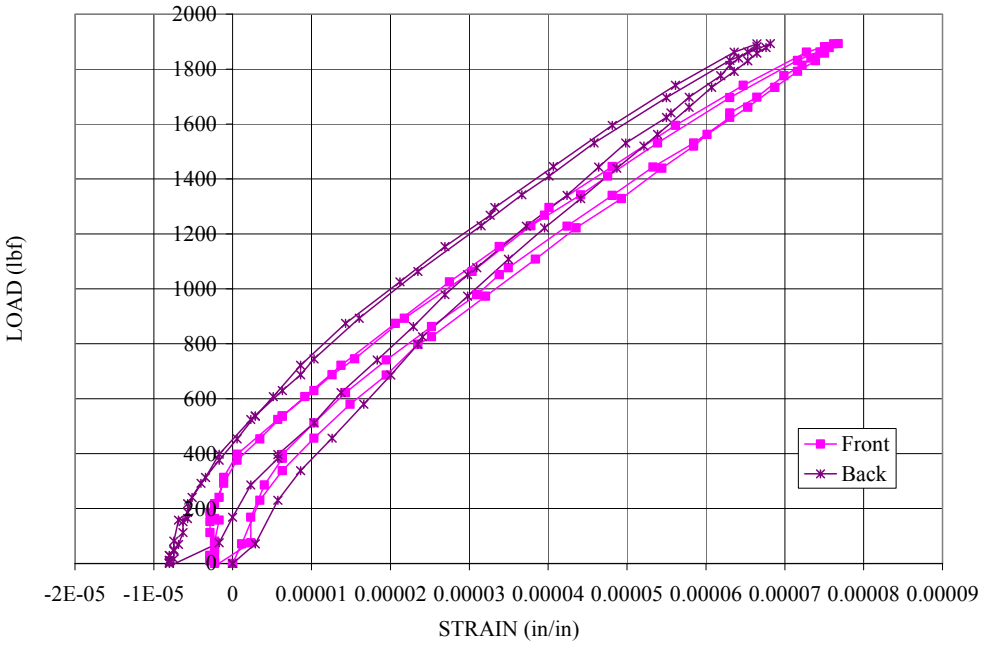

Figure A.56: Load vs. Strain Data for SCG-7; 7.2K Cycles

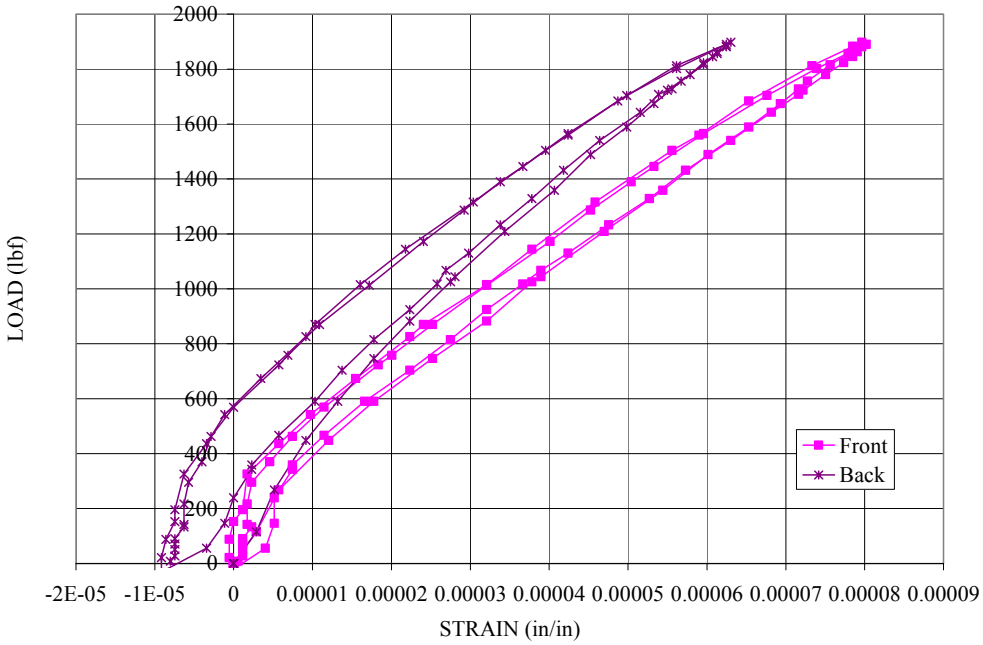

Figure A.57: Load vs. Strain Data for SCG-7; 12.4K Cycles

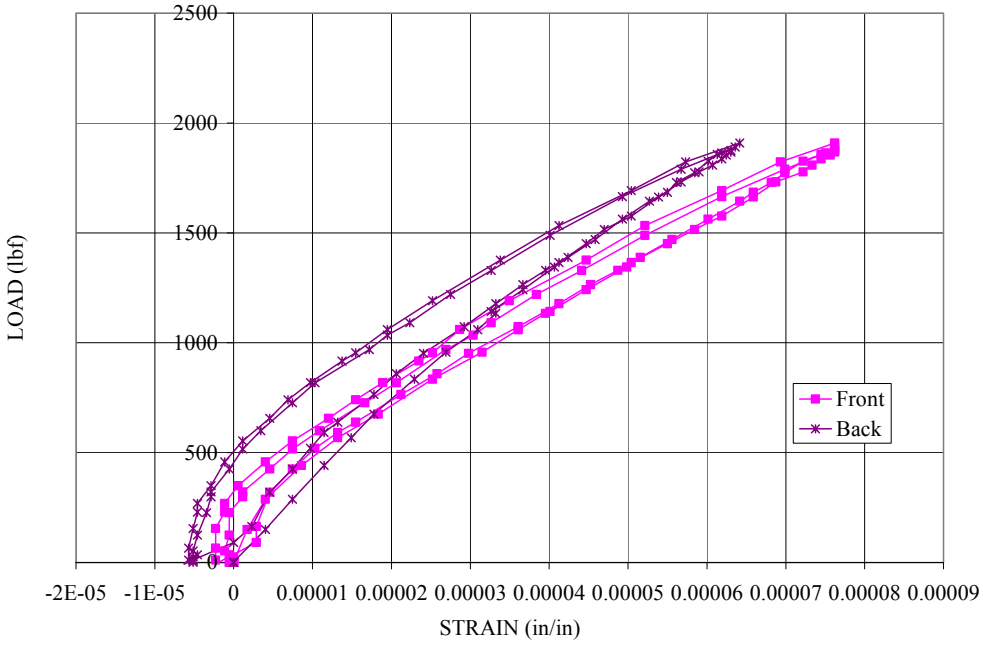

Figure A.58: Load vs. Strain Data for SCG-7; 22.8K Cycles

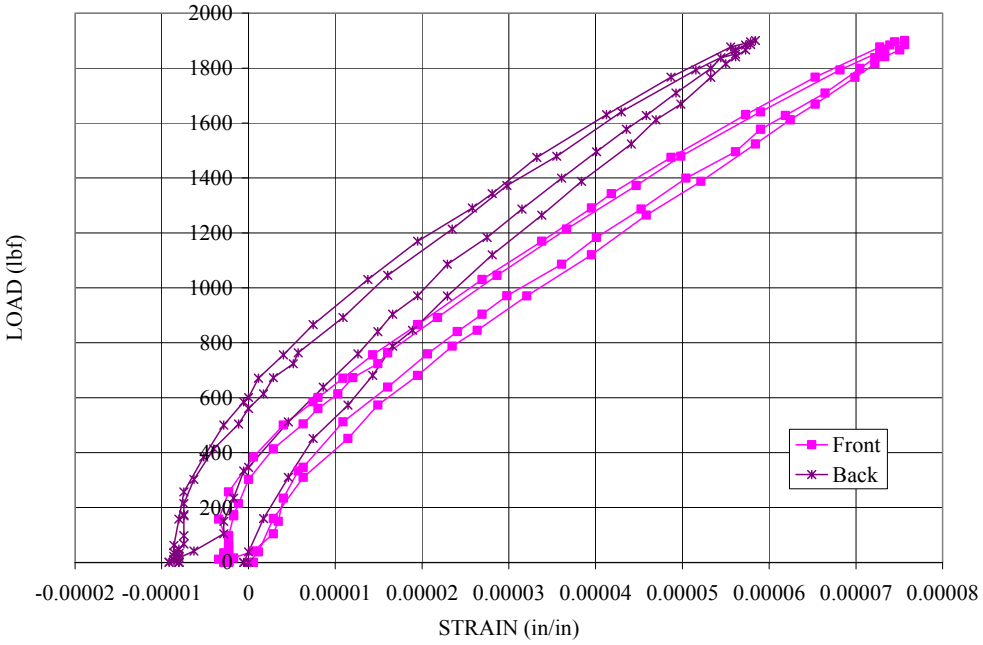

Figure A.59: Load vs. Strain Data for SCG-7; 30.3K Cycles

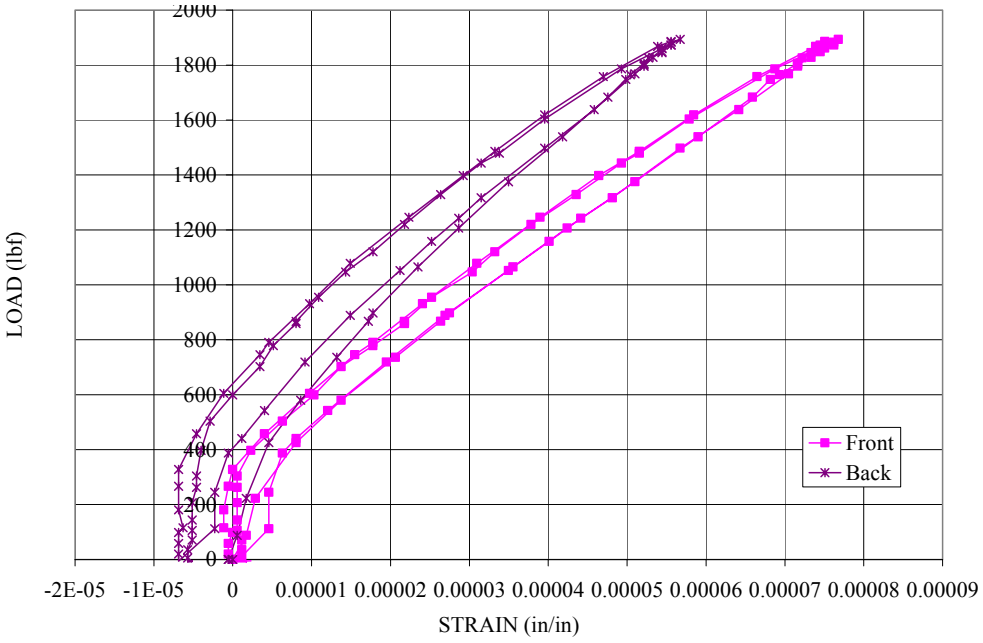

Figure A.60: Load vs. Strain Data for SCG-7; 37.8K Cycles

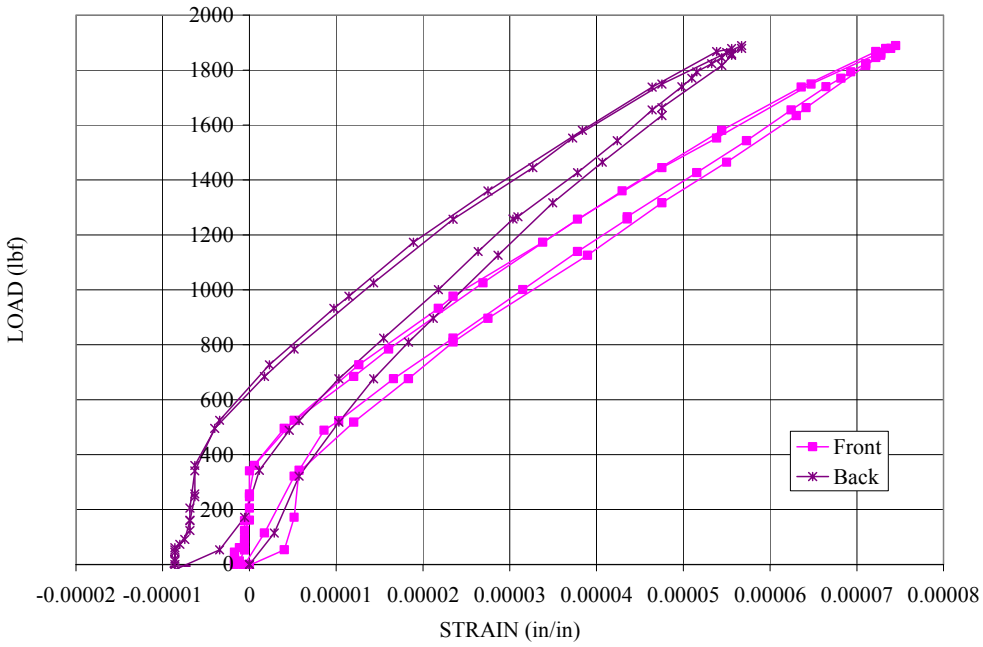

Figure A.61: Load vs. Strain Data for SCG-7; 45.3K Cycles

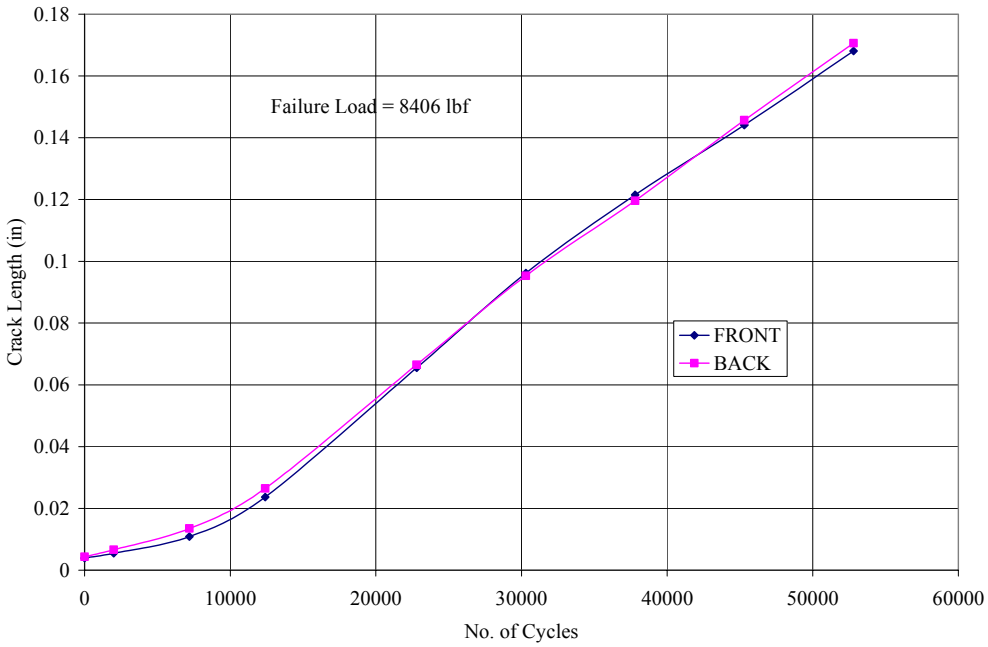

Figure A.62: Crack Length vs. Cycles for SCG-7

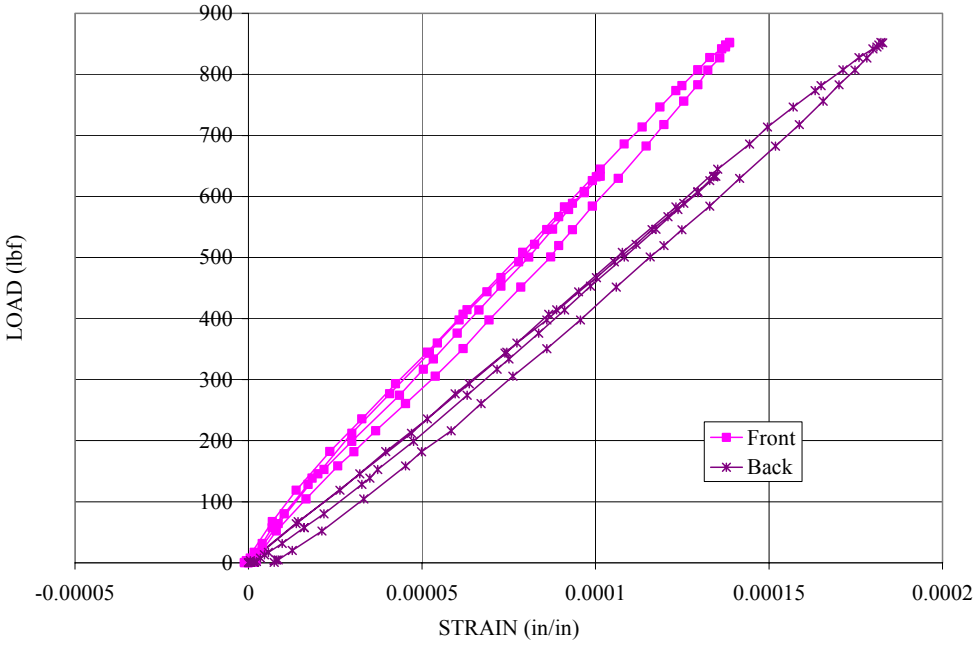

Figure A.63: Load vs. Strain Data for SCG-8; Calibration

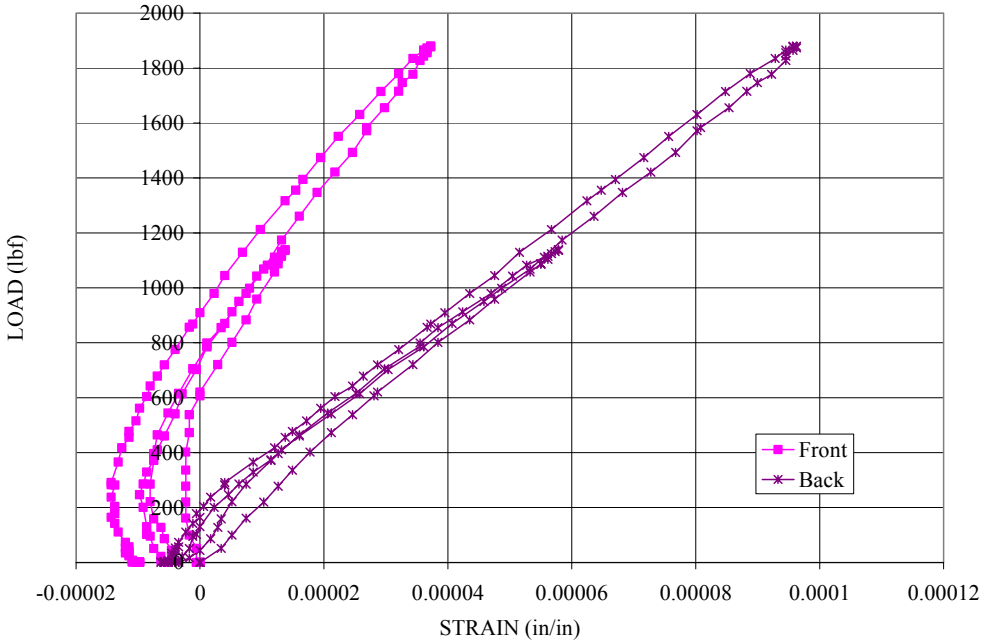

Figure A.64: Load vs. Strain Data for SCG-8; 0 Cycles

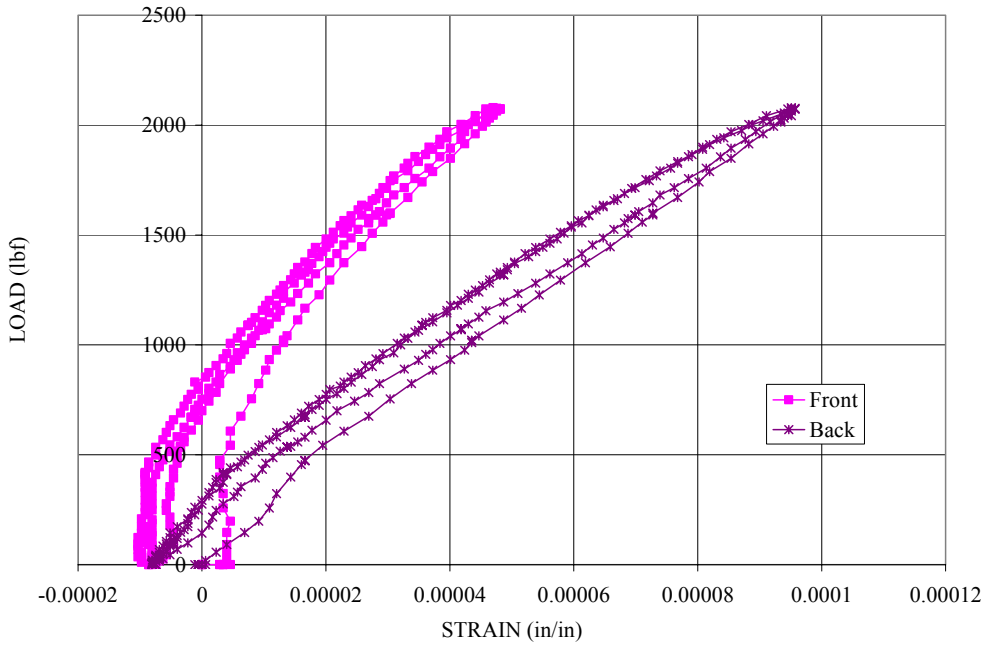

Figure A.65: Load vs. Strain Data for SCG-8; 325K

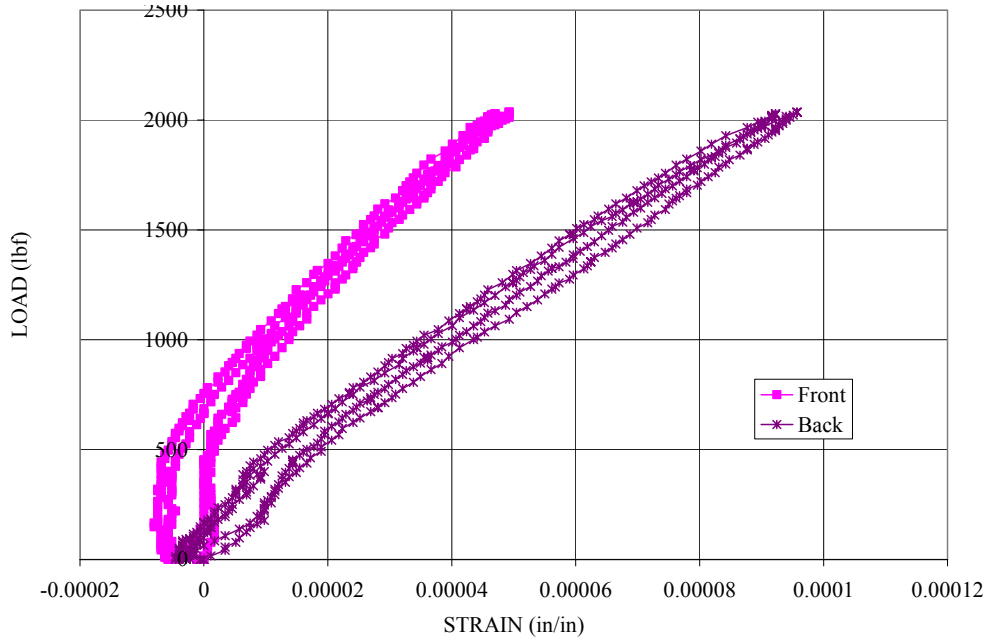

Figure A.66: Load vs. Strain Data for SCG-8; 725K Cycles

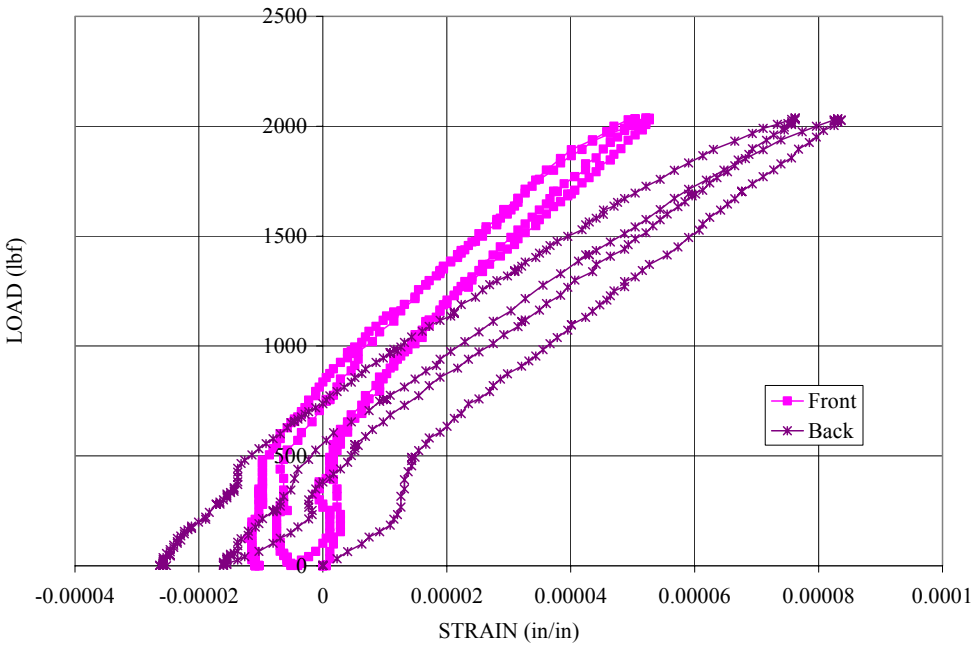

Figure A.67: Load vs. Strain Data for SCG-8; 825K

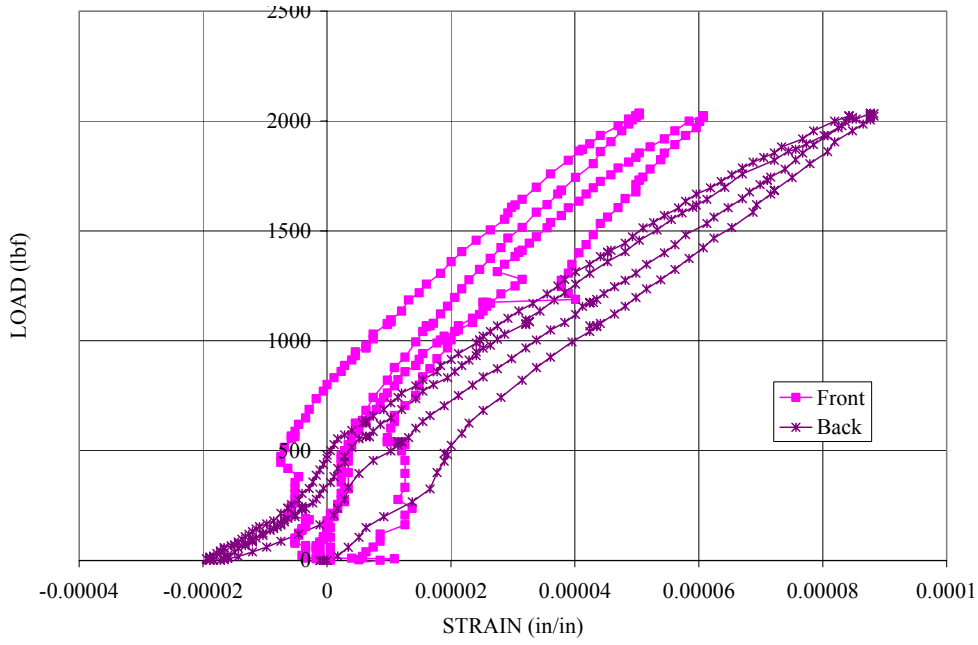

Figure A.68: Load vs. Strain Data for SCG-8; 925K Cycles

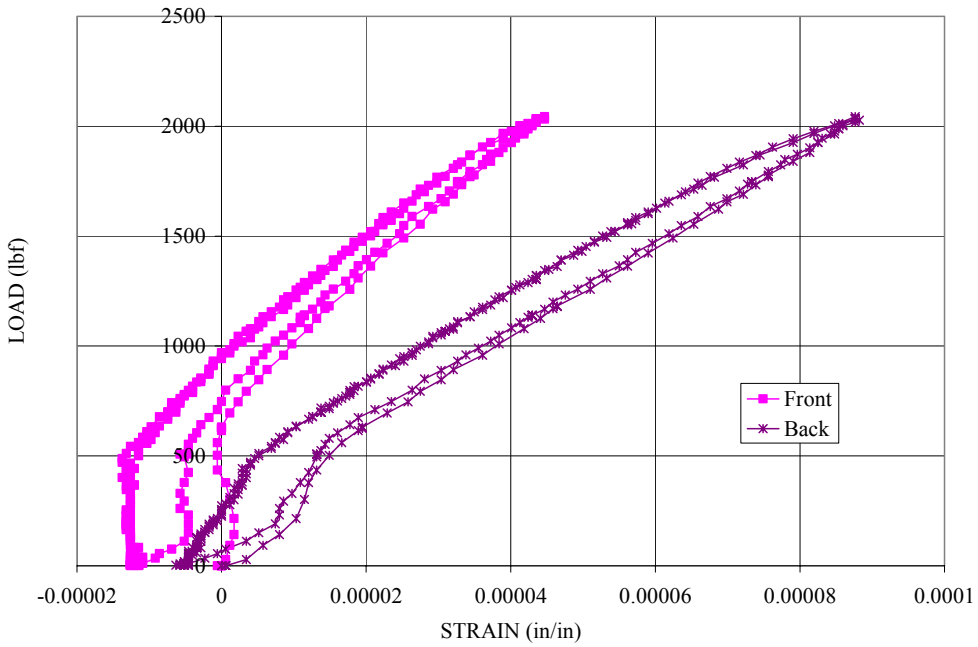

Figure A.69: Load vs. Strain Data for SCG-8; 1025K

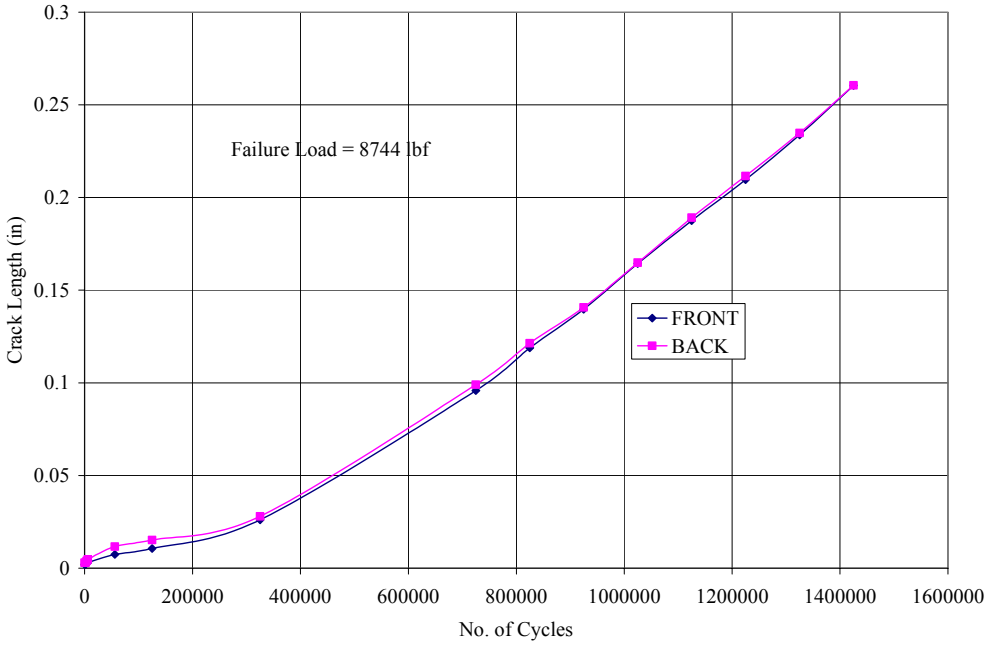

Figure A.70: Crack Length vs. Cycles for SCG-8

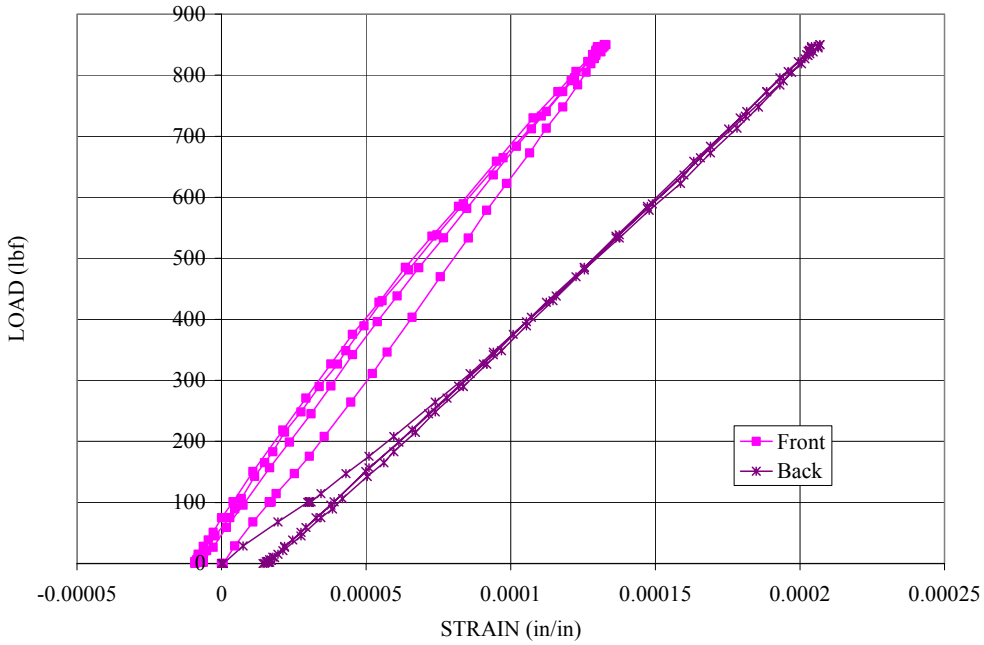

Figure A.71: Load vs. Strain Data for SCG-9; Calibration

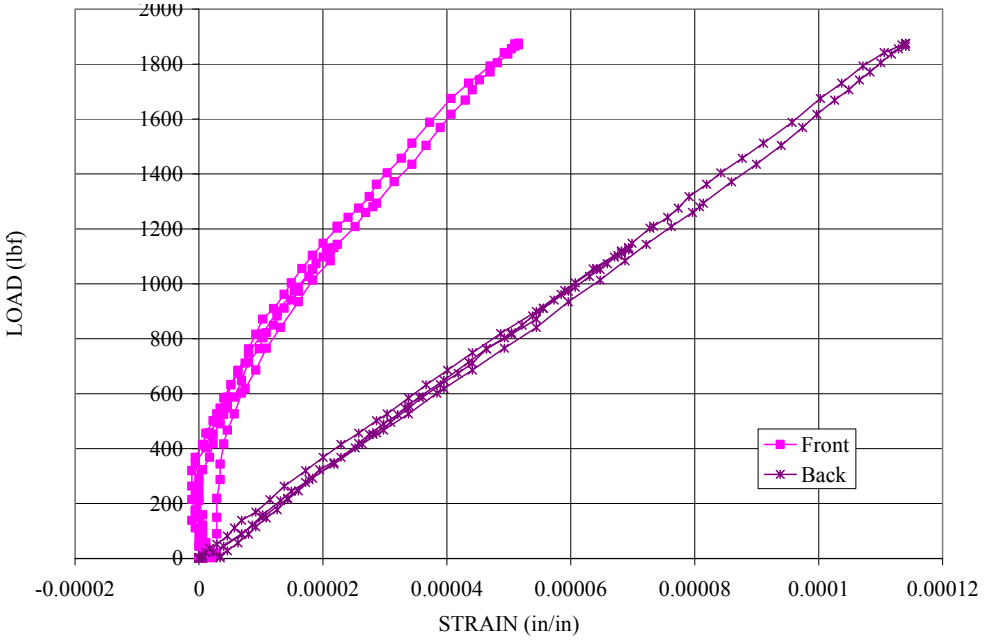

Figure A.72: Load vs. Strain Data for SCG-9; 0 Cycles

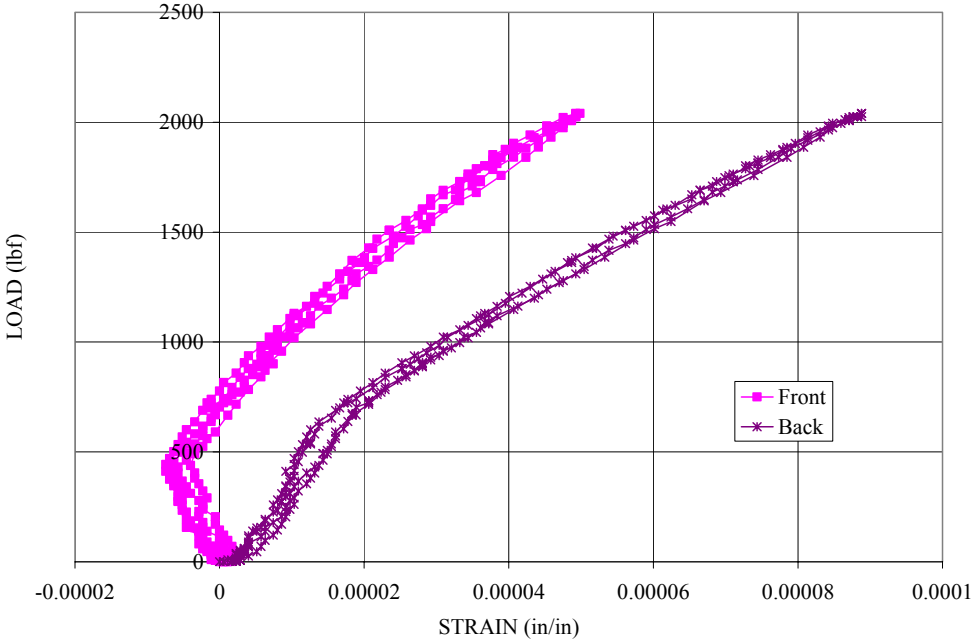

Figure A.73: Load vs. Strain Data for SCG-9; 1100K Cycles

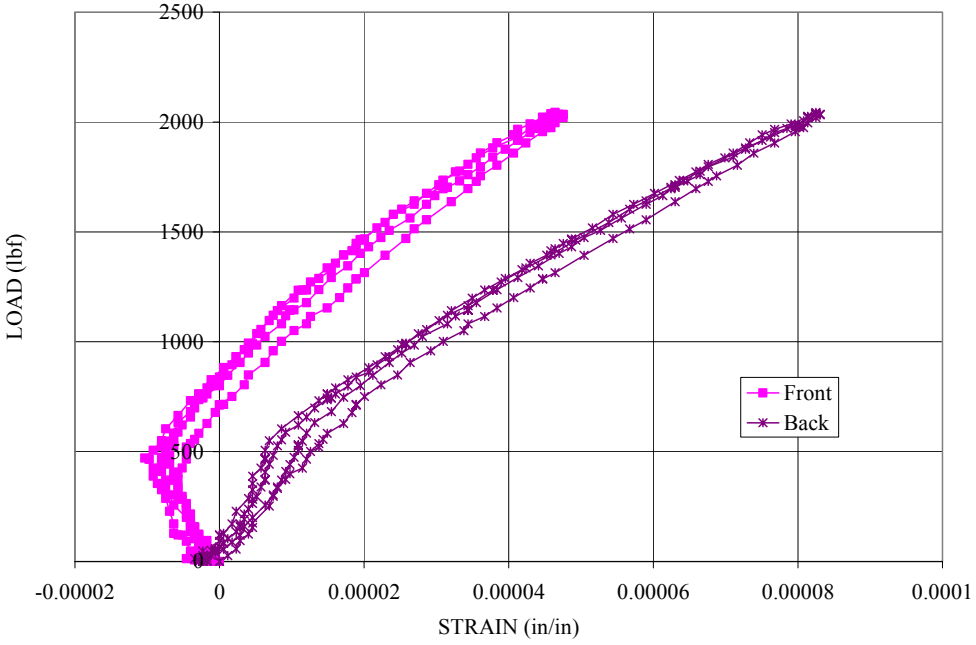

Figure A.74: Load vs. Strain Data for SCG-9; 1200K Cycles

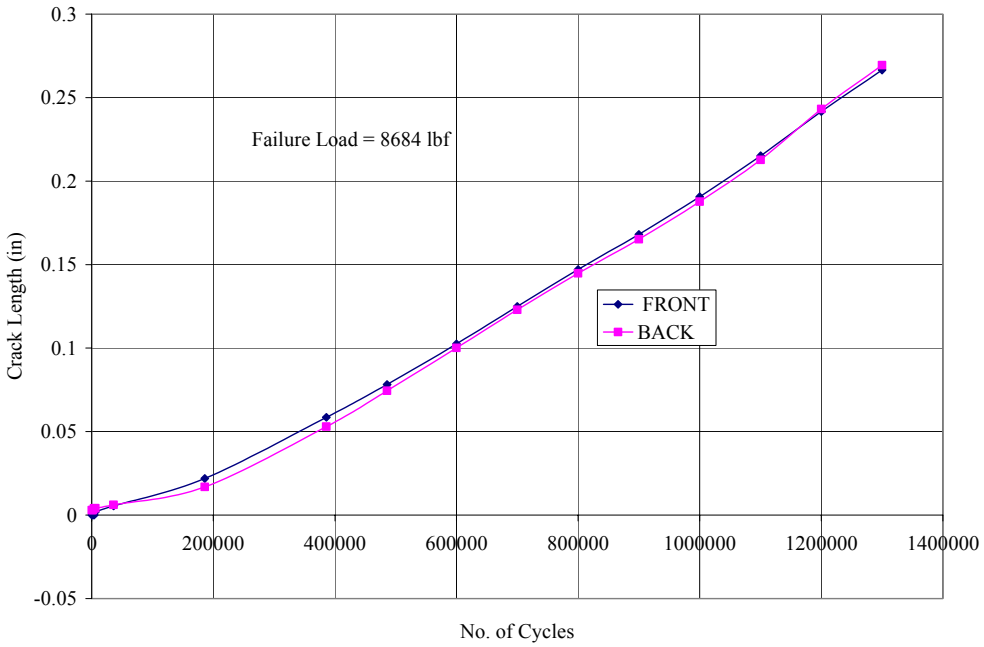

Figure A.75: Crack Length vs. Cycles for SCG-9

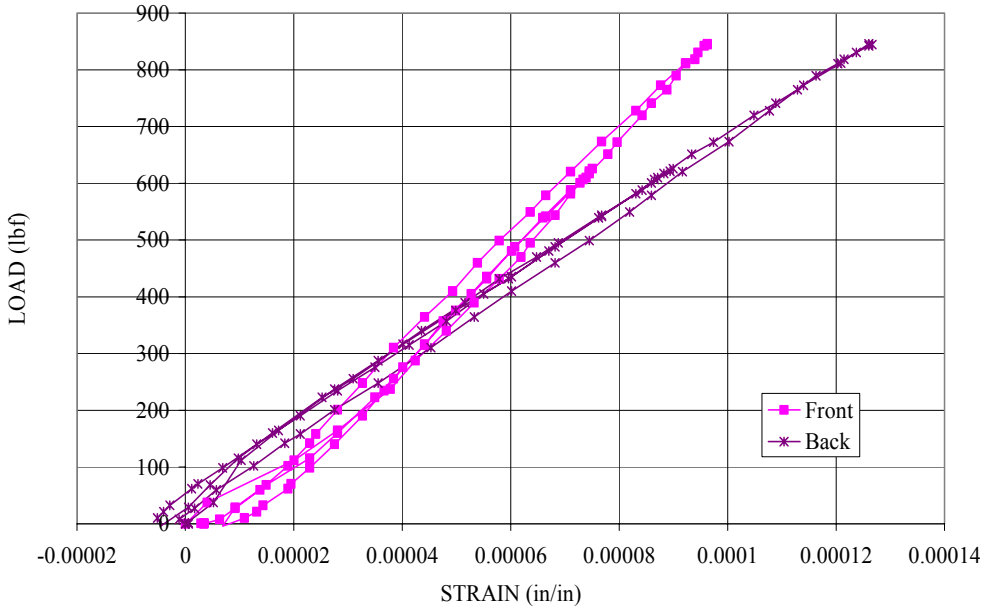

Figure A.76: Load vs. Strain Data for SCG-11; Calibration

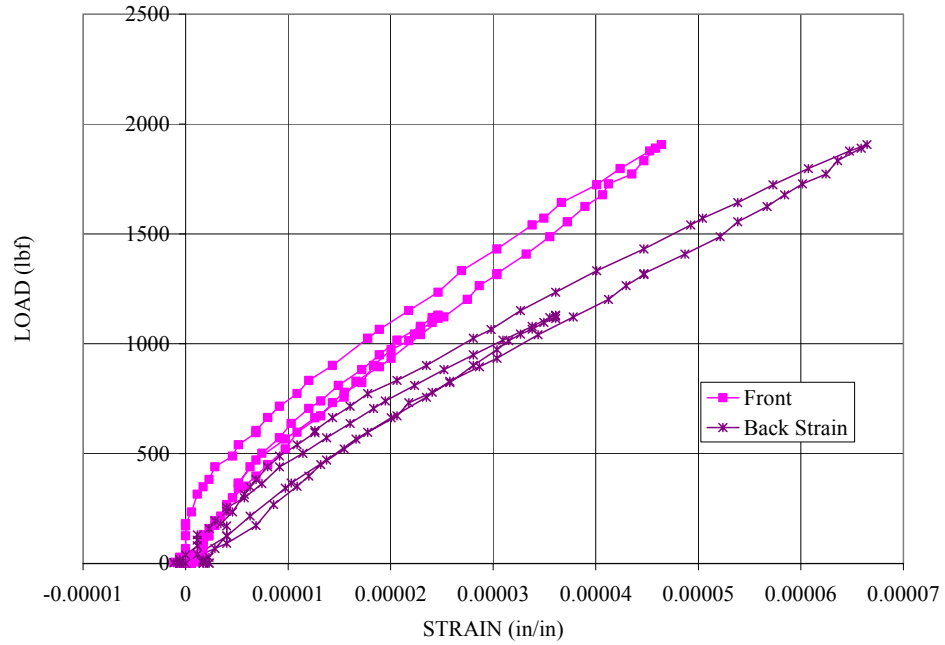

Figure A.77: Load vs. Strain Data for SCG-11; 0 Cycles

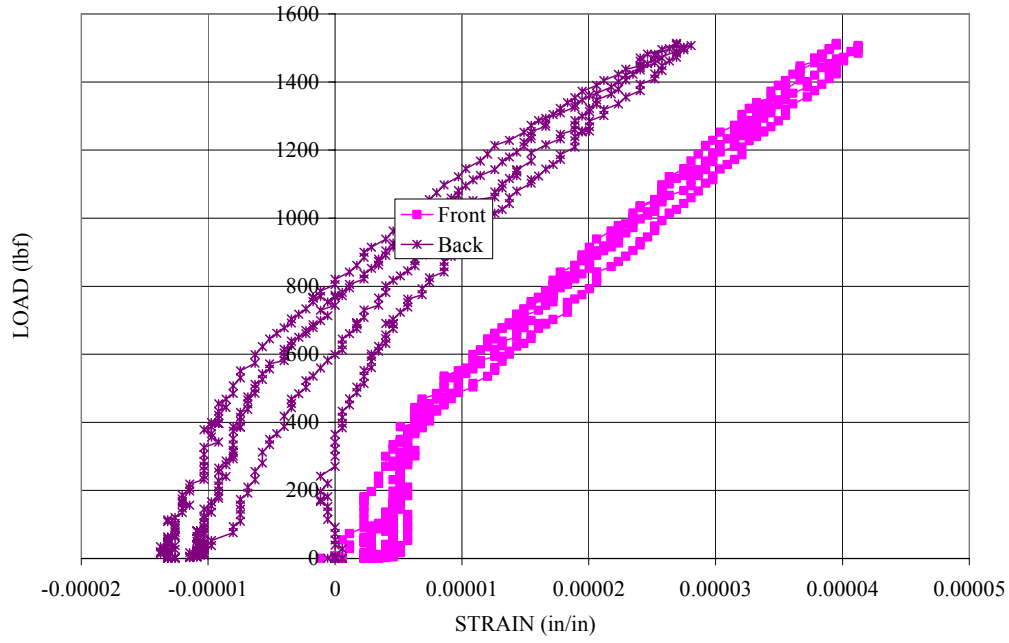

Figure A.78: Load vs. Strain Data for SCG-11; 30K Cycles

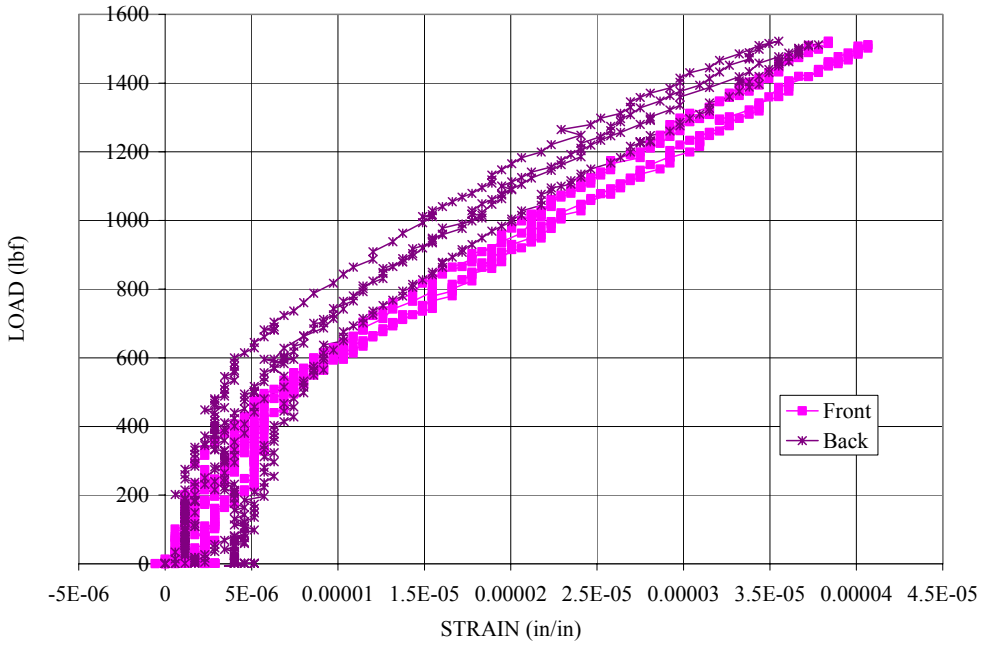

Figure A.79: Load vs. Strain Data for SCG-11; 50K Cycles

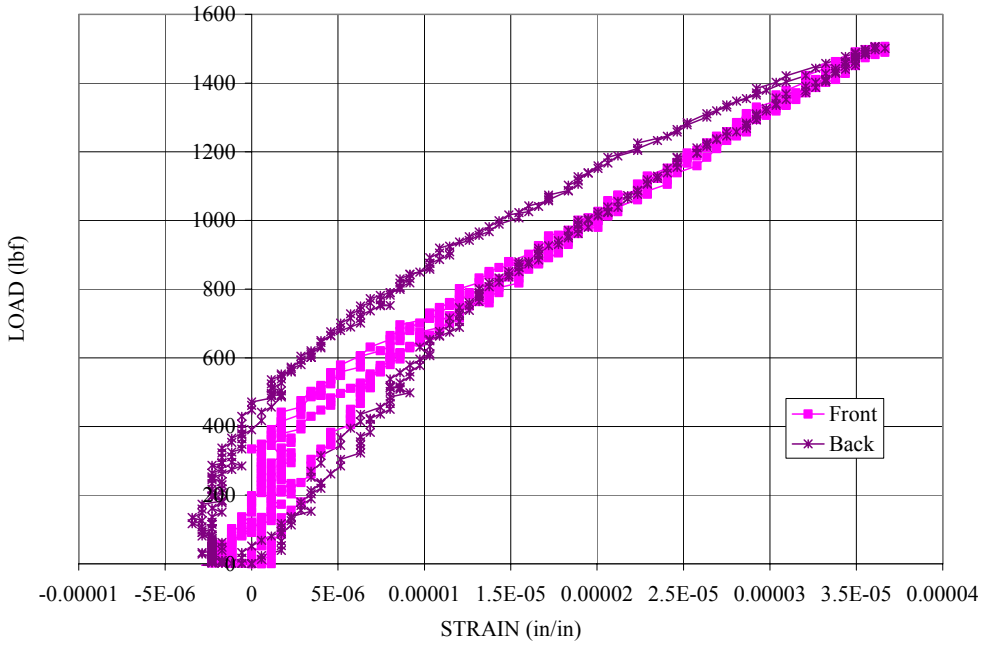

Figure A.80: Load vs. Strain Data for SCG-11; 60K Cycles

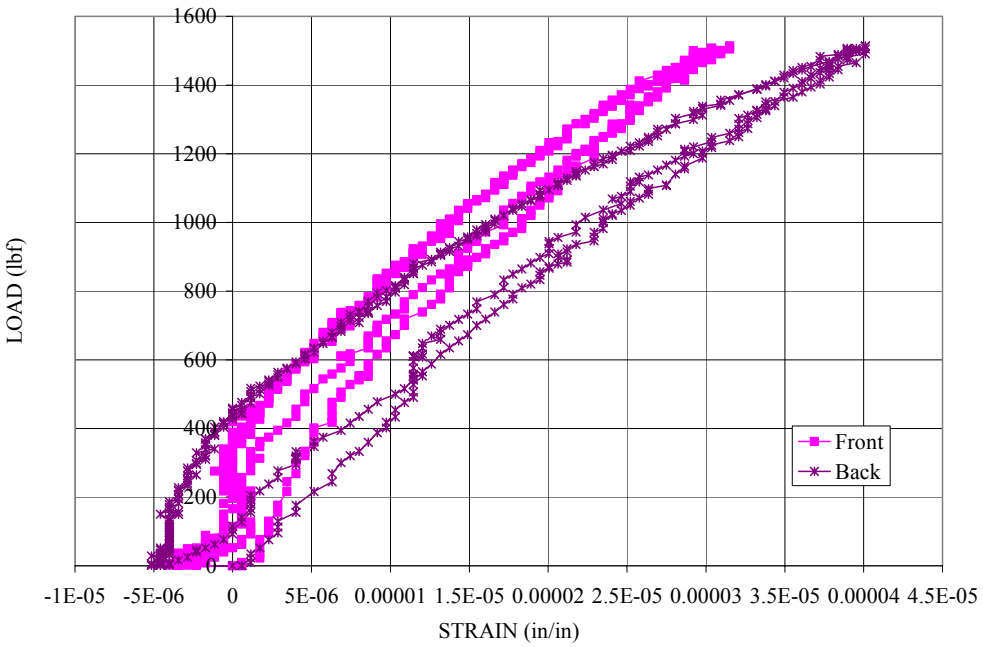

Figure A.81: Load vs. Strain Data for SCG-11; 80K Cycles

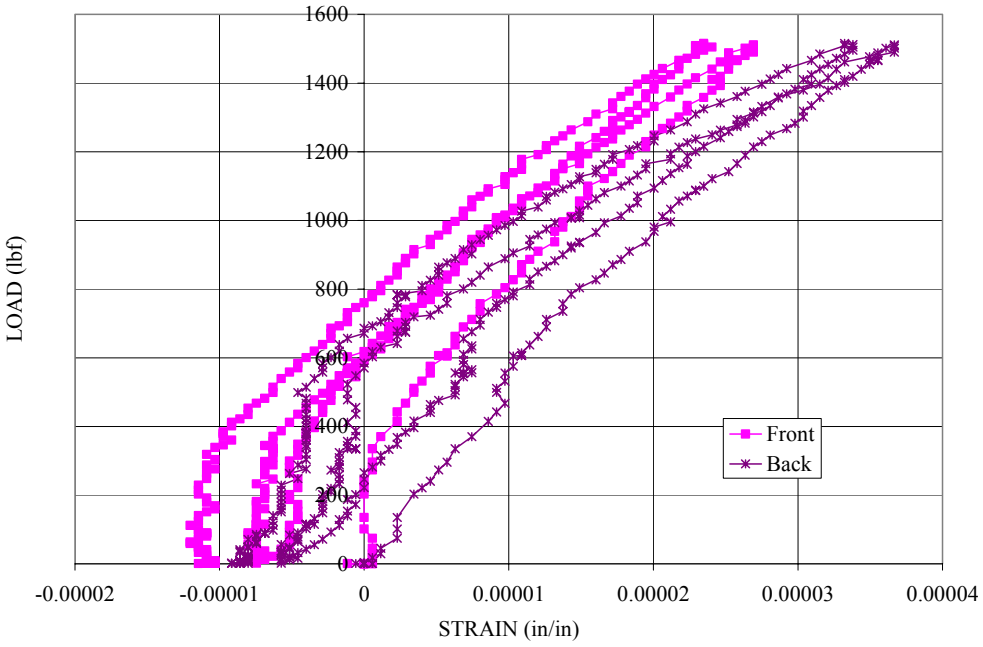

Figure A.82: Load vs. Strain Data for SCG-11; 95K Cycles

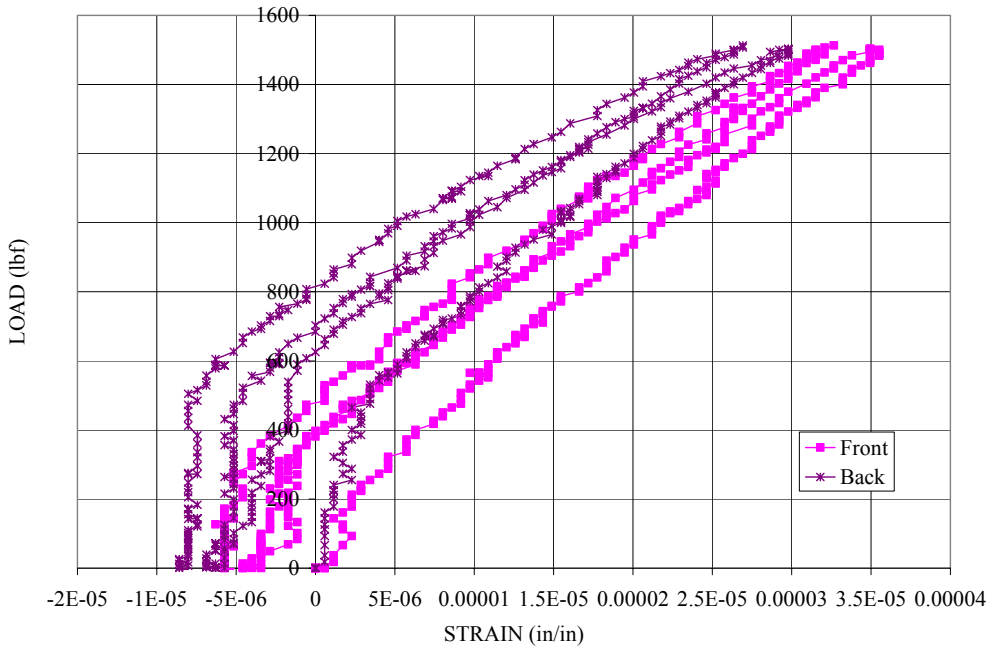

Figure A.83: Load vs. Strain Data for SCG-11; 110K Cycles

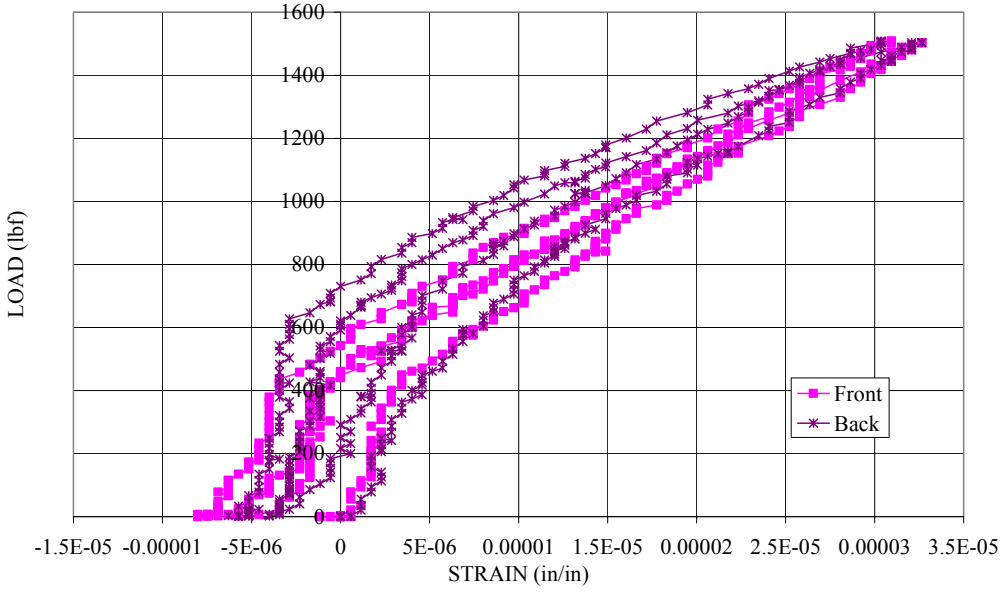

Figure A.84: Load vs. Strain Data for SCG-11; 130K Cycles

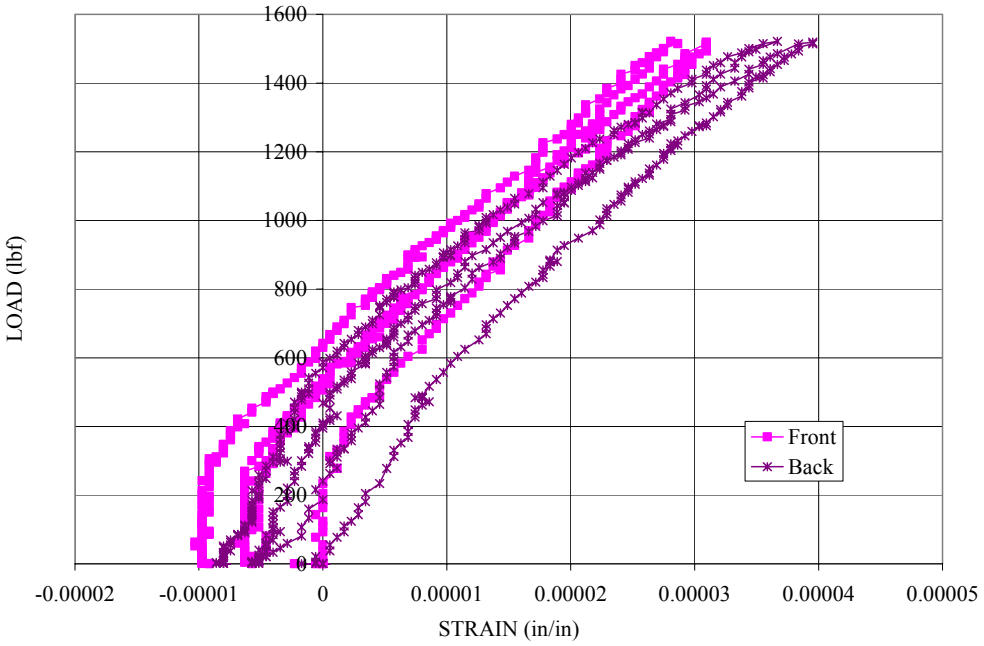

Figure A.85: Load vs. Strain Data for SCG-11; 145K Cycles

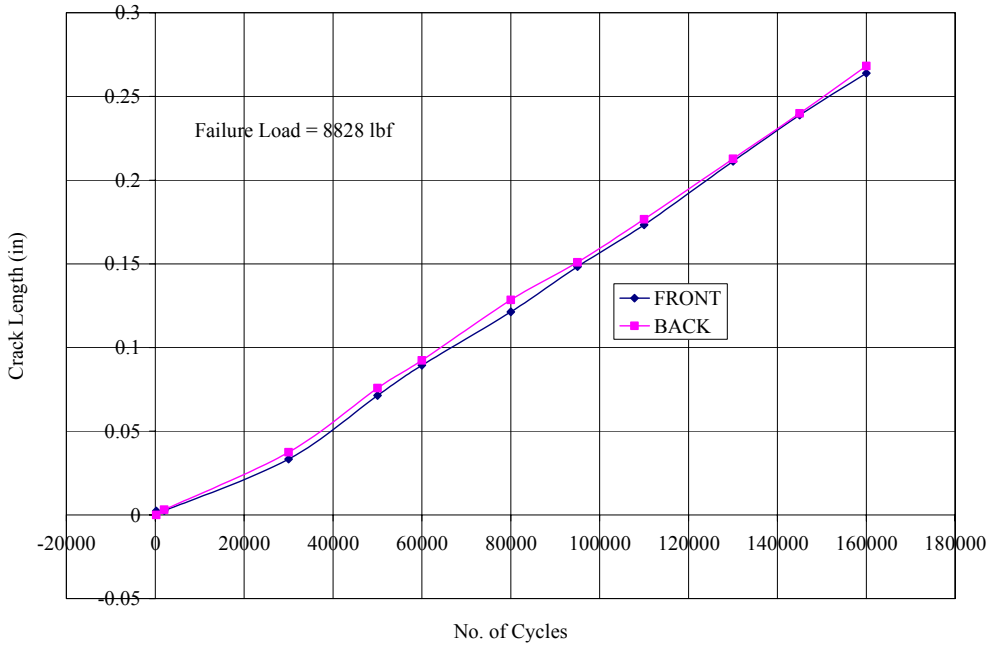

Figure A.86: Crack Length vs. Cycles for SCG-11

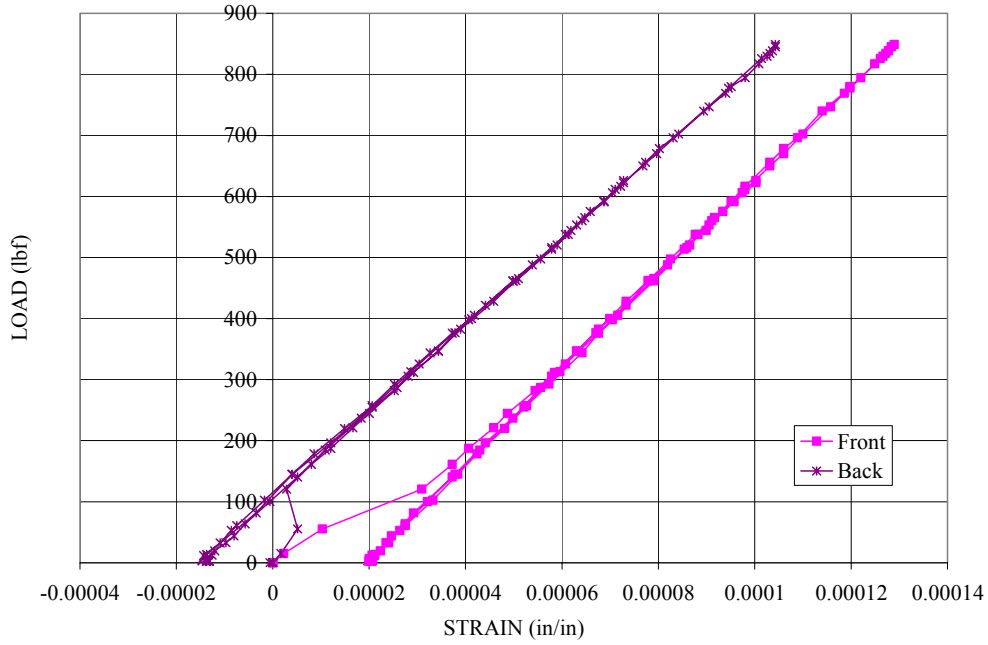

Figure A.87: Load vs. Strain Data for SCG-12; Calibration

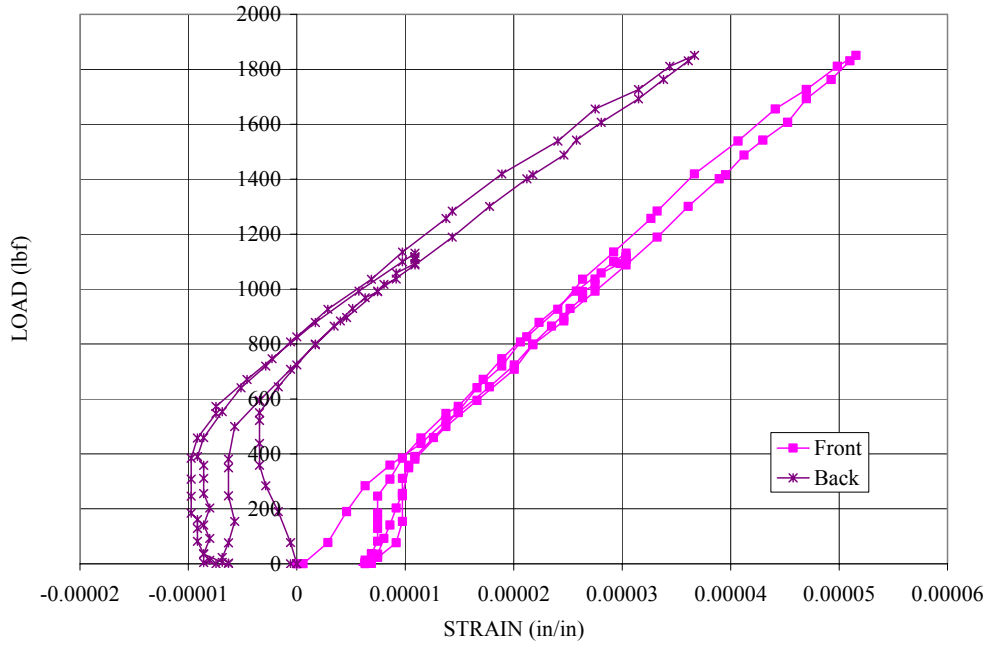

Figure A.88: Load vs. Strain Data for SCG-12; 0 Cycles

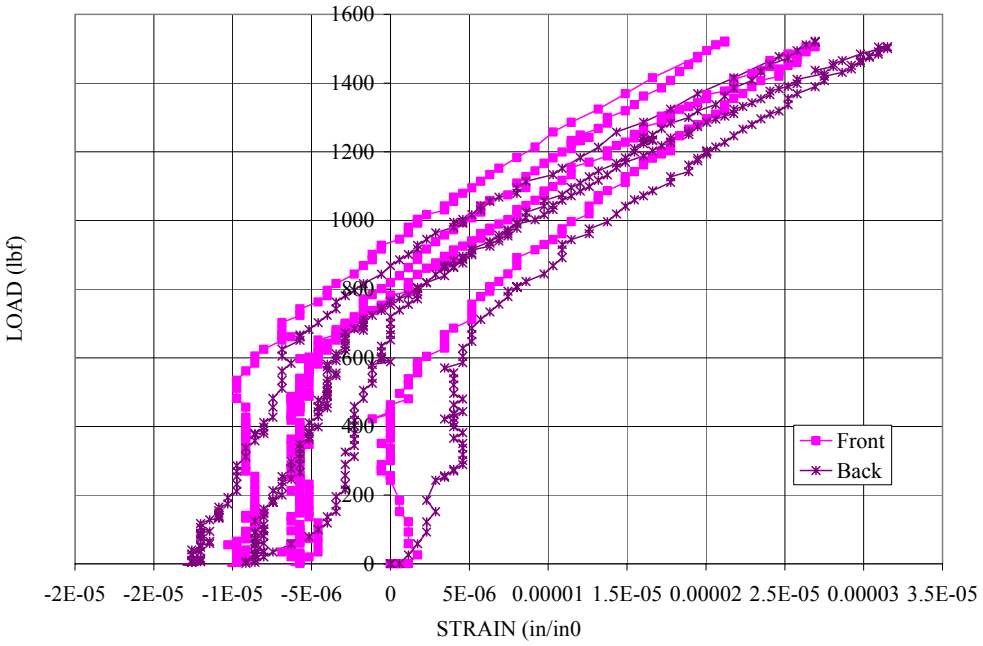

Figure A.89: Load vs. Strain Data for SCG-12; 11K Cycles

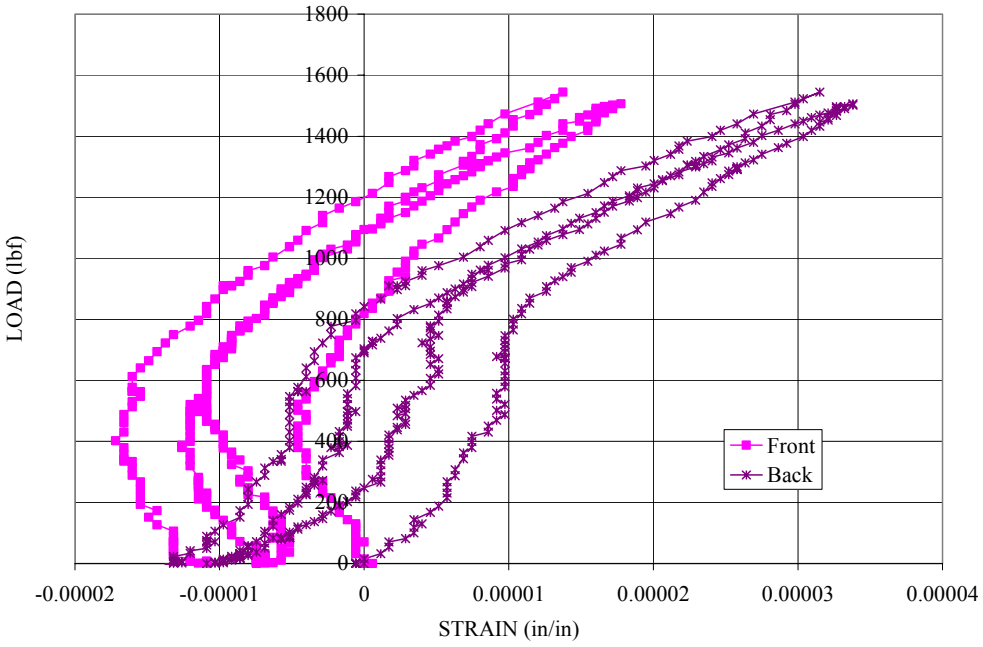

Figure A.90: Load vs. Strain Data for SCG-12; 15K Cycles

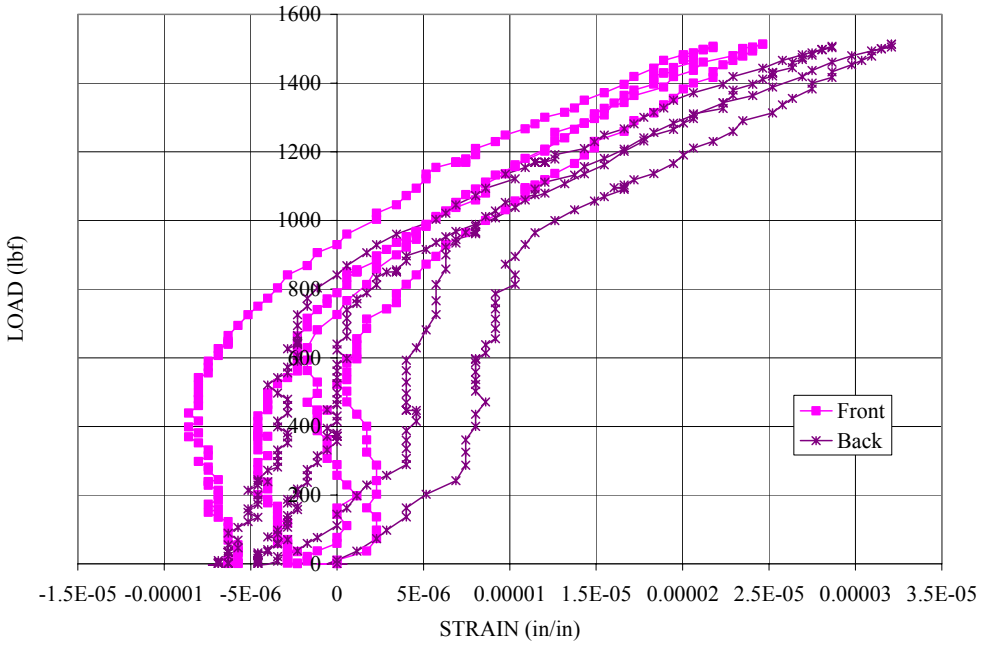

Figure A.91: Load vs. Strain Data for SCG-12; 39K Cycles

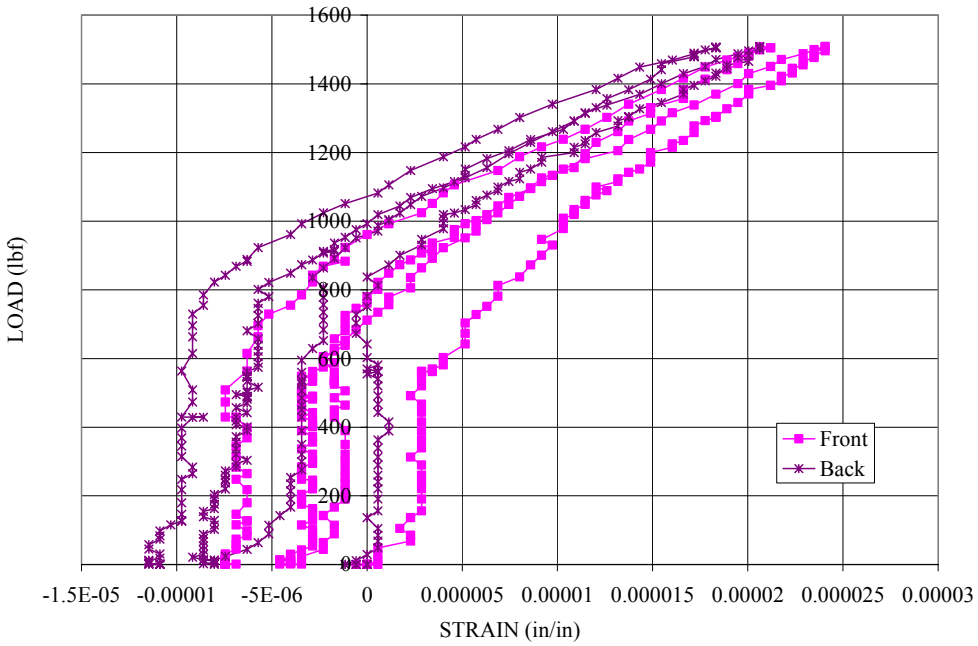

Figure A.92: Load vs. Strain Data for SCG-12; 50K Cycles

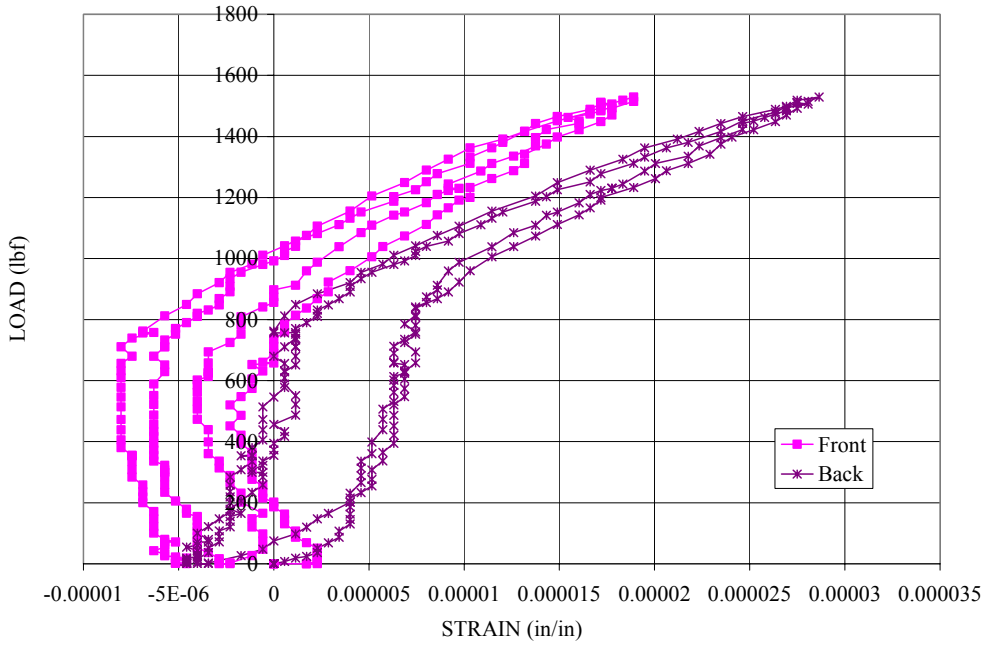

Figure A.93: Load vs. Strain Data for SCG-12; 69K Cycles

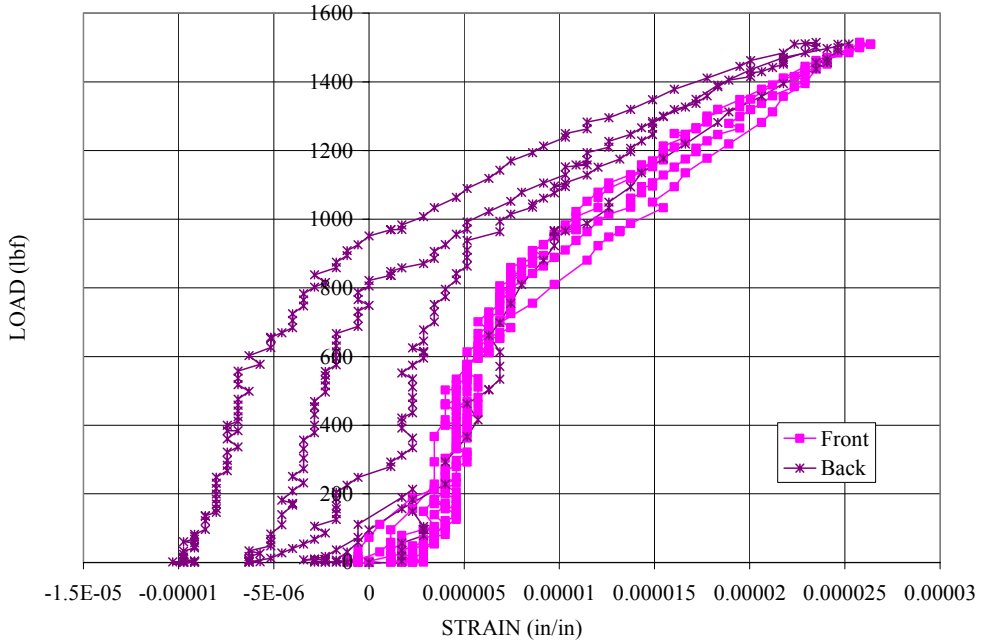

Figure A.94: Load vs. Strain Data for SCG-12; 150K Cycles

Appendix B
Crack Growth Data

Table B.1: Crack Growth Data for SCG-1S

CYCLE	FRONT	BACK	FRONT OPPOSITE	BACK OPPOSITE
200	0.00855	0.00739		
2200	0.0121	0.01227		
4200	0.02096	0.02173		
9400	0.04531	0.04509		
14600	0.0712	0.07153		
19800	0.09224	0.09407		
25800	0.11347	0.11739		
31800	0.13843	0.1431		
37800	0.16081	0.16405		
43800	0.18461	0.18594		
51800	0.22273	0.21913		0.00535
57800	0.2539	0.24894		0.01271

Failure Load: 8678 lbf.

Table B.2: Crack Growth Data for SCG-2

Cycles	FRONT	BACK
0	0.0625	0.0628
2000	0.07328	0.07635
4000	0.08594	0.0887
6000	0.09637	0.09917
8000	0.10476	0.10783
10000	0.11545	0.11766
12000	0.12487	0.12575
14000	0.13347	0.1344
20000	0.16522	0.16513
26000	CYCLES	0.19343
32000		0.22284
38000	0.24899	0.25303

Failure Load: 8964 lbf.

Table B.3: Crack Growth Data for SCG-5

CYCLES	FRONT	BACK
500	0.00852	0.00713
5700	0.03063	0.02328
10900	0.0506	0.05081
16100	0.07756	0.07991
21300	0.10375	0.10334
26500	0.12451	0.12634
31700	0.14616	0.14678
36900	0.17365	0.17254
42100	0.19837	0.19821
47300	0.22443	0.2268
52500	0.25319	0.25642

Failure Load: 8822 lbf

Table B.4: Crack Growth Data for SCG-6

CYCLE	FRONT	BACK	FRONT OPPOSITE	BACK OPPOSITE
0	0.0042	0.00181		
5200	0.0126	0.00849		
10400	0.02373	0.02113		
20800	0.05918	0.05796		
28600	0.08433	0.08306		
36600	0.11004	0.10618		
44400	0.13215	0.12859		
52200	0.14946	0.14916		
62600	0.1742	0.17744		
73000	0.207	0.20664		
83400	0.24146	0.24393	0.06528	0.05081

Failure Load: 8542 lbf.

Table B.5: Crack Growth Data for SCG-7

CYCLES	FRONT	BACK	FRONT OPPOSITE	BACK OPPOSITE
0	0.00394	0.00432		
2000	0.00548	0.00661		
7200	0.01085	0.01351		
12400	0.02369	0.02647		
22800	0.06548	0.06652		
30300	0.09618	0.0953		
37800	0.12149	0.11964		
45300	0.14408	0.14571		
52800	0.16812	0.17059		0.00241

Failure Load: 8406 lbf.

Table B.6: Crack Growth Data for SCG-8

CYCLES	FRONT	BACK
100	0.00203	0.0029
2000	0.00216	0.00302
4000	0.00295	0.00392
6000	0.00304	0.00463
56000	0.00742	0.01164
125000	0.01063	0.01521
325000	0.02606	0.02795
725000	0.09575	0.09904
825000	0.11889	0.12144
925000	0.13969	0.14079
1025000	0.1644	0.16481
1125000	0.18749	0.18908
1225000	0.20963	0.21165
1325000	0.23377	0.23487
1425000	0.26048	0.26053

Failure Load: 8744 lbf.

Table B.7: Crack Growth Data for SCG-9

CYCLES	FRONT	BACK
200	0	0.00295
2000	0	0.00299
4000	0	0.00402
6000	0.00187	0.00414
36000	0.00548	0.00611
186000	0.02189	0.01679
386000	0.05851	0.05296
486000	0.07816	0.0744
600000	0.10256	0.10008
700000	0.12498	0.12293
800000	0.14705	0.14471
900000	0.16812	0.16516
1000000	0.19058	0.18768
1100000	0.21513	0.21272
1200000	0.24168	0.24313
1300000	0.2665	0.26943

Failure Load: 8684 lbf.

Table B.8: Crack Growth Data for SCG-11

CYCLES	FRONT	BACK
200	0.00238	0
2000	0.00263	0.00307
30000	0.03332	0.03745
50000	0.07133	0.07578
60000	0.08939	0.09237
80000	0.12131	0.12848
95000	0.14831	0.15097
110000	0.17331	0.17662
130000	0.21122	0.21278
145000	0.23884	0.23984
160000	0.26387	0.26814

Failure Load: 8828 lbf.

Table B.9: Crack Growth Data for SCG-12

CYCLES	FRONT	BACK
200	0	0
2000	0	0
4000	0	0
6000	0	0
11000	0	0.0054
13000	0	0.00622
15000	0	0.00739
17000	0.00482	0.00913
27000	0.01572	0.02358
39000	0.03714	0.04481
49000	0.0581	0.06125
69000	0.09089	0.09451
85000	0.11629	0.12138
100000	0.14164	0.14368
120000	0.17571	0.17758
135000	0.20305	0.20379
150000	0.23196	0.23088
165000	0.25889	0.25831

Failure Load: 8844 lbf.

Table B.10: Crack Growth Data for SCG-16

CYCLE	FRONT	BACK
0	0	0
100	0	0.00414
500	0	0.00413
2000	0	0.00412
4000	0	0.00452
6000	0	0.00529
8000	0	0.00632
10000	0.00178	0.00748
12000	0.00261	0.00884
17200	0.00811	0.01414
21200	0.01684	0.02106
23200	0.02033	0.0245
33200	0.04632	0.04857
43200	0.07583	0.07673
53400	0.10457	0.10578
63400	0.13837	0.13564
73400	0.17371	0.17305
83400	0.20969	0.21073
95900	0.26217	0.26075

Residual Strength: 8934 lbf.

Table B.11: Crack Growth Data for SCG-17S

CYCLES	FRONT	BACK
0	0.02668	0.02715
200	0.02817	0.02726
2000	0.03258	0.03356
7000	0.0472	0.04372
13000	0.0463	0.04956
50000	0.11166	0.11342
58500	0.12868	0.13306
65500	0.14845	0.15311
70500	0.15961	0.16683
76500	0.17555	0.1832
82000	0.18587	0.20002
88000	0.19936	0.21639
94000	0.22007	0.23143
99000	0.23368	0.245
104500	0.25121	0.26366

Residual Strength: 7864 lbf.

Table B.12: Crack Growth Data for SCG-18S

CYCLES	FRONT	BACK
0	0.0155	0
50000	0.0155	0.001
100000	0.027	0.0165
200000	0.054	0.043
250000	0.065	0.0595
300000	0.077	0.067
350000	0.09	0.082
450000	0.1155	0.1075
500000	0.1315	0.1195
600000	0.1585	0.1495
700000	0.191	0.18
800000	0.2185	0.2165
850000	0.238	0.231
900000	0.2565	0.247

Pull to Failure @ 8.396 KIP

Table B.13: Crack Growth Data for SCG-19S

CYCLES	FRONT	BACK
0	0.0155	0
50000	0.0155	0.001
100000	0.027	0.0165
200000	0.054	0.043
250000	0.065	0.0595
300000	0.077	0.067
350000	0.09	0.082
450000	0.1155	0.1075
500000	0.1315	0.1195
600000	0.1585	0.1495
700000	0.191	0.18
800000	0.2185	0.2165
850000	0.238	0.231
900000	0.2565	0.247

Pull to Failure @ 8.396 KIP

Table B.14: Crack Growth Data for SCG-20S

CYCLES	FRONT	BACK
0	0.0025	0.0015
10000	0.024	0.0185
20000	0.057	0.033
30000	0.089	0.0905
35000	0.1155	0.112
40000	0.139	0.132
45000	0.1575	0.157
50000	0.183	0.1745
55000	0.2035	0.201
60000	0.224	0.226
65000	0.2545	0.2535
75000	0.313	0.312
85000	0.3835	0.388
95000	0.472	0.475
98000	0.503	0.5045
108000	0.613	0.613
118000	0.753	0.7585
126562	Failed	

Table B.15: Crack Growth Data for SCG-21

CYCLES	FRONT	BACK
0	0	0.002
5000	0	0.01
10000	0	0.012
15000	0	0.0135
25000	0	0.019
35000	0	0.0255
45000	0.003	0.037
55000	0.0065	0.039
65000	0.0065	0.053
75000	0.0065	0.0675
85000	0.014	0.088
95000	0.1125	0.122
105000	0.1685	0.1705
115000	0.232	0.2325
125000	0.3225	0.321
135000	0.462	0.456
145000	0.678	0.6685
152216	Failed	

Note: For the front crack growth readings scratches, marks, and surface roughness prevented accurate measurements of crack accurate measurements of crack

Appendix C
Fracture Surface Photographs

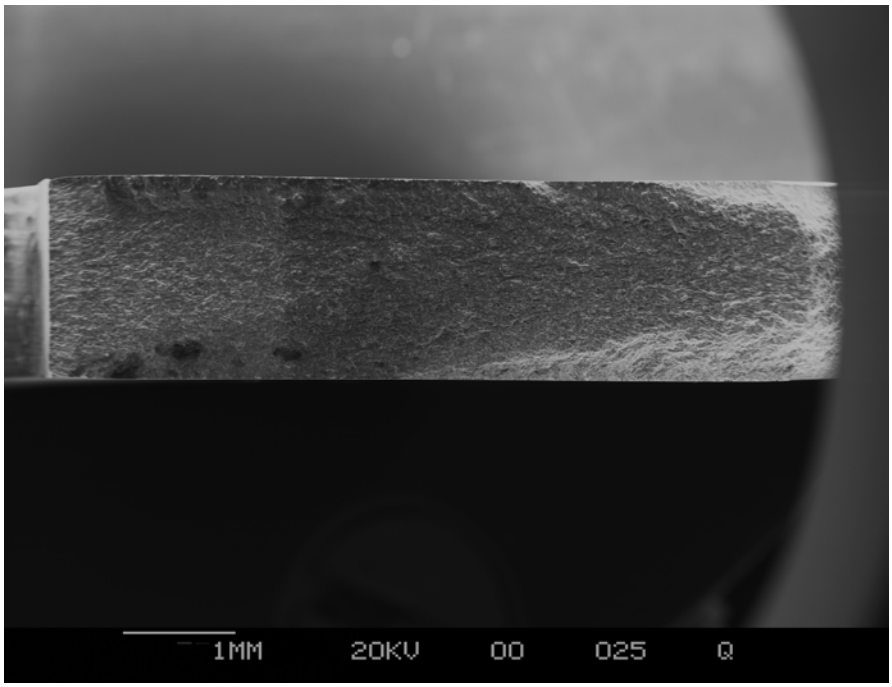

Figure C.1 Entire Fatigue Area for Scg 1S

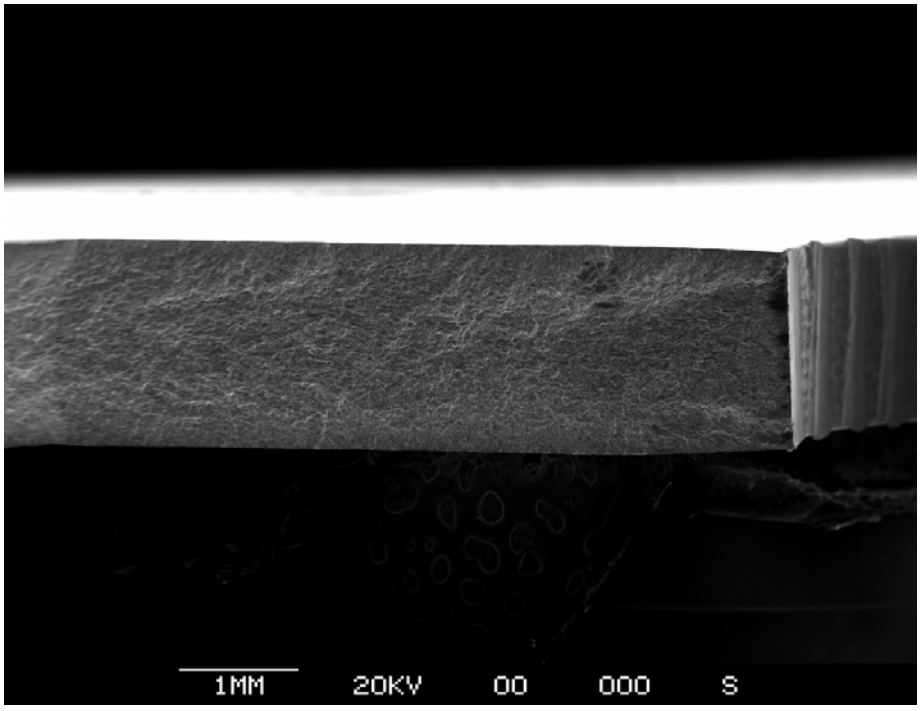

Figure C.2 Entire Fatigue Area for Scg 2

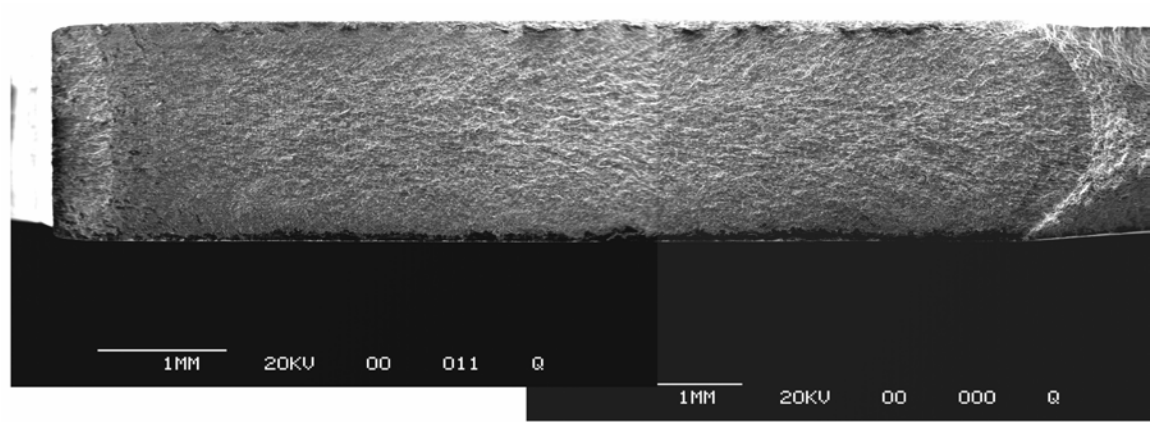

Figure C.3 Entire Fatigue Area for Scg 3S

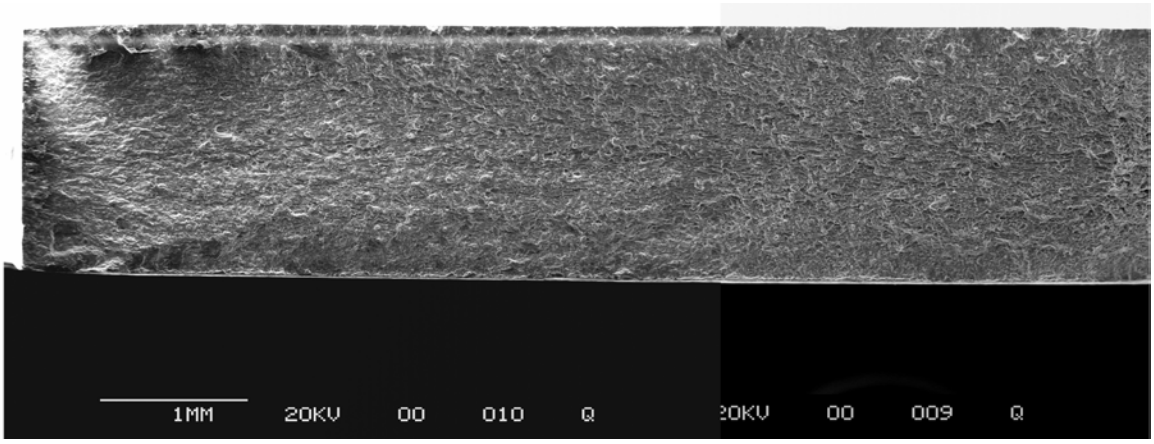

Figure C.4 Entire Fatigue Area for Scg 5

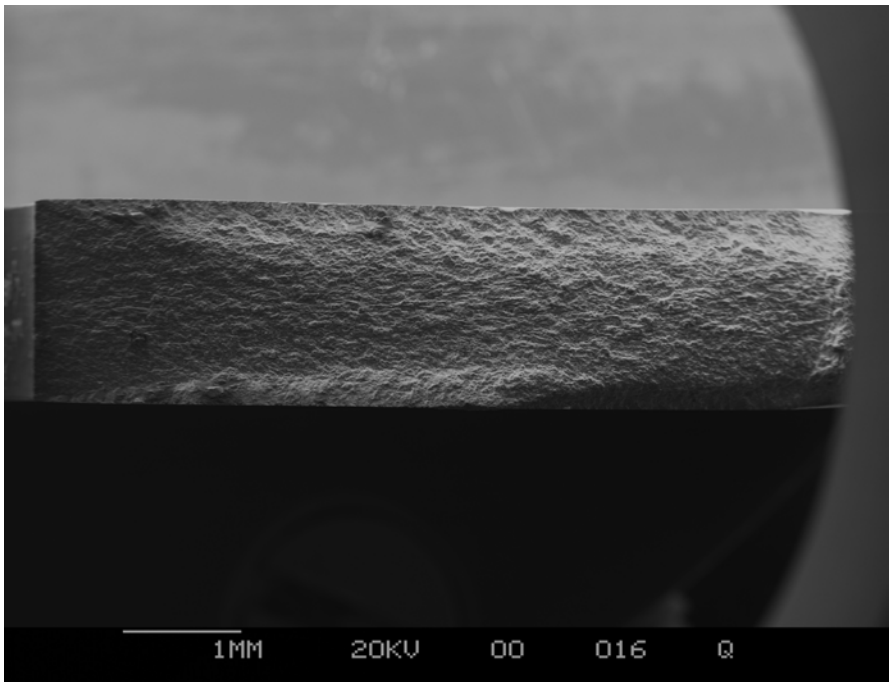

Figure C.5 Entire Fatigue Area for Scg 6

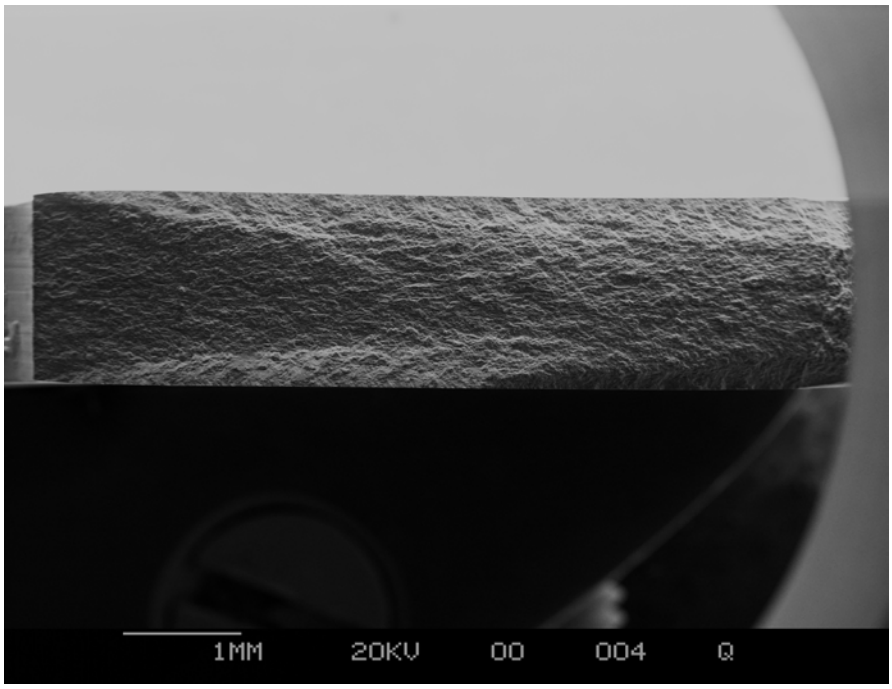

Figure C.6 Entire Fatigue Area for Scg 7

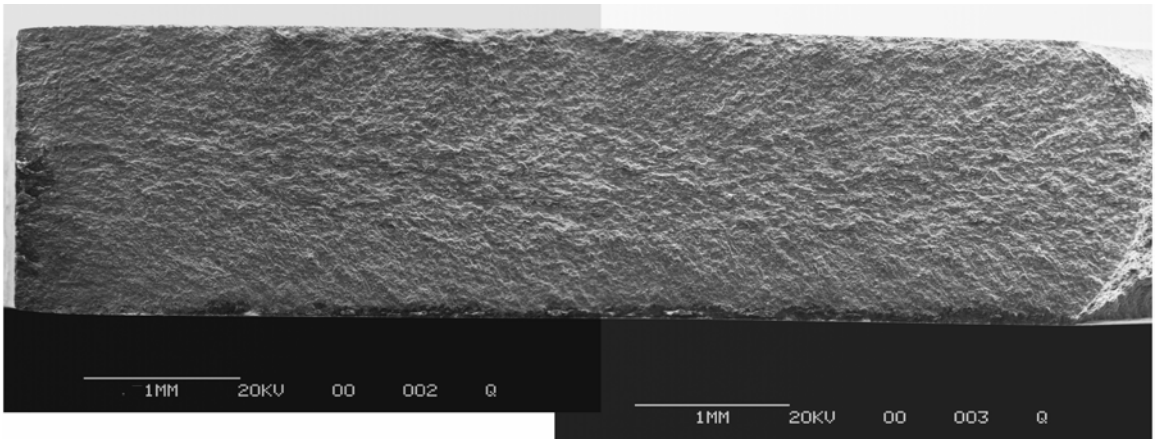

Figure C.7 Entire Fatigue Area for Scg 8

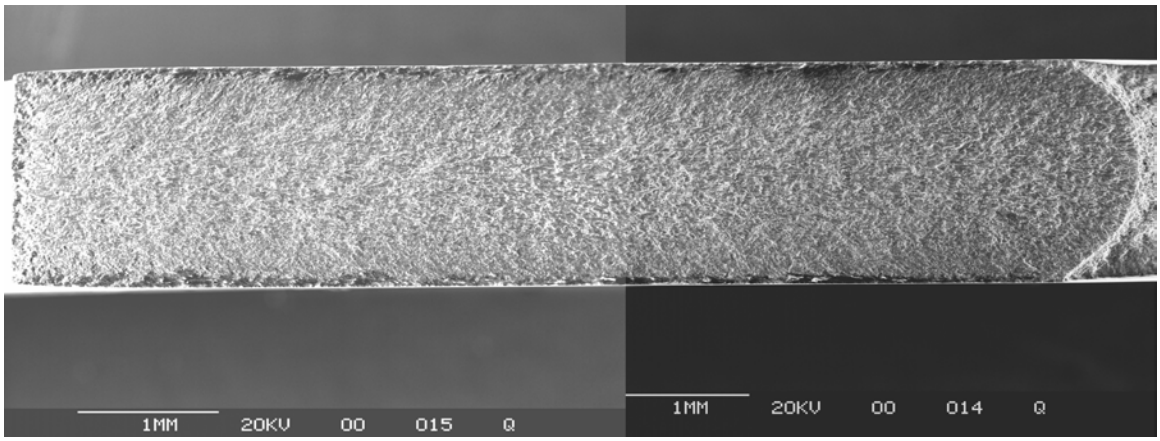

Figure C.8 Entire Fatigue Area for Scg 9

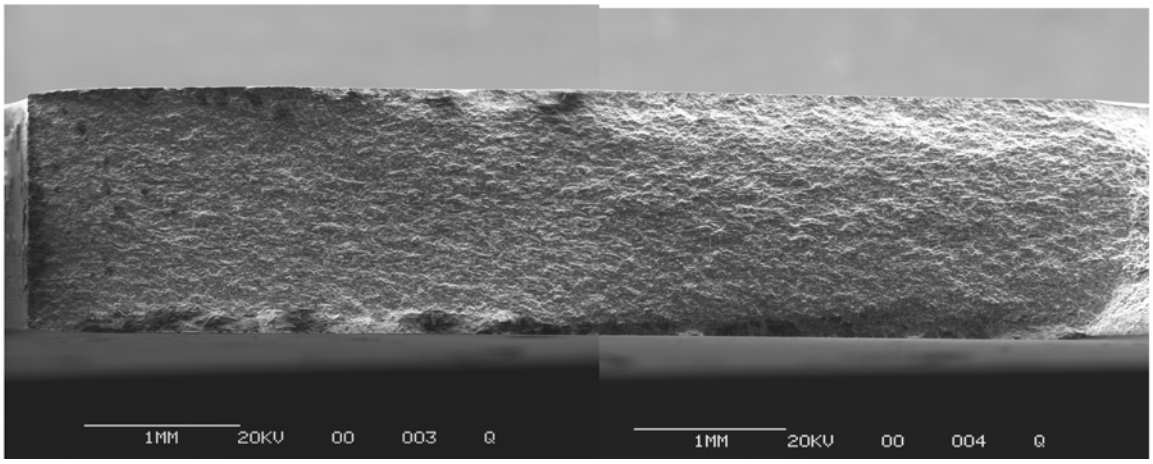

Figure C.9 Entire Fatigue Area for Scg 11

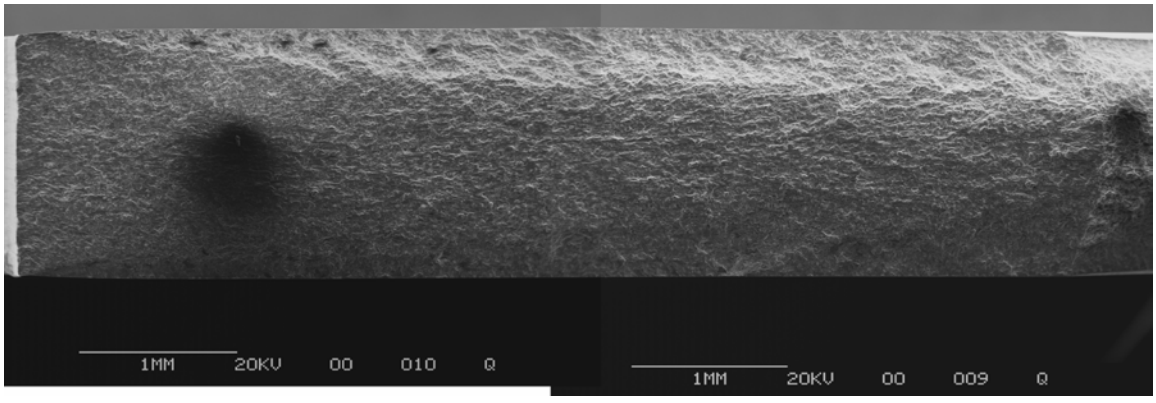

Figure C.10 Entire Fatigue Area for Scg 12

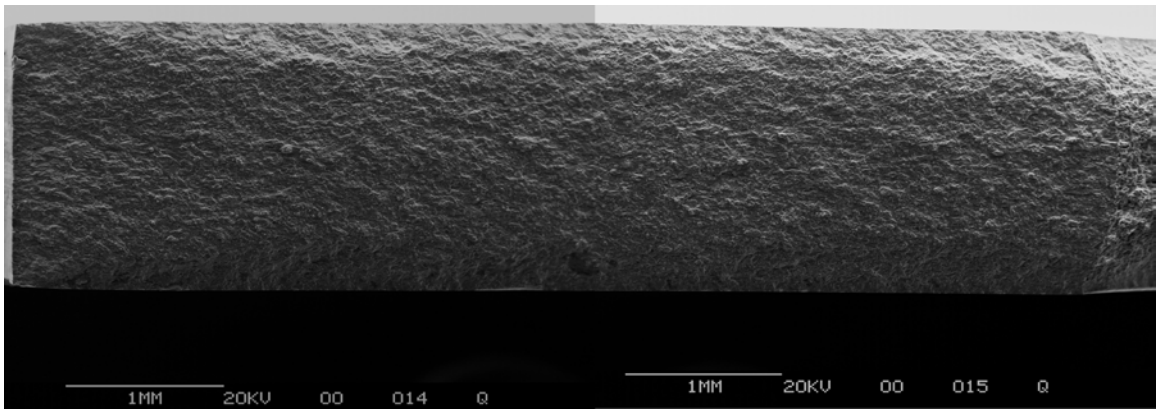

Figure C11 Entire Fatigue Area for Scg 12S

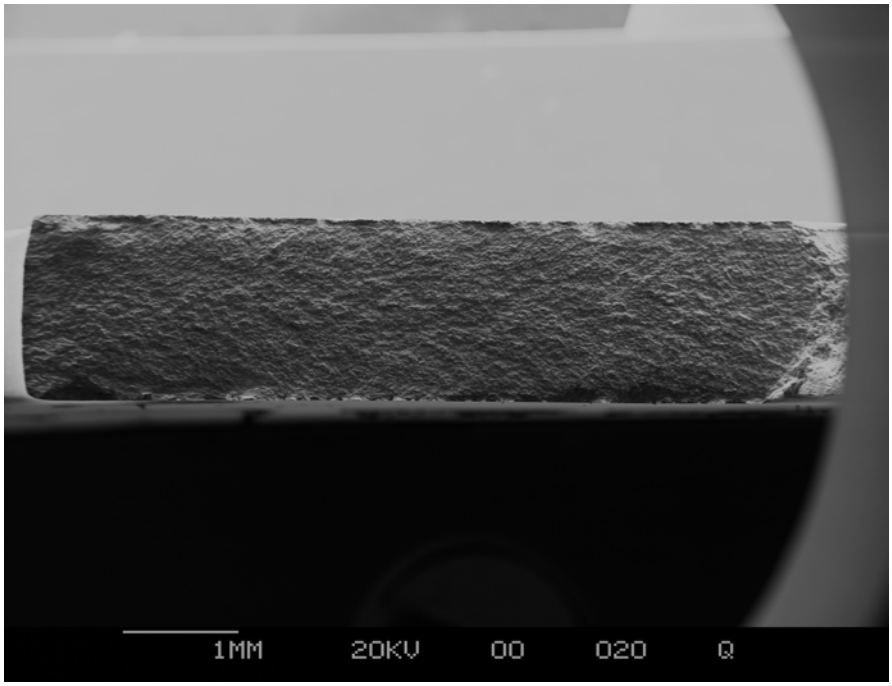

Figure C.12 Entire Fatigue Area for Scg 13S

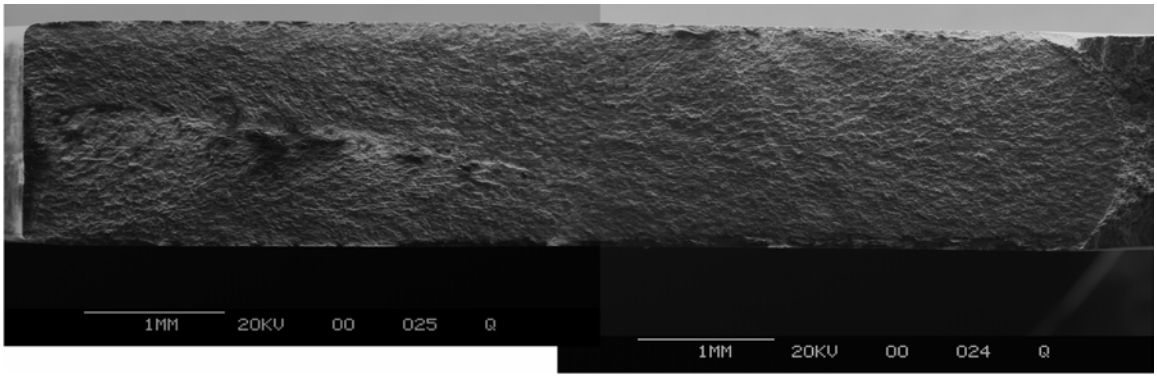

Figure C.13 Entire Fatigue Area for Scg 14

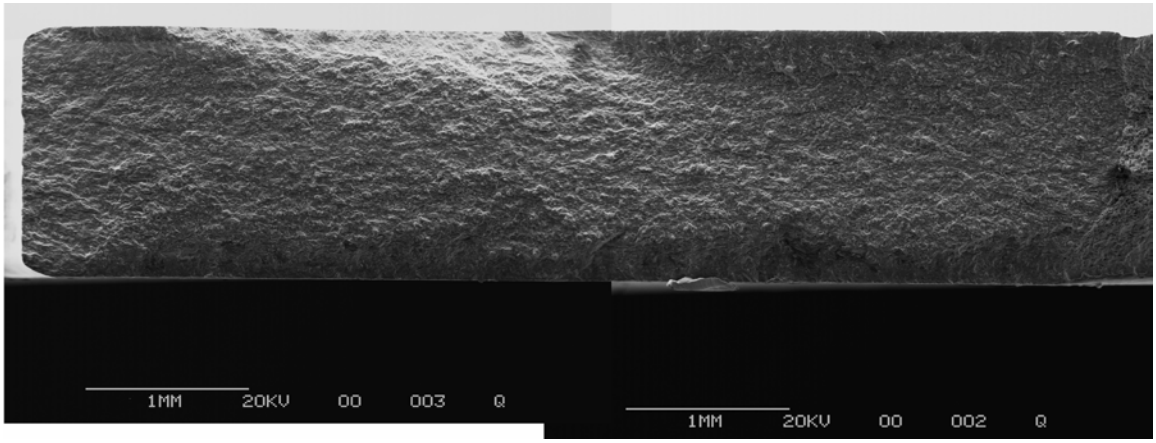

Figure C.14 Entire Fatigue Area for Scg 17S

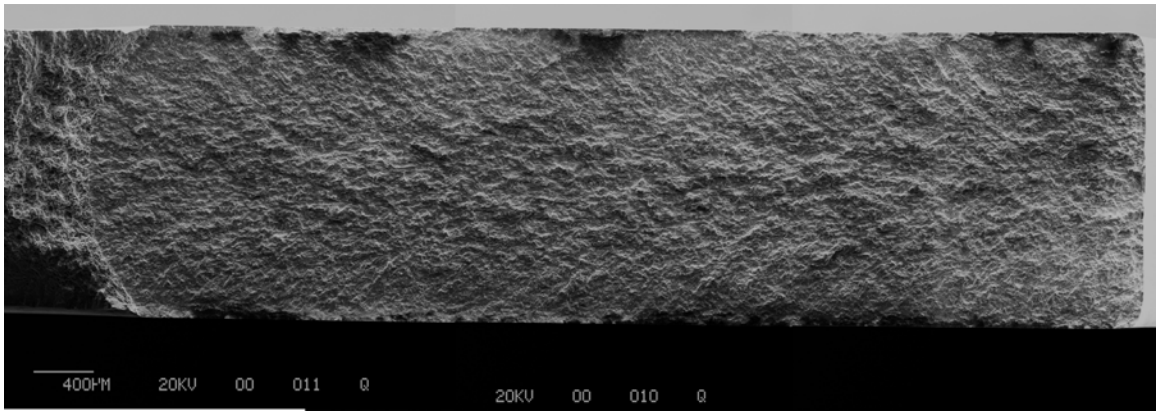

Figure C.15 Entire Fatigue Area for Scg 18S

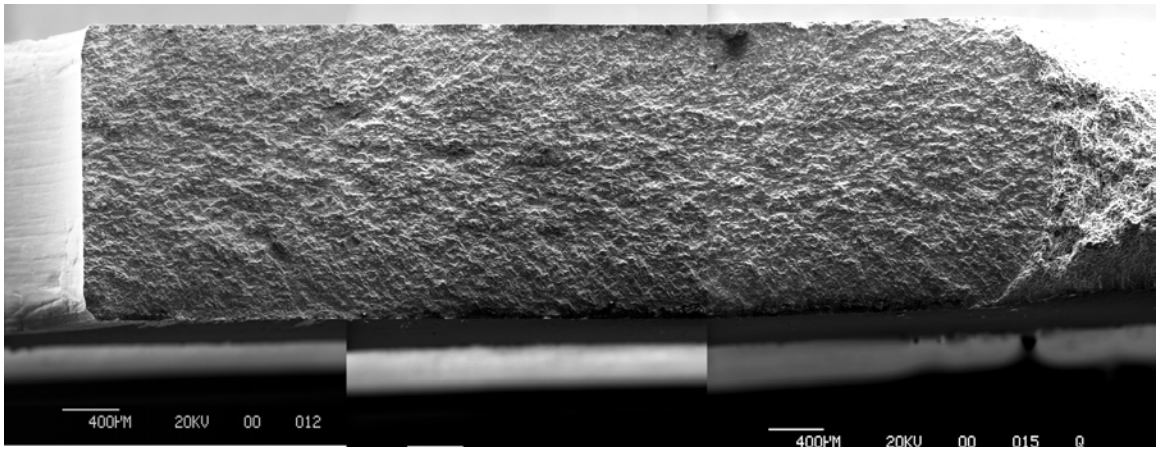

Figure C.16 Entire Fatigue Area for Scg 19S

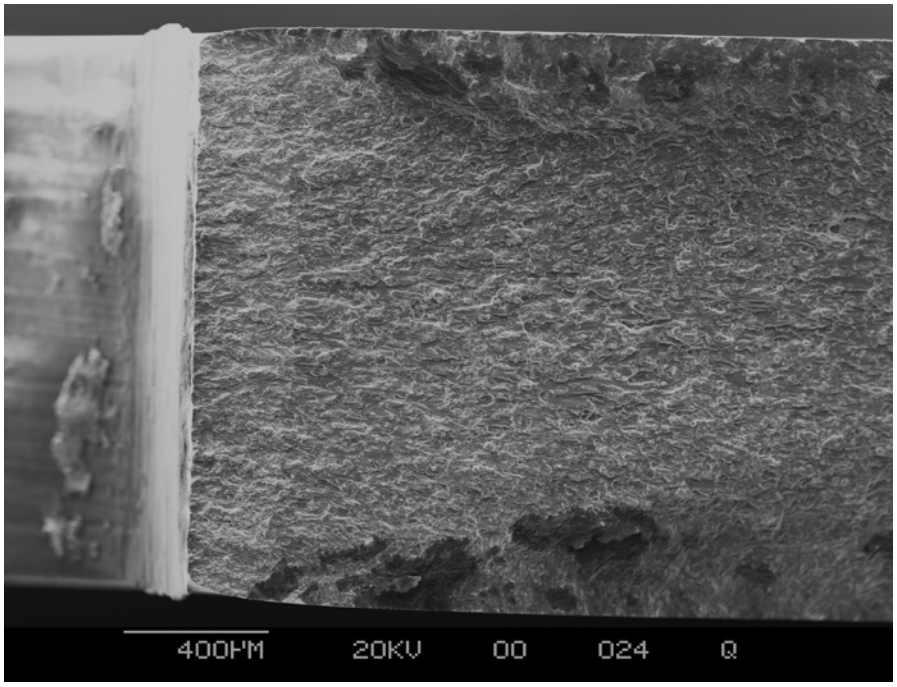

Figure C.17 Fracture Surface of specimen 1S showing crack initiation area

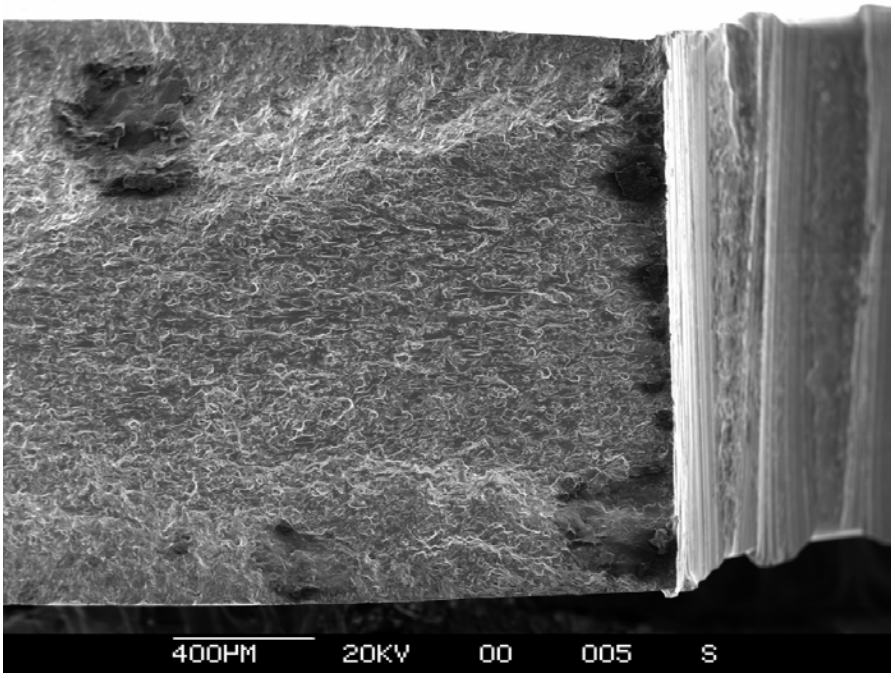

Figure C.18 Fracture Surface of specimen 2 showing crack initiation area

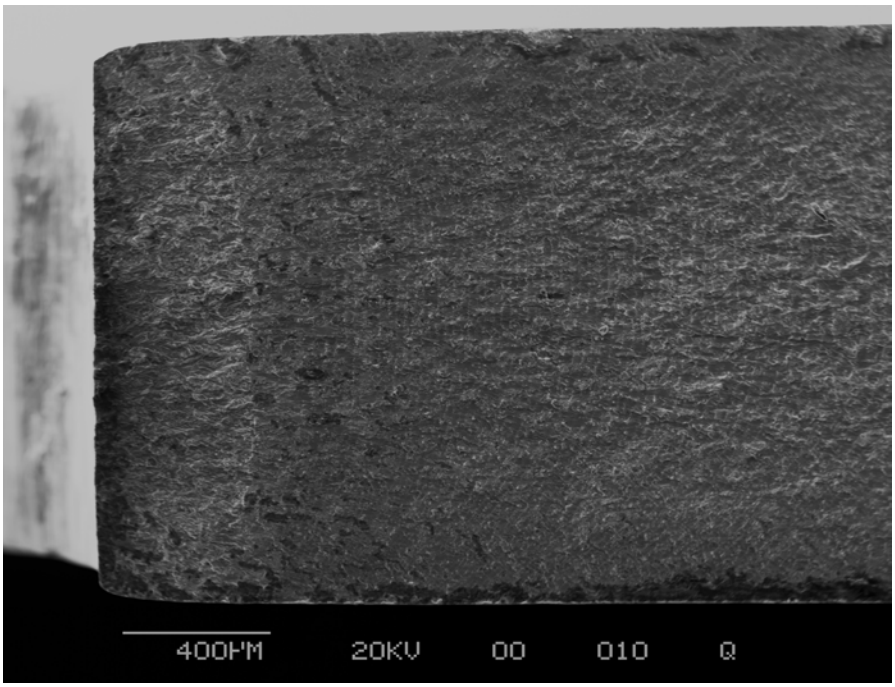

Figure C.19 Fracture Surface of specimen 3S showing crack initiation area

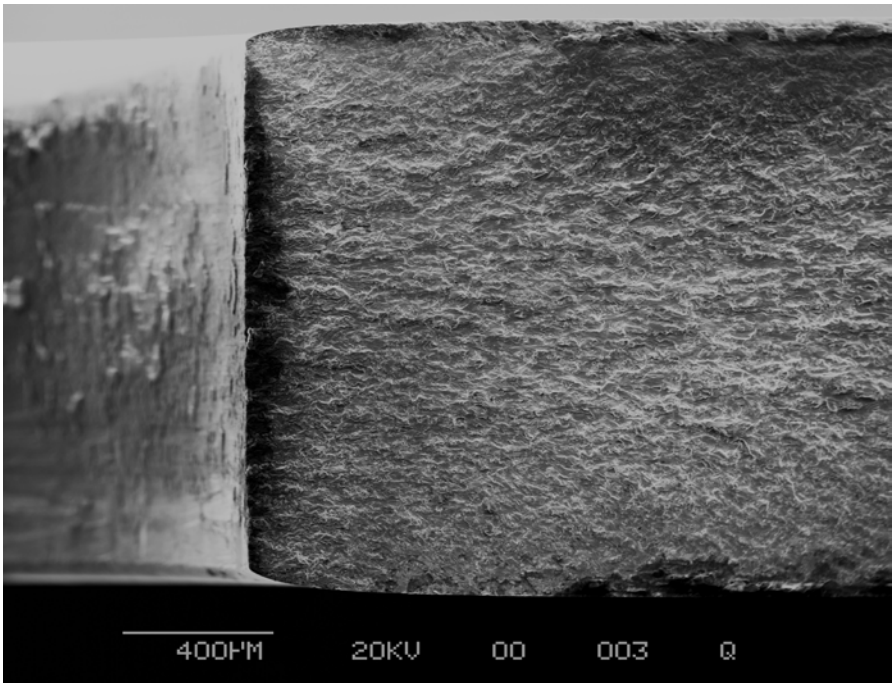

Figure C.20 Fracture Surface of specimen 3S showing crack initiation area

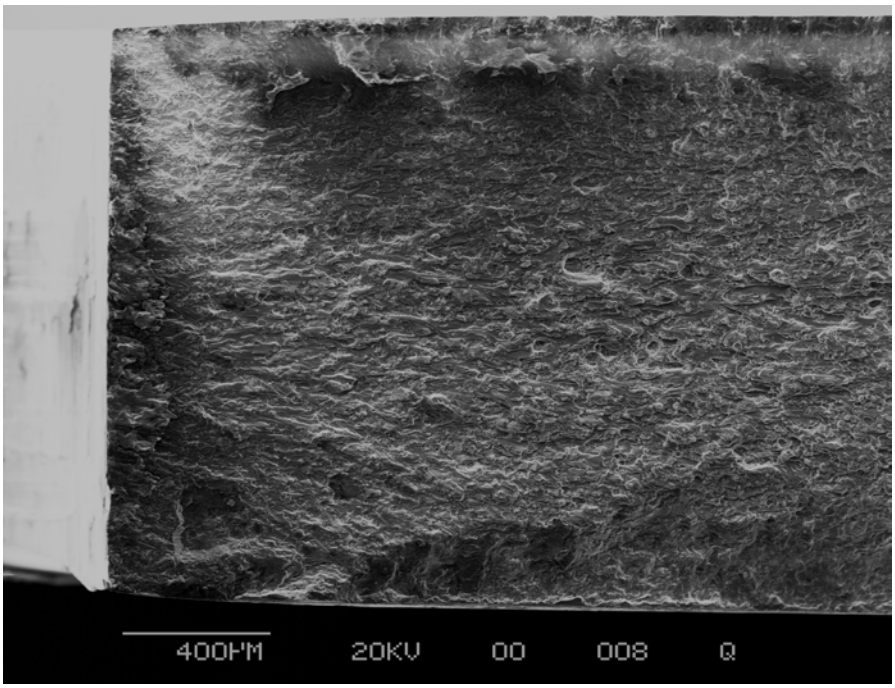

Figure C.21 Fracture surface of specimen 5 showing crack initiation area

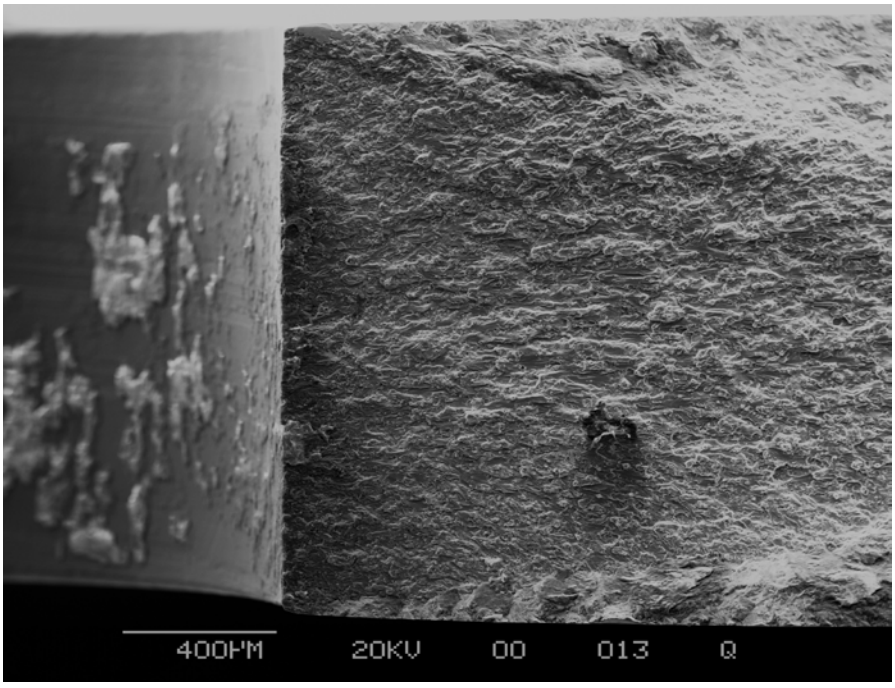

Figure C.22 Fracture surface of specimen 6 showing crack initiation area

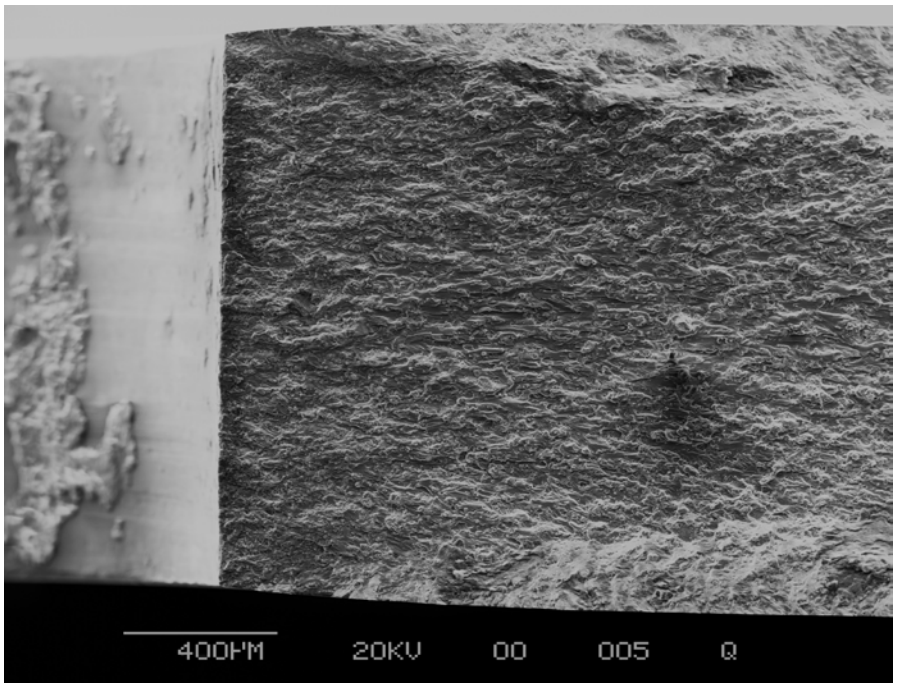

Figure C.23 Fracture surface of specimen 7 showing crack initiation area

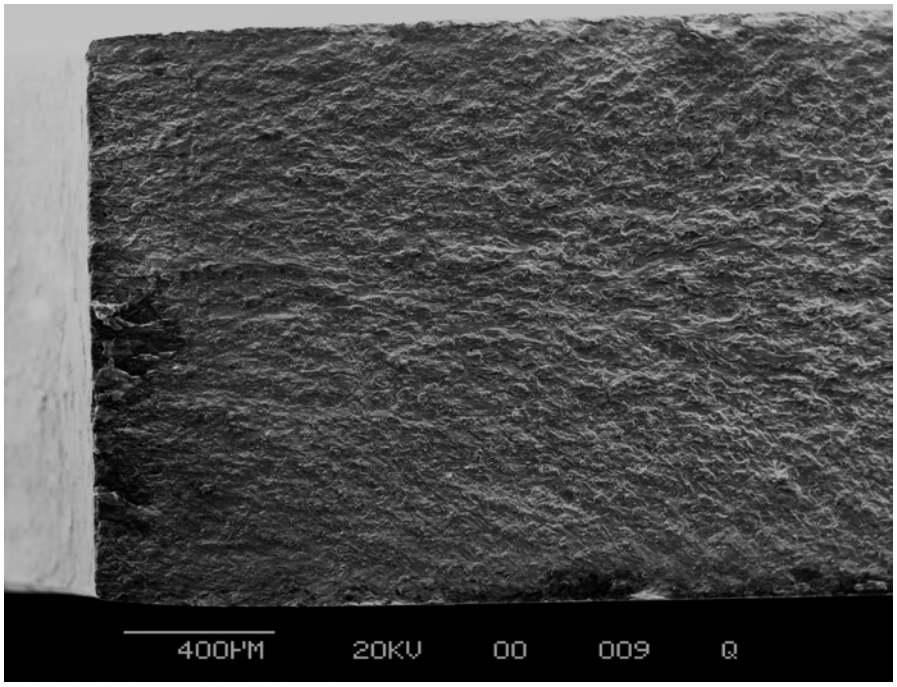

Figure C.24 Fracture surface of specimen 8 showing crack initiation area

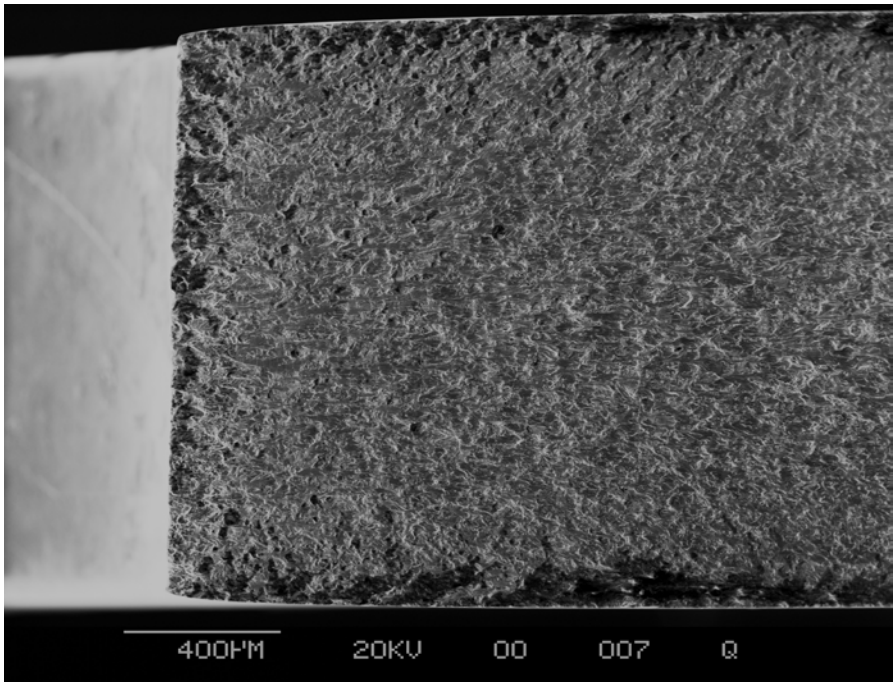

Figure C.25 Fracture surface of specimen 9 showing crack initiation area

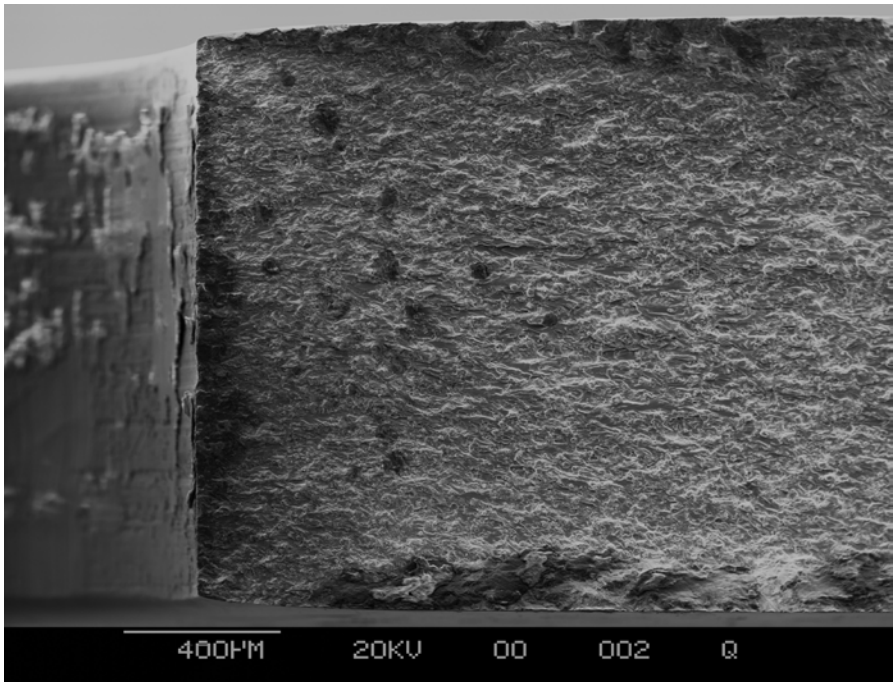

Figure C.26 Fracture surface of specimen 11 showing crack initiation area

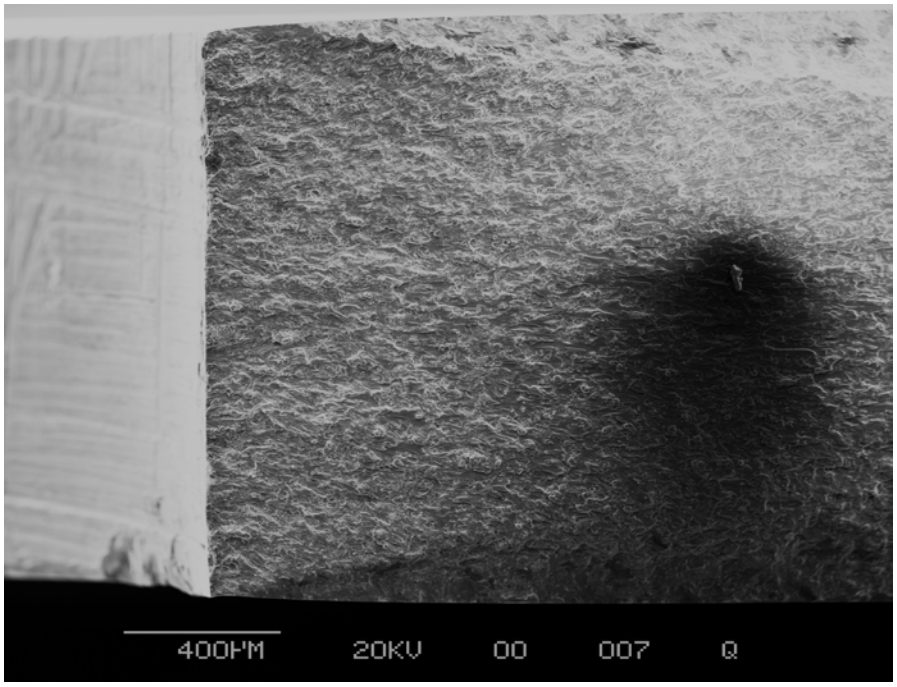

Figure C.27 Fracture surface of specimen 12 showing crack initiation area

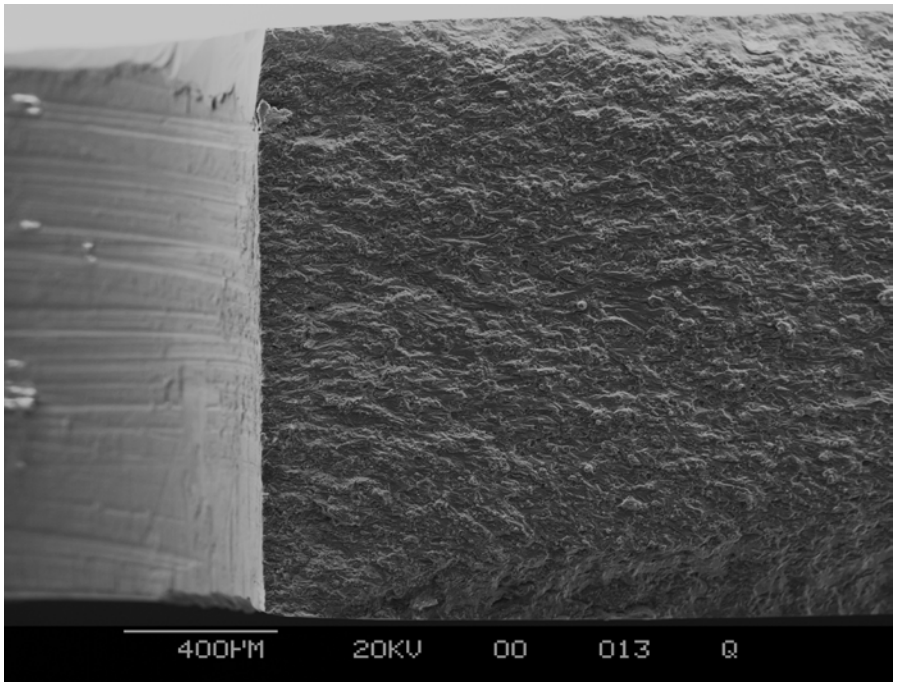

Figure C.28 Fracture surface of specimen 12s showing crack initiation area

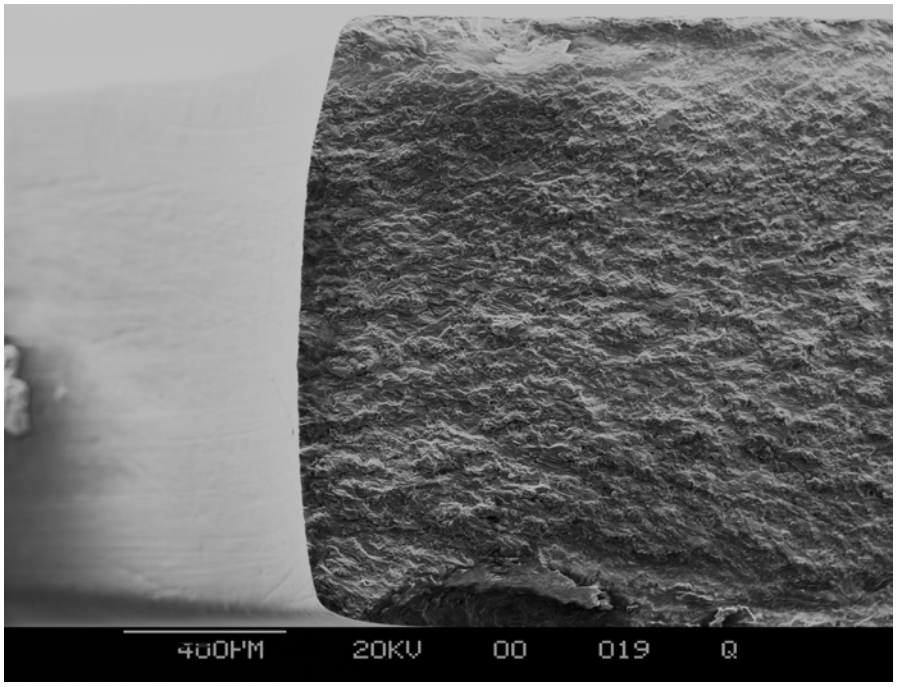

Figure C.29 Fracture surface of specimen 13s showing crack initiation area

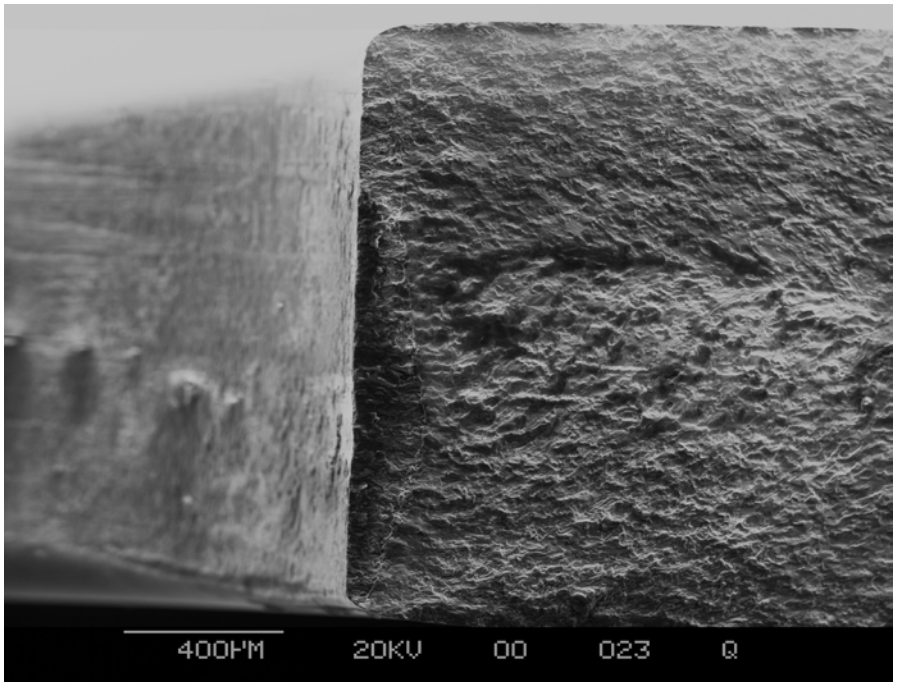

Figure C.30 Fracture surface of specimen 14 showing crack initiation area

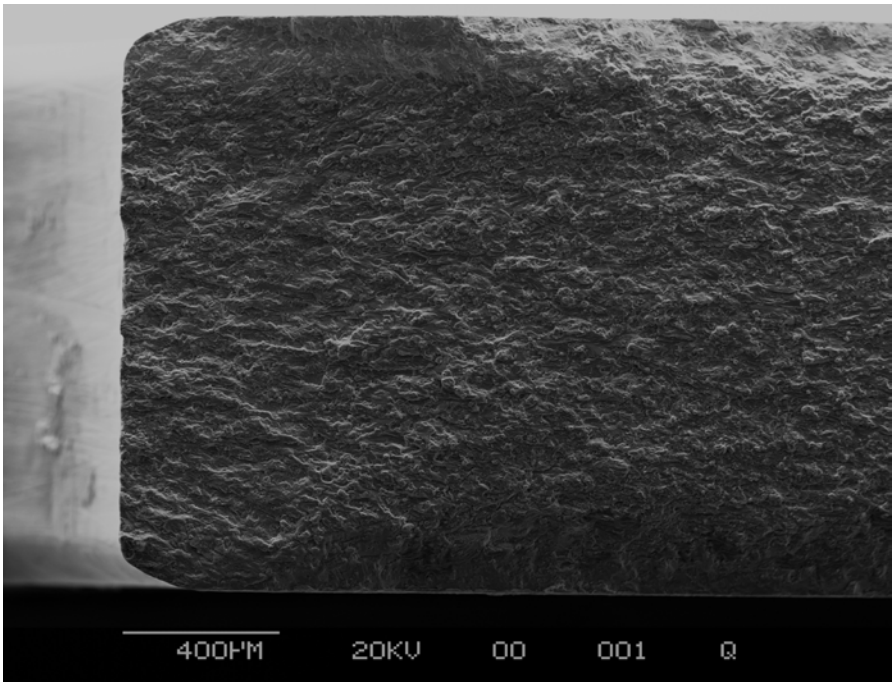

Figure C.31 Fracture surface of specimen 17s showing crack initiation area